DISS. ETH NO. 27335

FULLY WEARABLE POWERED WRIST EXOSKELETON FOR REHABILITATION TRAINING AFTER STROKE

A thesis submitted to attain the degree of

DOCTOR OF SCIENCES of ETH ZURICH

(Dr. sc. ETH Zurich)

presented by

CHARLES OLIVIER LAMBELET

MSc in Microengineering, Ecole Polytechnique Fédérale de Lausanne

born on 08.08.1988

citizen of Forel (Lavaux) VD

accepted on the recommendation of

Prof. Dr. Nicole Wenderoth (examiner)
Prof. Dr. Roger Gassert (co-examiner)
Dr. Walter Karlen (co-examiner)

2021

Give a man a fish, and you feed him for a day.
Teach a man to fish, and you feed him for a lifetime.
— Confucius

To my parents, sister, brother, and their family…

Acknowledgements

A PhD is an enriching and challenging adventure that everyone will experience in a different way. Among the many parameters that can influence this adventure, one remains common to all PhDs. This constant is the people. Indeed, a PhD cannot be accomplished alone, and as the adventurer of this journey, I would like to express my gratitude to a number of people.

My supervisor, Nici Wenderoth, who gave me substantial freedom to steer this project in the direction I desired. Perhaps too much freedom which proved to be a test of patience towards the end;). Her ability to supervise such an heterogeneous lab as the NCM is remarkable.

My co-supervisors, Roger Gassert, whose guidance and supportive feedback on technical aspects were more than helpful. His fascination for transparency planes can be contagious. Walter Karlen, who gave me the opportunity to do an internship in his lab in the first place and put me in touch with Nici.

Dan Woolley, who was the person I could most liken to an engineer in the NCM Lab. His continuous support and indefectible commitment in proofreading my manuscripts ended up making him my official mentor towards the end of this journey.

Olivier Lambercy, with whom I share a first name and half a last name. His feedback during our meetings and when reviewing manuscripts have always been relevant and constructive.

The NCM Lab is filled with heteroclite and talented people that I would like to thank for their support and daily social interactions (in alphabetic order for the sake of simplicity): Caroline Heimhofer, who seems to be a very motivated young woman (typical of young PhDs) judging by her more than early morning arrivals in the lab (according to Google Calendar). Caroline Lustenberger, whose presentation skills must be taken as an example. Christina Grimm, whom I suspect of leaving breadcrumbs in her path so that we can find her. Ernest Mihelj, who taught me poetic spoken English with a slight Croatian touch. Felix Thomas and Finn Rabe, with whom I would love to create a guitarists' boyband and hit the strings along the way. Gabrielle Zbaeren, who was to me like a French-speaking island surrounded by English and German international waters. Ingrid Odermatt, who is Swisser than the Swissest Swiss person from Obwalden, and who can eat slower than me. Iurii Savvateev, whose mere mention of his first name reminds me the glory of the Russian space conquest. Manuel Carro Dominguez, whose multicultural roots fit perfectly this lab. Marc Bächinger, who let me live and do a PhD in HIS city and canton. Marija Markicevic, with whom I shared the longest journey but whose glide seems to have caught some thermals and will continue a little further. Miriam Schrafl-Altermatt, whose academic trajectory strongly resembles that of a cosmic particle. Sanne Kikkert, who believed me more than she would trust the King of the Netherlands himself!

Acknowledgements

Abstract

The human wrist is to the hand, as what the pen is to the poet. The latter cannot work without the former. The wrist not only serves to orientate the hand before a grasp, but also to stabilize it during a grasp. These two functions of the upper limb are inseparable, and a disorder of the wrist joint negatively affects dexterity and grip strength of the hand. Upper limb paresis is the most common impairment following neurological disorders such as stroke, and affects more than 3'700 individuals in Switzerland each year. Stroke survivors often suffer from abnormal muscle tone such as spasticity, tremors, and pain, which affects wrist function and negatively impacts independence and quality of life.

The rehabilitation of these functions is possible during conventional therapy and can be enhanced through high dose and intensive movement-based training delivered by robotic systems. Robot-assisted therapy promotes active participation combined with proprioceptive feedback that reinforces motor learning and somatosensory recovery. By quantitatively assessing the recovery and providing a motivating environment, robot-assisted therapy stands as an adequate candidate to supplement conventional therapy. Nevertheless, therapy administered via robotic devices remains in the minority of treatments and many patients after discharge from the hospital suffer from persistent wrist and hand impairments. Therefore, novel and accessible technologies that empower the patient to self-initiate and continue rehabilitation training must be developed and made commonplace.

Home-based rehabilitation using robotic technologies is a promising and growing field that has triggered the development of many devices. In addition to promoting independent rehabilitation training, powered wearable devices have the potential to provide assistance during functional everyday tasks. However, besides meeting the requirements for supporting a given motor function, the development of such solutions must strike a balance between functionality, usability and wearability. In particular, the ease to mount and unmount (don and doff) is an essential aspect that has so far been rarely addressed in many projects targeting home-based therapy.

The aim of this thesis was to develop, characterize and evaluate a fully wearable wrist exoskeleton - the *eWrist* - that actively supports extension and flexion movements. Envisioned as a tool for assistance during daily tasks, the development focused on usability and wearability of the device. Furthermore, this thesis aimed at implementing a robust and intuitive control scheme on a wearable exoskeleton that promotes voluntary effort using physiological signals.

To achieve this goal, existing technologies targeting the upper limb were reviewed and requirements for a wearable wrist exoskeleton were determined. Weight, size, actuation torque,

Abstract

angular velocity, range of motion, and most importantly ease of implementation were aspects considered when choosing an appropriate transmission type that meets the requirements. With the goal of building a device for independent use, a mechanism to don the *eWrist* with a single hand was implemented. Moreover, the development of the first prototype and subsequent iterations prioritized the selection of widespread and affordable components, and the use of 3D printing techniques and open-source software that would facilitate potential integration into maker communities. The non-backdrivability of the transmission imposed the implementation of an admittance control scheme that allowed smooth and stable interactions between the user and the robot. To investigate the feasibility of intuitive control promoting voluntary effort, an sEMG-based controller was implemented and evaluated on a single healthy subject. The results showed that the fastening system enabled quick and easy donning and doffing, and a firm attachment to the forearm and hand. Moreover, the sEMG controller proved to drive the assistance support in accordance with the intention of the user.

To further improve functionality and wearability, a new iteration of the *eWrist* was characterized and evaluated in fifteen healthy participants and two stroke survivors. Shortcomings of the previous iteration were addressed by: reducing weight and physical profile, increasing durability, improving interaction with the device, and further improving the donning procedure. A novel fastening system including electronics and battery was developed that enabled donning of the entire exoskeleton using one hand. Standardized human-robot interaction metrics and impedance planes were used to characterize and evaluate the various behaviours that can render the device. Based on the established requirements, the developed solution fulfilled or even outperformed expectations. The time required to mount the *eWrist* revealed that after a few practice trials participants could don it independently in about 1 min. In addition, standardized usability questionnaires completed by the participants showed that they all embraced the device and found its attachment system efficient and simple to use.

The non-backdrivability of the transmission combined with a stiffening of the wrist joint generates instabilities in the physical human-robot interaction (pHRI) that were assessed in a goal-directed visuomotor task. A variable admittance control scheme was implemented to detect and dampen these disturbances, and was evaluated in ten healthy participants and six stroke survivors performing the task. In addition, an improved sEMG-based controller, together with a gravity compensation controller were implemented to promote voluntary effort and support wrist weakness. The stability and transparency of the pHRI, characterized by metrics such as jerk, interaction force, and angular velocity/acceleration, was used to assess the effectiveness of the variable admittance scheme. In the context of the visuomotor task, the variable admittance controller proved to significantly reduce instabilities in the human-robot interaction with healthy participants. Additionally, both controllers could enhance wrist functionality of stroke survivors, especially in the most extreme angular positions and more impaired patients.

After many iterations, the latest version of the *eWrist* exoskeleton has resulted in a solution that combines lightweight, low physical profile, ease of donning, and intuitive control to support extension and flexion wrist function in patients with neuromotor impairment. Furthermore, the portability of the *eWrist* makes it suitable for deployment in various environments whether

in a clinic or at an individual's home. Finally, thanks to a focus on accessibility and simplicity throughout the design process, the *eWrist* meets an optimal trade-off between complexity and functionality to increase access to affordable orthoses for stroke rehabilitation.

Résumé

Le poignet humain est à la main, ce que la plume est au poète. Ce dernier ne peut pas fonctionner sans le premier. Le poignet sert non seulement à orienter la main avant une prise, mais également à la stabiliser pendant une prise. Ces deux fonctions du membre supérieur sont indissociables, et un trouble de l'articulation du poignet péjore la dextérité et la force de préhension de la main. La parésie du membre supérieur est la déficience la plus fréquente à la suite de troubles neurologiques tels qu'un accident vasculaire cérébral (AVC), et elle touche chaque année plus de 3'700 personnes en Suisse. Les personnes ayant subi un AVC souffrent souvent d'un tonus musculaire anormal tel que la spasticité, de tremblements, et de douleurs, qui affecte la fonction du poignet et a un impact négatif sur l'autonomie et la qualité de vie.

La réhabilitation de ces fonctions est possible durant une thérapie conventionnelle et peut être intensifiée à travers une thérapie à forte dose et à base de mouvements répétitifs délivrée par des systèmes robotiques. La thérapie assistée par robot favorise la participation active du patient combiné à un retour proprioceptif qui renforce l'apprentissage moteur et la restauration somatosensorielle. En évaluant quantitativement la rémission et en fournissant un environnement motivant, la thérapie assistée par robot s'avère être une méthode adaptée pour compléter la thérapie conventionnelle. Néanmoins, ce type de thérapie reste minoritaire et de nombreux patients, après leur sortie de l'hôpital, souffrent de déficiences persistantes du poignet et de la main. Il faut donc développer et démocratiser des technologies nouvelles et accessibles qui permettent au patient d'initier et de continuer lui-même sa réhabilitation.

La réhabilitation à domicile à l'aide de technologies robotiques est un domaine prometteur et en pleine croissance qui a déclenché le développement de nombreux appareils. En plus de promouvoir une réhabilitation autonome, les appareils portables motorisés peuvent fournir une assistance lors de tâches fonctionnelles du quotidien. Cependant, en plus de répondre aux exigences de soutien d'une fonction motrice donnée, le développement de telles solutions doit trouver un équilibre entre fonctionnalité, facilité d'utilisation et portabilité. En particulier, la facilité pour revêtir et dévêtir l'appareil est un aspect essentiel qui, jusqu'à présent, a rarement été abordé dans de nombreux projets ciblant la thérapie à domicile.

Le but de cette thèse a été de développer, caractériser et évaluer un exosquelette du poignet entièrement portable - le *eWrist* - qui soutient activement les mouvements de flexion et d'extension. Conçu comme un outil d'assistance pour les tâches quotidiennes, le développement s'est concentré sur la facilité d'utilisation et de port de l'appareil. En outre, cette thèse a visé à mettre en œuvre un contrôle robuste et intuitif d'un exosquelette portable qui promeut l'effort volontaire en utilisant des signaux physiologiques.

Résumé

Pour atteindre cet objectif, les technologies existantes ciblant le membre supérieur ont été passées en revue et les exigences relatives à un exosquelette portable du poignet ont été déterminées. Le poids, la taille, le couple d'actionnement, la vitesse angulaire, l'amplitude de mouvement et, surtout, la facilité de mise en œuvre ont été des aspects pris en compte lors du choix d'un type de transmission répondant aux exigences. Afin de construire un dispositif qui peut s'utiliser de manière indépendante, un mécanisme permettant de revêtir l'*eWrist* d'une seule main a été mis en place. De plus, le développement du premier prototype et les itérations ultérieures ont donné la priorité à des choix de composants répandus et abordables, et à l'utilisation de techniques d'impression en 3D et de logiciels libres qui faciliteraient une intégration potentielle dans des communautés de maker. L'unidirectionalité de la transmission a imposé la mise en place d'un système de contrôle d'admission qui a permis des interactions douces et stables entre l'utilisateur et le robot. Pour étudier la faisabilité d'un contrôle intuitif favorisant l'effort volontaire, un contrôleur basé sur le signal électromyographique de surface a été mis en place et évalué sur un seul sujet sain. Les résultats ont montré que le système de fixation permettait de revêtir et de dévêtir rapidement et facilement l'exosquelette, et offrait une fixation solide à l'avant-bras et à la main. De plus, le contrôleur basé sur le signal électromyographique de surface s'est avéré capable de piloter l'assistance conformément à l'intention de l'utilisateur.

Pour améliorer encore la fonctionnalité et la portabilité, une nouvelle itération de l'*eWrist* a été caractérisée et évaluée avec quinze participants sains et deux survivants d'un AVC. Les lacunes de la version précédente ont été comblées en réduisant le poids et l'encombrement, en augmentant la durabilité, en améliorant l'interaction avec l'appareil et en simplifiant encore la procédure pour revêtir l'exosquelette. Un nouveau système de fixation, comprenant l'électronique et la batterie, a été mis au point, afin de pouvoir revêtir l'exosquelette complet d'une seule main. Des mesures standardisées évaluant l'interaction homme-machine et des rendus d'impédance ont été utilisés pour caractériser et évaluer les différents comportements dynamiques que peut rendre l'appareil. Sur la base des exigences établies, la solution développée a répondu aux attentes, voire les a dépassées. Le temps nécessaire pour revêtir l'*eWrist* a révélé qu'après seulement quelques essais, les participants pouvaient le revêtir de manière autonome en 1 minute environ. De surcroît, les réponses aux questionnaires standardisés remplis par les participants ont mis en exergue la simplicité d'utilisation de l'appareil ainsi que l'efficacité de son système de fixation.

L'unidirectionalité de la transmission combinée à un raidissement de l'articulation du poignet génère des instabilités dans l'interaction homme-machine qui ont été évaluées dans une tâche visuomotrice où des cibles doivent être atteintes. Un système de contrôle d'admission variable a été mis en place pour détecter et réduire ces perturbations. Il a été évalué avec dix participants sains et six survivants d'AVC. De plus, une amélioration du contrôleur basé sur le signal électromyographique de surface, ainsi qu'un contrôleur de compensation de la gravité ont été mis en place pour promouvoir l'effort volontaire et soutenir les faiblesses du poignet. La stabilité et la transparence de l'interaction homme-machine, caractérisée par des mesures telles que les saccades dans l'interaction, la force d'interaction et la vitesse/accélération angulaire, ont été utilisées pour évaluer l'efficacité du système d'admission variable. Dans

le contexte de la tâche visuomotrice, le contrôleur d'admission variable a réduit de manière significative les instabilités dans l'interaction homme-machine avec les participants sains. Les deux contrôleurs ont par ailleurs pu améliorer la fonctionnalité du poignet des survivants d'AVC, en particulier dans les positions angulaires les plus extrêmes et chez les patients présentant des déficiences plus importantes.

Après plusieurs itérations, la dernière version de l'exosquelette *eWrist* a abouti à une solution qui combine légèreté, peu d'encombrement, facilité à revêtir et contrôle intuitif afin de soutenir les fonctions d'extension et de flexion du poignet chez les patients atteints de troubles neuromoteurs. D'autre part, la portabilité de l'exosquelette *eWrist* le rend adapté à un déploiement dans de nombreux environnements, que ce soit dans une clinique ou au domicile. Enfin, grâce à l'effort mis sur l'accessibilité et la simplicité tout au long du processus de conception, l'*eWrist* répond à un compromis optimal entre complexité et fonctionnalité visant à accroître l'accès à des orthèses abordables pour la réhabilitation après un AVC.

Contents

Contents

Contents

List of Figures

List of Tables

List of acronyms

ADL	activities of daily living
BIM	bimanual intensive therapy
CIMT	constraint-induced movement therapy
CVA	cerebrovascular accident
DOF	degree of freedom
FDM	finite difference method
FM-UE	Fugl-Meyer assessment of the upper limb
IQR	interquartile range
IMU	inertial measurement unit
MAS	modified Ashworth scale
NASA-TLX	NASA-task load index
NIJ	normalized integrated jerk
pHRI	physical human-robot interaction
PI	proportional-integral
ROM	range of motion
RPM	rotation per minute
RT	robot-assisted therapy
sEMG	surface electromyography
SUS	system usability scale
TTL	transistor-transistor logic
VMT	visuomotor task

1 General introduction

If I had nine hours to chop down a tree,
I'd spend the first six sharpening my axe.
— Abraham Lincoln

1.1 The importance of wrist function

In all mammals such as humans, distal limbs like hands, paws or feet are linked to the body with a highly flexible joint. The function of this joint is to orientate the distal part of the limb to its direct environment. For the hand this joint is the wrist. In the case of the wrist, it not only serves to orientate the hand before a grasp, but also to stabilize it during the grasp (Palmer et al., 1985).

The human wrist is an ellipsoidal type synovial joint, which allows movement along two axes - extension and flexion, and radial and ulnar deviation. Moreover, pronation and supination of the forearm provides an additional degree of freedom (DOF) to orientate the hand. The wrist joint is a complicated assembly of bones, ligaments, nerves, and vessels all gracefully packed into a rather small volume. It can withstand heavy stress but can also actuate the hand in a delicate manner. All muscles actuating the wrist are located in the forearm. The principal muscles are the extensor and flexor carpi radialis and ulnaris. Their interplay gives the wrist its mobility, but also allows it to stiffen and become stable.

Among the DOF of the wrist (see Fig. 1.1), extension is the most important in terms of range of motion and frequency of use during functional everyday tasks (Palmer et al., 1985). The position of the wrist affects grip strength (Burssens et al., 2015; Hazelton et al., 1975; O'Driscoll et al., 1992; Pryce, 1980), and optimal stabilization of the wrist enhances grip force (LaStayo et al., 1999). Moreover, movement of the wrist in the direction of flexion to extension induces synergistic finger joint motion due to the tenodesis effect that closes the fingers and can be used for grasping objects (Su et al., 2005).

Flexion   Extension   Radial deviation   Ulnar deviation   Pronation   Supination
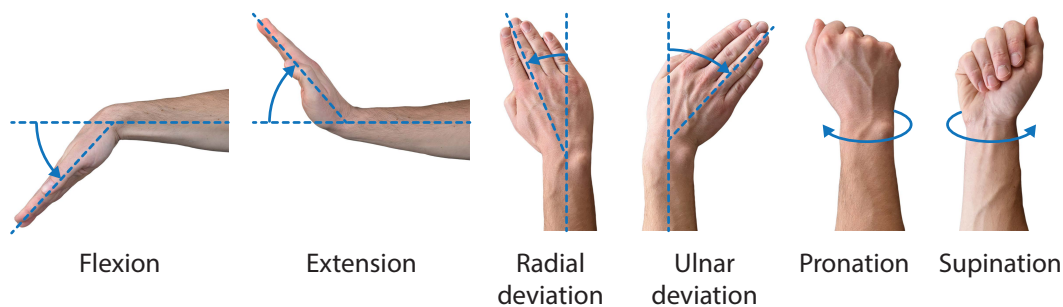
Figure 1.1: The six movements of the wrist.

Interestingly, whereas the English language emphasizes the function of the hand to open a door with *"the handle"*, the French language emphasizes wrist function. Indeed, the French translation for handle is *"la poignée"* and for wrist is *"le poignet"*. It is also said that a person who is strong and vigorous has *"de la poigne"*. This linguistic perspective highlights that in addition to being essential for good hand function, healthy and strong wrist function even holds cultural significance.

1.2   Stroke and motor recovery

Wrist function can be severely impacted by neurological disorders such as stroke. Stroke, or a cerebrovascular accident (CVA), is caused by an acute disruption of oxygen to the brain caused either by a blockage (ischemic stroke) or a rupture (hemorrhagic stroke) of blood vessels (Ojaghihaghighi et al., 2017). A consequence of an interrupted blood supply to a given brain area is cell necrosis (Sherwood, 2015), leading to irreversible brain injury. With over ten million new incidents every year (Mackay et al., 2004), stroke is among the leading causes of serious long-term disability and dependency throughout the world (Benjamin et al., 2018). Whereas only 5% to 20% of stroke survivors demonstrate complete functional recovery, more than 50% do not recover fully (Kwakkel et al., 2003), which means this disease is an enormous burden on the health care system and ultimately on society as a whole (Lapchak et al., 2017; Thrift et al., 2017). In Switzerland alone, stroke events occur on average every 30 minutes leaving more than 5000 stroke survivors each year with long-term disability (Faeh et al., 2010).

Impairments following stroke can vary widely across individuals and depend on the location and extent of the lesion (Laredo et al., 2018). In addition to sensory (i.e. proprioception, touch) loss, cognitive impairment (e.g., in the domains of memory, attention, language), and emotional aspects (e.g., depression), the characteristic effect of stroke is to disconnect a part of the body from the mind (McKenna et al., 2017). Motor deficits, which can vary between full paralysis to a slight disturbance of fine motor skills (Brunnstrom, 1970), are the most common form of impairment. Paresis in a limb is caused by a degradation of motor commands from the contralateral (opposite side) motor regions of the brain (McKenna et al., 2017). A paresis, unlike a plegia (i.e. paralysis), is defined as a weakness in performing voluntary movements, and a decrease in strength and dexterity. Upper limb paresis is the most common impairment following stroke and affects more than 75% of stroke survivors (Langhorne et al., 2011; Langhorne et al., 2009; Rathore et al., 2002). As a result of the degeneration of motor commands and reduced activity in the descending motor tracts, increased agonist-antagonist co-contractions in skeletal muscles are observed (Sommerfeld et al., 2004). Excessive muscle co-contractions, but also involuntary and increased stiffness of the limbs, is referred to as spasticity. Often linked to hemiparesis, spasticity is an abnormal muscle tone (hypertonia) clinically recognized as a resistance to passive muscle stretch that increases with the speed of the stretch (Bobath, 1978; Lance, 1980). This hypertonia and abnormal synergies not only generate pain, but often result in tremor and increased stiffness of the joint, and ultimately in a reduced range of motion(Kamper et al., 2006; McKenna et al., 2017). As an example, Fig. 1.2a depicts a typical impairment seen in stroke survivors, which is defined as hyperflexion of the wrist and fingers, which limits the ability to voluntarily extend the wrist and use the hand. These impairments negatively impact activities of daily living (ADL) and independence, which ultimately affects quality of life.

Rehabilitation of impaired motor function is possible but requires extensive training and motivation (Colombo et al., 2007; Maclean et al., 2000; 2002). Various treatments such as occupational and movement-based therapy, electrical and non-invasive brain stimulation,
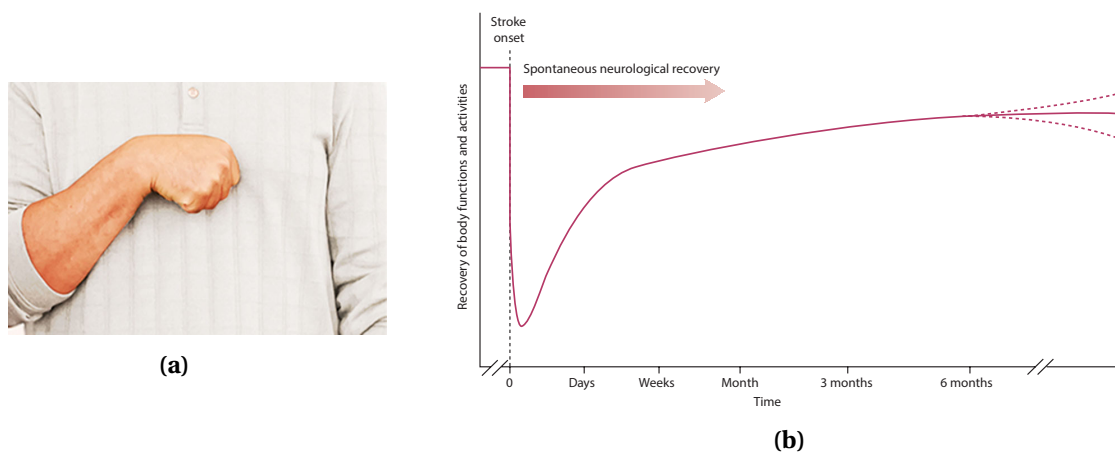
Figure 1.2: a Hyperflexion of the wrist and fingers caused by abnormal muscle synergies (iDryNeedle, 2021). **b** Spontaneous neurological recovery in the acute (1-7 days), sub-acute (7 days - 6 months) and chronic (> 6 months) poststroke phases (Langhorne et al., 2011).

anti-spastic medication and orthopaedic surgery have been shown to improve upper limb function (Langhorne et al., 2009). With regard to movement based therapies, there is a large consensus among therapists and the scientific community that intensity and training dose are important factors for optimizing recovery (Kleim et al., 2008; Langhorne et al., 1996). However, based on the site and initial extent of the lesion, age and neurological status before the stroke, recovery after stroke is a complex process that varies extensively across individuals (Cramer et al., 2000; Langhorne et al., 2011). Neuroplasticity, i.e. the ability/capacity of the central nervous system to reorganize/change and adapt both its structure and function (e.g., activity-dependent changes due to training), is one crucial mechanism underlying the observed improvements in motor function with rehabilitation training. In the acute and sub-acute phases after stroke (0-6 months), there is thought to be a peak in neural plasticity, suggesting that this time window offers the best opportunity to maximize rehabilitation treatment gains (Biernaskie et al., 2004; Jung, 2017). Nevertheless, irrespective of the type and amount of therapy, a spontaneous "return" of neurological functions also usually occurs poststroke (see Fig. 1.2b), making it difficult to assess objectively the efficacy of any treatments applied during these phases (Kwakkel et al., 2006).

Somatosensory functions, and proprioception in particular, play a major role in the process of relearning movements (Kessner et al., 2016; Vidoni et al., 2009; Yekutiel, 2000). Proprioception is the sense of position and movement of the limbs, but also the sense of force, heaviness, and effort. Proprioceptive receptors are located in the skin, muscles, and joints (Proske et al., 2012). The loss of this sense directly affects motor functions that require proprioceptive information to adapt the motor command based on predicted sensory inputs (Shadmehr et al., 2010). Proprioception is essential in the coordination of goal-oriented movements, and to accurately aim at and reach for objects (Ghez et al., 1990; Sarlegna et al., 2009; Sober et al., 2003). Although the effect of stroke on somatosensory functions remains poorly understood, it

is estimated that proprioceptive functions are impaired in 35%-50% of stroke patients (Carey et al., 1996). Recovery of proprioceptive function usually evolves with motor rehabilitation training, however, the detailed mechanisms of this process and its interaction with motor recovery are still largely unknown (Winward et al., 2007). Various studies have shown that proprioceptive deficits after stroke do have an impact on motor recovery and functional outcomes (Carey, 1995; Fang et al., 2003; Feys et al., 2000; Tyson et al., 2008). Moreover, the combination of motor and somatosensory deficits poststroke alter functional recovery to a greater extent than when only motor impairments are present (Patel et al., 2000; Reding et al., 1988). For these reasons, it is important that rehabilitation therapy equally address the recovery of both proprioceptive and motor function.

1.3 Current movement-based rehabilitation therapies in stroke

Traditional movement-based rehabilitation options for stroke patients include therapist-based treatments with hands-on physical and occupational therapy in rehabilitation centers. The treatment, which includes weekly blocked practice over several weeks during the acute and subacute phases poststroke, usually leads to improvements in motor and sensory function (Ottenbacher et al., 1993). However, not only does overall training time remain low compared to the time that the patient is inactive at home (Bernhardt et al., 2004; Lang et al., 2009), but stroke patients are discharged at an increasingly early stage (Hall et al., 2012; Ramirez et al., 2016). Moreover, without incentives to use their affected limb and with a lack of motivation, paretic patients are prone to learned non-use by depending on their unaffected limbs (Taub et al., 2006). Bimanual intensive therapy (BIM) and constraint-induced movement therapy (CIMT) are two therapeutic approaches aimed at preventing learned non-use (Ballester et al., 2016; Liepert et al., 1995). Whereas BIM engages the paretic limb with the non-paretic limb in mirror movements, CIMT forces the use of the impaired limb by immobilizing the unimpaired limb (Barzel et al., 2015; Marumoto et al., 2011). Both methods have been shown to promote cortical reorganization and improve recovery (Liepert et al., 1998; Schaechter et al., 2002).

In the past years - thanks to improvements notably in the field of actuator miniaturization, power electronics, and control electronics - robot-assisted therapy (RT) in stroke has attracted increasing attention (Bos et al., 2016; Maciejasz et al., 2014). Advantages of this approach compared to conventional therapy are many and include: 1) increasing dose and intensity of training (Kwakkel et al., 2008; Norouzi-Gheidari et al., 2012; Pila et al., 2017; Ward et al., 2019) while reducing the physical burden on therapists (Fong et al., 2019), 2) enabling quantitative measurements to assess performance and recovery of the patient more precisely than conventional rehabilitation training (Zollo et al., 2011), 3) tracking the longitudinal effect of the therapy over the time of hospitalization (Lambercy et al., 2018) and 4) engaging the patient in a motivating and stimulating environment (Colombo et al., 2007; Maclean et al., 2002). RT empowers the patient to actively participate in the rehabilitation process. Active-assisted movement and assistance-as-needed rehabilitation strategies require voluntary effort from the patient and are known to trigger more cortical reorganization resulting in more

significant motor improvements than conventional therapy (Hu et al., 2009a; Lotze et al., 2003; Perez et al., 2004). Interactive treatments including active robotic support based on the intention of the patient have been developed (Hu et al., 2015; Lenzi et al., 2012; Song et al., 2013). Moreover, the combination of active participation and proprioceptive feedback from the supported and moving limb further reinforce motor learning and somatosensory recovery (Boyd et al., 2003; Lotze et al., 2003; Vahdat et al., 2019; Wong et al., 2012). This is especially true for the generation of coordinated and fine movements (Ghez et al., 1990; Hasan, 1992), and for improving adaptation following perturbation to movement (Miall et al., 2018).

(a)   **(c)**

(b)
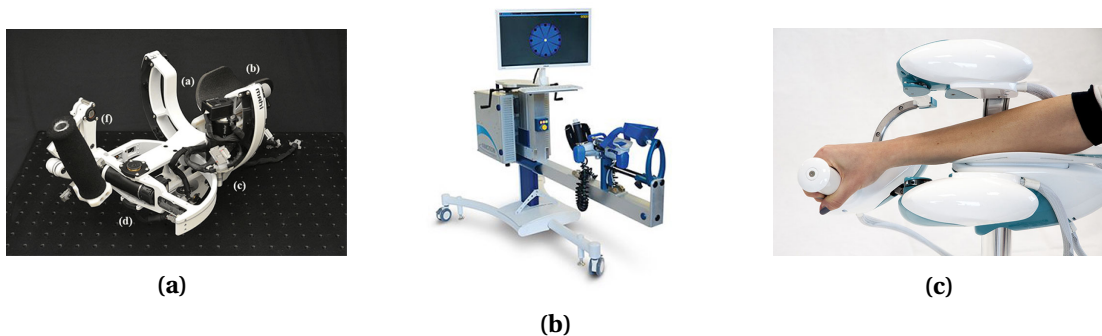
Figure 1.3: A collection of research and commercially available stationary robotic devices for wrist rehabilitation training. **a** The *OpenWrist* research project (Pezent et al., 2017). **b** The *InMotion WRIST* (NeuroRehab, 2021). **c** The *Wristbot* (IIT, 2021).

Powered devices for wrist rehabilitation training are mainly prototypes and remain in the domain of research projects (Martinez et al., 2013; Pehlivan et al., 2014; Pezent et al., 2017). There are a few products that specifically target wrist function, such as the *InMotion WRIST* (BIONIK, Canada) or the *Wristbot* (Italy), that are commercially available (or will be soon) (see Fig. 1.3). These are stationary devices that are well suited for providing precise kinesthetic feedback and for training specific movements during the early stage of rehabilitation. Moreover, they actively support multiple DOF movements in engaging environments such as virtual reality (Buongiorno et al., 2018). In these stimulating and immersive environments, training is performed on functional tasks such as orientating, reaching and grasping an object. However, due to their cost, form factor, and usability, they are best suited for use in clinical settings with qualified personnel (Lo et al., 2019).

Currently, RT is mainly administered to inpatients as a supplement to conventional therapy (Masiero et al., 2014; Norouzi-Gheidari et al., 2012), since only specialized clinics can afford the infrastructure needed. For these clinics, RT is also promoted as a sign of prestige. In this regard, access to RT remains limited to privileged patients and still represents a minority of treatments. After being discharged from the hospital, many stroke survivors experience persistent impairments leading to compensatory strategies and learned non-use (Cirstea et al., 2000; Montagnani et al., 2015). Therefore, a need for novel approaches supplementing conventional therapy that can be continued after leaving clinical settings remains. These novel approaches must be effective (Brewer et al., 2007; Pignolo, 2009) and ideally empower

the patient to self-initiate independent rehabilitation training.

1.4   Envisioned movement-based rehabilitation approach

The lack of training opportunities outside the hospital environment and the large proportion of stroke survivors who experience persistent impairment following clinical treatment needs to be addressed (Ostwald et al., 2008). To this end, one solution is to pursue rehabilitation training at home. Robotic technology can play an important role here since the user can be remotely monitored and guided (Feng et al., 2005). Robotic devices could be first introduced and used in the clinical setting as an adjunct to conventional therapy to familiarize the patient with the system. In this familiarization phase, the therapist could tailor the device to the patient's anthropometric measurements and level of impairment. After discharge from the hospital, the device could be used independently by the patient in home and community settings (Lee et al., 2018). Close monitoring of the home-based rehabilitation process would 1) provide valuable information about the patient's ability to translate the motor skills acquired during conventional therapy sessions to real life situations (Bhatnagar et al., 2020; Leuenberger et al., 2017; Van Meulen et al., 2016), 2) allow therapists to track motor recovery, and 3) prescribe individualized therapy plans. Such an approach would typically be applied in patients with mild-to-moderate upper-limb deficits since they may already have a certain level of independence.

An interesting and potentially promising approach to provide functional, intensive and task-specific training would involve using wearable robotic devices that assist the paretic limb during ADL. In this way, the affected limb can be used repeatedly and for extended periods of time during functional tasks (Radder et al., 2019). Nevertheless, there are several technical challenges for portable robotics aimed at assisting ADL. First, the technology must be safe, reliable and affordable (Sivan et al., 2014). Second, weight and form factor must be minimized while still meeting the requirements for supporting a given motor function. Aesthetics is also an important factor to consider for use in community settings (Power et al., 2016). Last but not least, the technology must be easy to use and especially easy to set up without requiring the help of a third person. Regarding the final point, mounting the device in the context of unsupervised rehabilitation is essential but has so far been rarely addressed in the scientific community (Kim et al., 2018b; Kozlowski et al., 2015; Meuleman et al., 2015; Tefertiller et al., 2017). Indeed, mounting the device is the first barrier that the user has to overcome. This step must be as straightforward as possible to keep patients motivated (Colombo et al., 2007; Juszczak et al., 2018).

In recent years, a myriad of home-based rehabilitation tools have been developed to assist ADL and by de facto train motor function (Bos et al., 2016) (see Fig. 1.4). Extensive effort has been devoted to detecting the user's intention to serve as a command signal for the device. The challenges here lie in the control of the robot, which must be intuitive and robust (Ison et al., 2014). The command signal can be based either on interaction forces between the

| (a) | (b) | (c) |
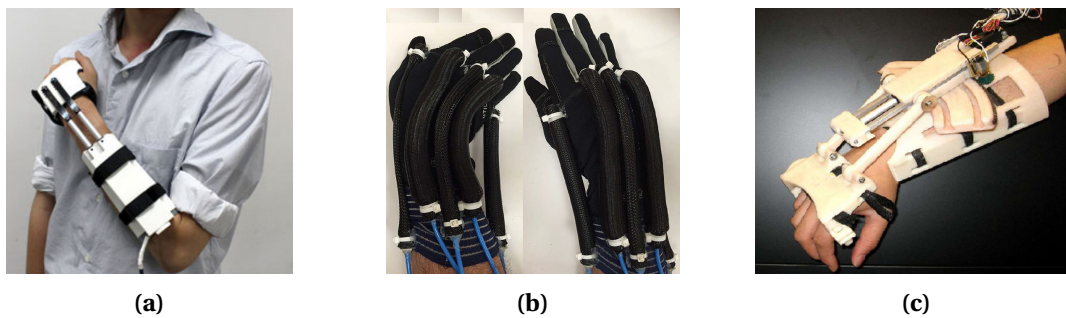
Figure 1.4: A collection of portable exoskeletons actively supporting wrist functions. **a** A spring-based prototype (Higuma et al., 2017). **b** A soft robotic glove (Al-Fahaam et al., 2016). **c** A prototype that supports 2 DOF (Khokhar et al., 2010).

user and the robot, or on physiological signals such as surface electromyography (sEMG). Both methods have been shown to be appropriate for proportional and intuitive control of a robotic device (Corbett et al., 2011; Lobo-Prat et al., 2014). The robustness of a force-driven control is particularly critical for rigid and non-backdrivable exoskeletons, which render a stiff environment to their user. By their nature, these devices are very sensitive to interaction forces and can become unstable in case of increased interaction forces, which can be provoked by stiffening of the assisted biological joint (Landi et al., 2017; Wang et al., 2015).

In the absence of physiological signals or in the case of an inability to generate force with the paretic limb, other approaches such as mirror therapy and gravity compensation are being considered (Ueki et al., 2010). In hemiparetic patients, mirror therapy with robotic devices consists of creating the assistance motion for the paretic limb with the healthy limb. However, since the impaired limb is passively moved without requiring voluntary effort from the affected motor region of the brain, this approach is less efficient. Therefore, an intuitive control actively involving the patient is not only beneficial for neurorehabilitation (Lotze et al., 2003), but also to achieve user acceptance (Bos et al., 2016). As a solution against muscular weakness, gravity compensation is commonly implemented in exoskeletons. This approach has mainly been applied to support the shoulder joint (Beer et al., 2007; Hsieh et al., 2015), and has been shown to increase the quality and dose of training by reducing fatigue (Kwakkel et al., 2013). Moreover, the positive effects of increased joint excursion and decreased spasticity have also been observed (Brewer et al., 2007; Prange et al., 2006).

Today, all the ingredients are available to offer innovative and affordable technologies to the stroke population, which could provide long-term rehabilitation options and supplement conventional therapy. Nevertheless, despite the effort toward this goal in recent years, there is still no solution that strikes a balance between lean design, ease of use, robustness, intuitive control, and wearability for use in home-based rehabilitation therapy and assistance in ADL. This thesis aims to investigate some of these aspects and bring novel ideas and solutions to the field.

1.5 Objectives of this thesis

The goal of this thesis is to address some of the shortcomings in the growing field of unsupervised rehabilitation training using powered wearable exoskeletons. This thesis consists of the development and evaluation of a fully portable wrist exoskeleton that actively supports extension and flexion movements. Besides meeting the technical requirements for a portable wrist exoskeleton (i.e. lightweight, low physical-profile, autonomy, and robust control), usability and portability of the device are crucial aspects that will be considered throughout the development phase. While simple solutions such as velcro and straps are commonly implemented to attach exoskeletons to the human body (Arata et al., 2013; Schabowsky et al., 2010), these fixations techniques are challenging when they have to be performed independently and with a single hand. Therefore, in the context of unsupervised and home-based therapy, a novel approach to mounting and unmounting (i.e. donning and doffing, respectively) will be investigated and evaluated with healthy participants and stroke survivors. The goal is that hemiparetic patients are able to don and doff the exoskeleton independently and in reasonable time after a short training phase.

In addition, this work explores the use of force-based and sEMG-based control strategies to proportionally trigger the mechanical support provided by the device. Extension and flexion wrist movements shall be actively assisted based on the user's intent. More specifically, the stability of the physical human-robot interaction will be examined during a goal-directed visuomotor task (Landi et al., 2017; Wang et al., 2015). The implemented controller will be evaluated to render maximal transparency of the device during smooth wrist motion, and to remain stable during stiffening of the wrist joint. Moreover, the developed wearable platform will enable investigation of a gravity compensation controller for patients with little ability to generate overt wrist movements or with weak physiological signals such as sEMG. In the context of the goal-directed visuomotor task, it is hypothesized that stroke survivors wearing the exoskeleton will be able to acquire more distant targets requiring more wrist extension/flexion with the aforementioned controllers than without. This would demonstrate that the system not only increases the excursion of the patients' wrist, but also allows them to remain stable and in control. These aspects are important in the context of a daily assistance for orientating the hand and steadily holding objects, and are also fundamental for adequate motor recovery.

1.6 Thesis outline

The core chapters of this thesis are composed of three research articles, two of which have already been published and one is in preparation for submission.

Chapter 2 describes a first functional prototype of a portable wrist exoskeleton implementing proportional sEMG-based force control that mechanically assists wrist extension and flexion movements. Existing technologies in wearable devices for the upper limb are reviewed and

trade-offs are made based on preliminary requirements. These requirements focus in particular on an acceptable weight and size for a wrist exoskeleton placed distally on the arm. The transmission type is selected based on the required actuation torque, velocity and range of motion, but also on the simplicity of its implementation and its impact on weight. The interaction force measurement and the intention detection method are two important aspects of the design since they must allow accurate proportional control while not altering usability. The rigid structure of the exoskeleton requires special attention regarding anatomical positioning on the wrist and ergonomics. An intuitive and efficient mechanism to fixate the exoskeleton on the forearm is implemented, however, an adequate fixation solution for the battery is not yet proposed. Finally, the technical aspects of the device are characterized, a succinct assessment of the donning time is performed, and the capability of the sEMG-based force controller demonstrated.

Chapter 3 presents an improved wrist exoskeleton. It is characterized more thoroughly and rigorously than in Chapter 2, highlights the wearability of the device and evaluates it in healthy participants and stroke survivors. As a fully portable device envisioned for assistance in ADL, shortcomings of the previous prototype are addressed and include: 1) reducing the weight placed distally and lowering the physical profile, 2) increasing the durability, 3) improving debugging and interaction with the device, and 4) improving the overall donning and doffing process. To address points 1) and 4), a novel fixation mechanism that includes electronics and the battery is developed in order to don the device with a single hand. The technical characterization focuses on standardized haptic and human-robot interaction metrics, and impedance planes present the various behaviours that can render the exoskeleton. In addition to the time required for donning and doffing the device, the wearabilty assessment collects subjective feedback from participants via standardized usability questionnaires.

Chapter 4 focuses on the stability of the exoskeleton during human-robot interaction in the context of a goal-directed visuomotor task. The stiffening of the wrist joint during target acquisition combined with the rigid structure of the non-backdrivable device can lead to instability in the human-robot interaction. A variable admittance control scheme that detects and reduces these disturbances is evaluated in the goal-directed visuomotor task performed by healthy participants and stroke survivors. Moreover, an improved proportional sEMG-based controller that actively supports extension and flexion of the wrist, together with a gravity compensation controller are also evaluated within the framework of the visuomotor task. Performance metrics such as jerk, interaction force, and angular velocity/acceleration provide valuable information on the stability and transparency of the interaction. These metrics are then used to compare the stability and transparency performance of both controllers (sEMG and gravity) to a third control modality. In this modality, the device provides no mechanical support, and does not offer any resistance to movement. Moreover, the number of acquired targets by stroke participants during the task is compared across all three modalities and provides insight into the functionality of the controllers and their potential benefits for stroke rehabilitation training.

Finally, the general discussion presents a plausible use of the current device, and elaborates on the potential implications of this project in the context of unsupervised rehabilitation training in community settings or at home. Limitations of the current work and suggestions on how to further develop this device into a functional assistive tool during ADL are also discussed.

2 The eWrist - A wearable wrist exoskeleton with sEMG-based force control for stroke rehabilitation

Charles Lambelet, Mingxing Lyu, Daniel Woolley, Roger Gassert, and Nicole Wenderoth

International Conference on Rehabilitation Robotics (ICORR), 2017

Chapter 2. The eWrist - A wearable wrist exoskeleton with sEMG-based force control for stroke rehabilitation

2.1 Abstract

Chronic wrist impairment is frequent following stroke and negatively impacts everyday life. Rehabilitation of the dysfunctional limb is possible but requires extensive training and motivation. Wearable training devices might offer new opportunities for rehabilitation. However, few devices are available to train wrist extension even though this movement is highly relevant for many upper limb activities of daily living. As a proof of concept, we developed the *eWrist*, a wearable one degree-of-freedom powered exoskeleton which supports wrist extension training. Conceptually one might think of an electric bike which provides mechanical support only when the rider moves the pedals, i.e. it enhances motor activity but does not replace it. Stroke patients may not have the ability to produce overt movements, but they might still be able to produce weak muscle activation that can be measured via surface electromyography (sEMG). By combining force and sEMG-based control in an *assist-as-needed* support strategy, we aim at providing a training device which enhances activity of the wrist extensor muscles in the context of daily life activities, thereby, driving cortical reorganization and recovery. Preliminary results show that the integration of sEMG signals in the control strategy allow for adjustable assistance with respect to a proxy measurement of corticomotor drive.

2.2 Introduction

In the United States alone, up to 795'000 people survive a stroke each year (Lloyd-Jones, 2009), more than half of which suffer from chronic hand impairments (Wade et al., 1983). Wrist and hand impairments after stroke negatively impact activities of daily living (Dipietro et al., 2007), with the patient often requiring the assistance of a third party. In addition to weakness in the extensors of the upper limb, spasticity, hypertonia and abnormal flexor synergies are common for many stroke patients and lead to hyperflexion of the wrist and fingers. It has been shown that upper limb recovery is closely linked to the duration and intensity of movement therapy (Kwakkel, 2009). Training has been shown to enhance plasticity and trigger cortical reorganization contributing to improved motor control following stroke (Liepert et al., 1998; Liepert et al., 2000).

Currently, most rehabilitation training is administered in physical therapy centres, but supervised practice could be supplemented with robot-assisted therapy. This approach has the potential to increase the amount of motor practice performed while reducing the workload of therapists (Kwakkel et al., 2007; Lum et al., 2002; Pignolo, 2009).

Even though robot-assisted devices can increase the number of repetitions performed within a single training session, overall training amount might be even further increased by wearable robotic devices which can be used in an unsupervised manner, e.g. in the patient's home (Ates et al., 2016; Ates et al., 2015).

Reaching toward an object is accomplished by a combination of shoulder and elbow movements, while grasping and releasing is achieved by the hand and fingers. In this long chain of
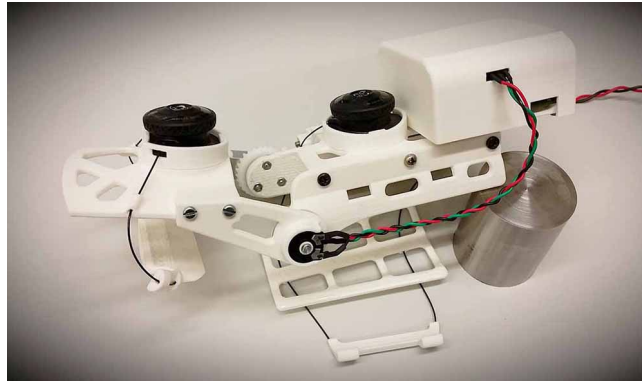
Figure 2.1: The *eWrist* - a proposed solution for a wearable powered exoskeleton for the wrist.

joints, it is easily overlooked that the wrist is essential for stabilizing the hand during all types of manipulation actions.

Even though wrist function is important in daily life activities, the recovery process in post stroke patients related to this joint is still not well understood. It has been shown that many stroke survivors experienced reasonable motor recovery of their proximal upper limb (shoulder and elbow), but limited recovery of the distal muscles e.g. the wrist (Chae et al., 2003; Chae et al., 2002).

In recent years, a myriad of passive and active wearable devices have been developed for hand/finger rehabilitation (Heo et al., 2012; Maciejasz et al., 2014), while relatively few have focused on the wrist (Al-Fahaam et al., 2016; Ates et al., 2016; Ates et al., 2015; Loureiro et al., 2005; Sasaki et al., 2005) and none have combined sEMG control with partial mechanical support to serve as a training device. Here we will use the wrist as a model joint to investigate whether rehabilitation training can be provided via a wearable "lazy" robotic device that measures sEMG activity of the wrist extensors as a proxy of a person's corticomotor driving signals, and implement a controller that further enhances these signals so that sufficient force is generated to perform daily life actions. A first step to answer this research question is to develop a prototype of the "*eWrist*" device (see Fig. 2.1).

Measuring residual sEMG is easily implementable for the upper limb and here we will use the Myo armband, a commercially available myoelectric measurement device which has been employed for similar projects (Lipovskã et al., 2015; Masson et al., 2016). Thanks to its ease of use and quick turnaround time (no wiring and no ponderous electrode placement required), the Myo armband stands out as an adequate solution for our application.

Previous studies have revealed that during volitional activation of wrist flexors and extensors, stroke patients exhibit extended periods of low amplitude sEMG indicating deficient muscle activity (Fitts et al., 1989). The lack of quantitative measurements to track the gradual changes during post stroke wrist training is a possible reason for the relatively poor understanding of this joint's rehabilitation process. The *eWrist* device might reveal important longitudinal data

to fill this knowledge gap.

Moreover, these data will provide initial insight into a core question for developing the *eWrist*, i.e. what is the optimal support strategy to enhance the rehabilitation process? We believe that the answer to this question is hidden in the concept of the so-called "lazy robot", which suggests that the assistance provided should strike a balance between active and passive support (Hu et al., 2009b; Marini et al., 2017).

This paper presents our first prototype of the *eWrist*, which will provide a framework for forthcoming experiments. The prototype was designed to fulfil the following requirements:

- can be used independently, e.g. at home

- monitors patient progress

- adaptability and versatility across users

- it must be safe, comfortable, easy to use, and affordable.

2.3 Design review and requirements

As an ultimate goal and to facilitate frequent use, a completely integrated and compact design including actuation, sensors, processing units and battery was desired (see Fig. 2.8). With this in mind, the weight and size of the different elements composing the device was prioritized during the development process.

2.3.1 Transmission type

Most active wearable exoskeletons for the wrist, hand and fingers fall within three general transmission types: pneumatic, cable-driven and linear actuator (DC motors). Pneumatic systems have been implemented in several projects (Al-Fahaam et al., 2016; Kline et al., 2005; Sasaki et al., 2005) and allow low weight at the distal extremity because the powered unit is carried on more proximal body parts. Major advantages of pneumatic exoskeletons include compliance to the human body and the soft mechanical support they offer. However, controlling the output force remains difficult and these systems require several components such as a pump, reservoir, regulator and valves which increase weight, size and cost.

Cable-driven systems benefit from the same aspects as pneumatic techniques while requiring less additional components. They can easily be interfaced with DC motors and offer a low physical profile when implemented in an orthosis (Ates et al., 2015; Mauricio Ochoa et al., 2009; Wege et al., 2007). Nevertheless, backlash and transmission losses render the control of such devices difficult.

Linear actuators have been mainly implemented in finger-based exoskeletons (Arata et al.,

2013; Ho et al., 2011; Iqbal et al., 2011) in order to precisely adjust position and velocity. When directly linked to the impaired limb, weight and backdrivability must be given special consideration. Nonetheless, linear actuators, and in a more general manner, electric motors placed distally offer high controllability and are simple to implement.
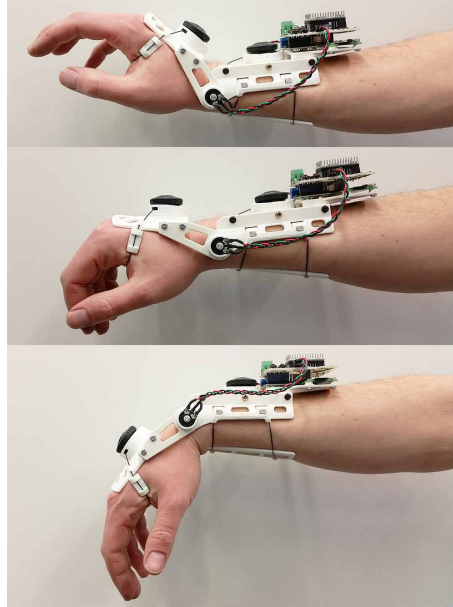
Figure 2.2: Natural (middle) and extreme (top and bottom) positions reached by the exoskeleton on a healthy subject. From top to bottom: Extension, Rest and Flexion.

2.3.2 Actuation output torque, velocity and range of motion

An output torque up to 3 Nm and a maximum range of motion of 140° (70° in flexion and extension) were chosen as design criteria based on previous work (see Fig. 2.2) (Rose et al., 2015; van Andel et al., 2008). Moreover, an angular velocity up to 180 deg/s (3.14 rad/s) was considered acceptable in a rehabilitation context.

2.3.3 Force measurement

With DC actuation, a simple way to estimate force (torque) is to measure the motor's current draw, since torque varies proportionally to current. However, when backdrivability is not ensured, force measurement with this method can only be achieved in the forward direction (i.e from motor to limb) but not in the reverse direction (i.e from limb to motor). A common method is to implement force/torque sensors in series with the kinematics (Mauricio Ochoa et al., 2009; Nef et al., 2006) which is the chosen approach for the current design. Those sensors are composed of several load cells, each of which measures the force in a different direction. Load cells can be manufactured in various shapes, for different loads and exhibit high linearity relative to the force.

2.3.4   sEMG measurements

Intention detection methods such as near-infrared spectroscopy (NIRS), electroencephalography (EEG) or electrooculography (EOG) are all valid approaches but difficult to implement in a wearable device (Canning et al., 2013; Wang et al., 2014). On the other hand, sEMG-based intention detection is the gold standard in portable devices (Ding et al., 2008; Ho et al., 2011; Lipovská et al., 2015; Masson et al., 2016; Mulas et al., 2005; Wege et al., 2007). Moreover, the Myo armband from Thalmic Labs has already been implemented in a rehabilitation context (Lipovská et al., 2015; Masson et al., 2016). Compared to other sEMG systems, the Myo armband is very easy to don and is user-friendly (Georgi et al., 2015).

2.3.5   Anatomical positioning

Two main approaches can be considered when designing an exoskeleton around a natural joint rotation: either the exoskeleton adapts to the natural joint (Al-Fahaam et al., 2016; Loureiro et al., 2005; Sasaki et al., 2005) or it imposes a mechanical axis that matches the biological joint. In the first case, the device is very compliant to the limbs but precise position control is difficult to implement. While in the second case, accurate placement of the exoskeleton is required to superimpose the anatomical joint with the mechanical axis, but rigorous position and force control can be more easily obtained. Therefore, we imposed a one degree-of-freedom axis which has the drawback of preventing radial and ulnar deviation of the wrist.

2.3.6   Exoskeleton weight, size and ergonomics

In order for our design to be wearable by a wide stroke population and in accordance with a previous study (Nycz et al., 2016), an ideal benchmark weight for the exoskeleton alone (without battery and Myo armband) is 250 g.

Moreover, when attached on the forearm, the device should not impede pronation and supination of the limb. Therefore, a short fixation structure is preferred in order to allow these movements and to leave space for the Myo armband. Considering the hand fixation, the palm should remain as free as possible ensuring that the hand can interact with the environment (Al-Fahaam et al., 2016; Nycz et al., 2016).

Finally, an important aspect to consider for daily utilization, is the set-up time and the ease to don and doff. Generally, straps and velcro are used to fix the orthosis to the limb. These methods have proved to be suitable in a clinical environment where the assistance of a third party may be requested. However, for home-therapy a novel technique must be employed to ensure the task can be performed with one hand.

2.4 Design and construction

Based on our criteria, a powered and wearable wrist exoskeleton was designed and constructed. Also, for the sake of simplicity, our entire setup is made from commercially available components which are low-cost and widely available.
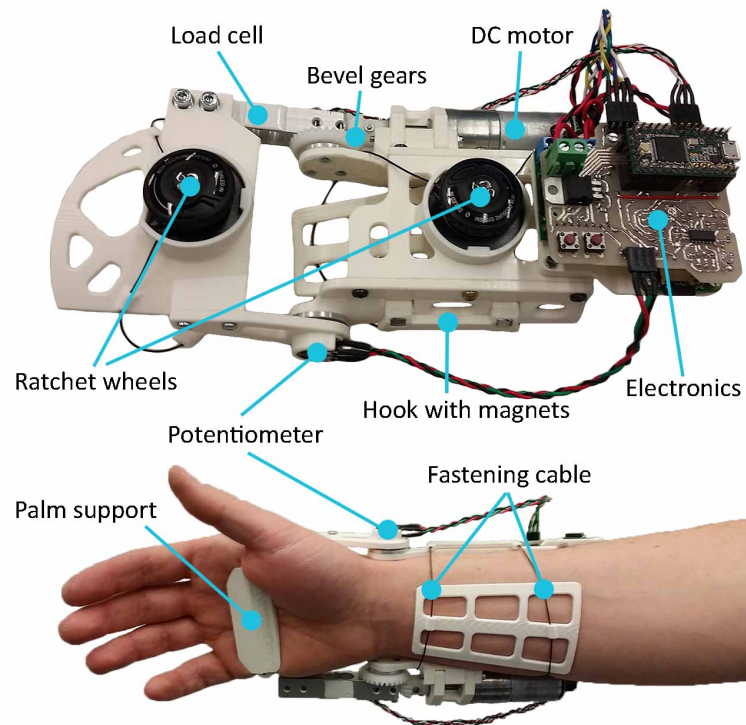
Figure 2.3: The exoskeleton prototype including the Boa Closure System.

2.4.1 Structure and fixation

Most of the parts of the exoskeleton are 3D printed in PLA[1], which is lightweight, allows for a small physical profile and high versatility to adapt to different users.

As depicted in Fig. 2.3, the exoskeleton is attached to the forearm and hand. A user-friendly fixation system allows for quick and easy placement, where the device is simply laid down on the forearm, locked and then tightened. With this approach, each fixation step can be achieved with only one hand. To don the device, the arm and hand are positioned inside the exoskeleton and two hooks with magnetic guidance lock the tightening system in place. The tightening system, i.e. the Boa Closure System[2] which is widely used in snowboard boots, is composed of a ratchet wheel around which a cable is wound. Two separate Boa Closure Systems are used: one for the forearm and one for the hand (see Fig. 2.3).

---

[1]Polylactic Acid is a biodegradable and bioactive thermoplastic aliphatic polyester derived from renewable resources.

[2]http://www.boatechnology.com/

When each wheel is turned, the cable is tightened and secures the exoskeleton around the forearm and hand. To release cable tension, the wheel is pulled. This system is lightweight and permits adjustment of the clamping force in a very intuitive way. Currently the battery is attached to the forearm with a strap that is not convenient to place with one hand, however, alternative solutions that meet the design criteria will be considered in the future.

2.4.2 Actuation

A 12V geared DC motor with a reduction ratio of 99:1 drives a bevel gear (see Fig. 2.3). The motor is placed along the forearm which minimizes impediment. Mechanical backdrivability is not ensured because of the high reduction ratio, nevertheless, transparency is rendered through active control. The bevel gears are made of POM[3], a light and strong polymer with a low friction coefficient. The ratio between bevel gears is 2:1. Moreover, the backlash between the gears can be reduced by slightly adjusting their position thanks to oblong fixations on the motor.

The motor driver is based on a VNH5019A chip which features up to 24 V operating voltage, a 3 V-compatible input command and a continuous output current of 12 A.

A two-channel Hall effect sensor is integrated within the motor and provides 48 counts per shaft revolution (Table 2.1). With a reduction ratio of 198:1 (99*2) between the motor shaft and the wrist angle, it gives 9504 counts per revolution which offers a resolution at the wrist of 0.038 edg/count.

Table 2.1: DC motor characteristics

Characteristics	Values
Weight [g]	130
Length[1] [mm]	66
Diameter [mm]	25
Rated voltage [V]	12
Stall current[2] [A]	5.6
No-load speed[2,3] [rpm]	100
Stall torque[2,3] [Nm]	2.1
Gear reduction ratio	99:1
Encoder resolution [cnt/rot]	48

[1] with encoder
[2] @ rated voltage
[3] @ gearhead output

---

[3]Polyoxymethylene

2.4.3 Sensing

Joint velocity is computed from the encoder on the motor shaft and absolute position of the wrist is given by a potentiometer placed on the rotational axis (see Fig. 2.3).

The joint torque is measured with a load cell mounted between the bevel gear and the hand fixation (see Fig. 2.3). The load cell can sustain a maximum force of 50N and must be calibrated. The cell is composed of four strain gauges mounted in a full Wheatstone bridge configuration for temperature compensation and high linearity. The output of the Wheatstone bridge is amplified by a rail-to-rail operational amplifier which provides an analog signal ranging from 0 to 3.3 V. The signal is then converted with a 12 bit ADC[4] which results in an accuracy of 0.012 N.

Myo armband

The Myo armband is a commercially available device from Thalmic Labs consisting of eight dry surface electromyography (sEMG) sensors, a nine-axis inertial measurement unit (IMU) and haptic feedback via vibrating motors. It has a sampling frequency of 200 Hz for raw sEMG data and communicates via Bluetooth Low Energy (BLE) making it easy to connect to other devices wirelessly.

The Myo armband was chosen for its ease of use compared to conventional sEMG data acquisition devices. It can be easily donned and doffed, and adjusted to any forearm size thanks to its expandable flex (see Fig. 2.4). Although not exploited in this project, the armband features a built-in classifier which recognizes 5 pre-set gestures out of the box.
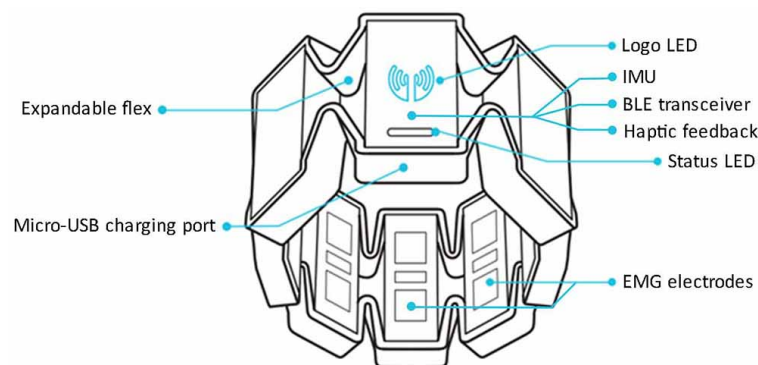
Figure 2.4: The Myo gesture control armband from Thalmic Labs. Figure adapted from https://developer.thalmic.com.

---

[4]Analog to Digital Converter

2.4.4 Electronics

Real-time control is performed by a Teensy 3.2[5] microcontroller. It collects the force data from the load cell, the absolute angle of the wrist from the potentiometer and also the angular velocity from the Hall sensor. It also runs the motor control loop and sends inputs to the motor driver.
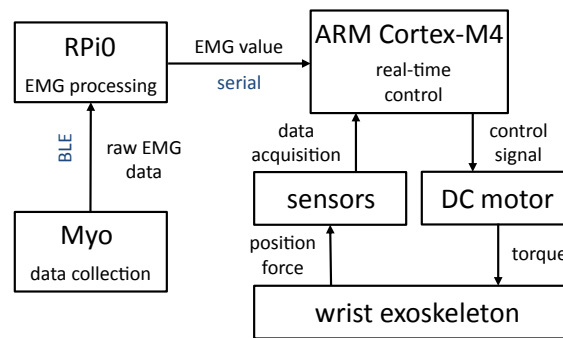
Figure 2.5: Block diagram showing system architecture. Firstly sEMG data are collected by the Myo armband, then processed by the RPi0, and finally computed by the Teensy 3.2 according to the measured force and position of the wrist.

A Raspberry Pi Zero[6] (RPi0) wirelessly collects raw sEMG data from the eight Myo armband electrodes. Low-pass filtering is performed on raw sEMG data which consists of a moving window average of 20 data samples. Then the difference between the electrode measuring the highest sEMG signal when performing extension of the wrist and the electrode measuring the highest sEMG signal when performing flexion is computed. This value is sent to the Teensy microcontroller as input for the controller (see Fig. 2.5). Finally, a custom PCB was created to connect the different elements composing the electronics design (see Fig. 2.6).

Motor and electronics are powered from an 11.1 V, 1100 mAh lithium-ion polymer battery. Under heavy use (maximum motor output torque (2.8 Nm) with a 50% duty cycle), the average current draw of our prototype was 2'850 mA, allowing for a battery life of about 0.35 hour.

2.4.5 Control

Real-time control is based on an admittance control with an inner velocity control loop. An admittance controller receives a force input and outputs motion in response. An inner motion control loop realised with a PD-controller is required to induce the desired motion at the end-effector (see Fig. 2.7). Virtual mass M_{virt} and virtual damping B_{virt} can be adjusted to modify the apparent behaviour of the exoskeleton.

---

[5]The Teensy is a USB-based development system implementation of the MK20DX256 32 bit ARM Cortex-M4 72 MHz. It features 256 kbytes of Flash Memory, 64 kbytes of RAM, 3.3V logic voltage but is 5V tolerant and has many I/O pins. Also, it is Arduino-compatible

[6]The RPi Zero is a microcomputer running a Linux OS and which features a 1 GHz Single-core CPU, 512 MB RAM and many GPIO ports.
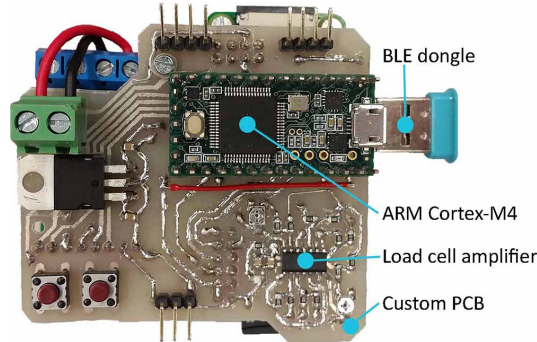
Figure 2.6: The Teensy microcontroller mounted on a custom board. The custom board includes a voltage regulator, the load cell amplifier, buttons to reset and shut down the RPi Zero and pins to connect the potentiometer, the Hall sensor and the load cell. Beneath are the Raspberry Pi Zero and the motor driver. The BLE dongle to communicate with the Myo armband is plugged into the RPi Zero USB port.

sEMG values from the Myo armband are relative measurements without unit, ranging from 0 (no muscle activity) to 2048 (highest measurable muscle activity). Therefore, these values are multiplied and down-scaled by a gain $k_{EMG} = 0.04$ in order to be introduced into the controller. Moreover, by adjusting k_{EMG}, one can control the amount of assistance the device provides when performing extension and flexion movements.
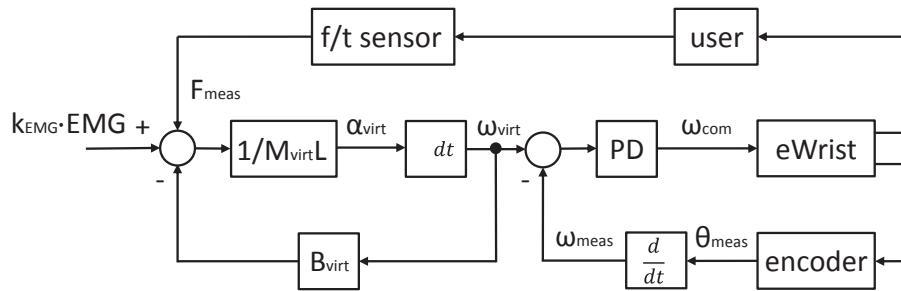
Figure 2.7: Block diagram of the admittance control with inner velocity control loop and sEMG input. The controller loop runs at 1 kHz.

2.5 Testing and characterization

The final design meets the definition of a wearable device since all actuation, control and energy storage are positioned on the arm. It was tested and characterized to determine if the initial requirements are fulfilled. Table 2.2 summarizes the different characteristics of the whole system.

Table 2.2: System characteristics

Characteristics	Target	Measured
Exoskeleton weight [g]	250	340
Battery weight [g]	-	80
Myo armband weight [g]	-	85
Exoskeleton size [mm]	-	225 x 110 x 85
Myo armband size [mm]	-	82 $\varnothing$ x 48
Battery size [mm]	-	73 x 35 x 22
Output max. torque [Nm]	3	2.8
Output max. angular velocity [deg/s]	180	270
Max. range of motion [deg]	140	154
Set-up time [s]	60	37.3
Battery capacity [Wh]	-	11.1

2.5.1 Weight and dimension

For now, our prototype does not meet our expectations, especially regarding weight (340 g without Myo armband and battery). The chosen DC motor is too heavy (130 g) and could be replaced by a smaller and lighter motor. However, smaller motors require larger gearboxes and a compromise must be found. The integration of a DC brushless motor is a valid possibility to reduce weight since they have a higher power density than DC brushed motors. As the motor makes up a significant part of the overall weight, it will be the first target before considering other weight reductions.

The current dimensions (length) leaves enough space (~ 2 cm) between the exoskeleton and the Myo armband for a rather tall male user (1.83 m) but must be reconsidered for persons with small arm lengths. Moreover, the fixation method permits free pronation movement but supination is impeded after about 45° from the neutral forearm position. To achieve supination angles greater than 45°, the radius must rotate around the ulna. However, the current exoskeleton design fixes the relative position of the radius and ulna.
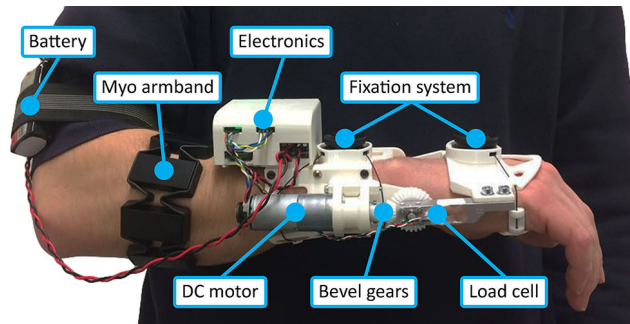
Figure 2.8: Healthy user wearing the *eWrist*. Shown are the wrist exoskeleton, the Myo armband and the battery.

24

2.5.2 Output torque, velocity and range of motion

The maximal output torque was measured with the load cell of the exoskeleton. The controller was programmed to output a motion opposite to the applied force while a precise application point of the resistive force was set to compute torque. The exoskeleton was kept fixed and the current gently increased. At some point, the structure deformed and the gears jumped. At that moment, the force was noted. A reinforcement of the structure around the motor and gears needs to be considered to increase the maximum acceptable torque. Also, the POM gears showed signs of weakness and may not be able to sustain higher torque.

The maximal angular velocity was recorded when the device was programmed to render transparency, i.e. low virtual mass (M_{virt}=0.1 kg) and low virtual damping (B_{virt}=0.1 Ns/rad). It was able to follow extension and flexion movements with an angular velocity up to 270 deg/s which is beyond our needs.

Finally, the range of motion was limited by the implemented potentiometer, however, the range is sufficient.

2.5.3 Fixation and set-up time

Five healthy subjects were asked to put on the exoskeleton, the Myo armband and the battery in order to measure the set-up time. Prior to the experiment, they were instructed on how to proceed. They were sitting at a table on which all the components were present. The time from when they first touched one of the components until they considered the elements to be attached and they were able to perform wrist movements was recorded. Table 2.3 shows the results.

Table 2.3: Set-up time of the *eWrist*, the Myo armband and the battery for five healthy subjects (4 females, mean age: 29±2.6, ranging: [27, 34] years).

Subject	Time [s]
1	30.6
2	41.3
3	35.5
4	43.4
5	35.8
Average	**37.3**

Note that about one third of the time was devoted to battery attachment.

2.5.4 Controller testing

In order to demonstrate the effect of sEMG assistance, two experiments consisting of executing vertical wrist movements (i.e. with or against gravity) with the exoskeleton were performed on a single healthy subject. Both experiments required repetitive extension and flexion movements while the virtual mass of the controller (see Fig. 2.7) was set to M_{virt}=15 kg and the virtual damping to B_{virt}=1 Ns/rad. In both experiments, the exoskeleton was actively driven by the motor. The difference between the experiments was that no sEMG assistance was provided in Exp. 1 (non-assisted condition) while in Exp. 2 (assisted condition), assistance controlled via the sEMG signal was added as depicted in Fig. 2.7. As mentioned above, the sEMG values represent the difference between the most activated channel (of the Myo armband) when performing an extension of the wrist and the most activated one when performing a flexion. Thus, a positive sEMG value corresponds to extensors activation while a negative value to flexors activation. The overall mean angular displacement in Exp. 1 was 77.9° (1.36 rad) and 87.6° (1.53 rad) in Exp. 2.

Fig. 2.9 shows the angular velocity (positive velocity corresponds to wrist extension) and the sEMG values over time when the exoskeleton was moved without sEMG assistance (Exp. 1, upper plot) or with sEMG controlled assistance (Exp. 2, lower plot). It can be seen that assistance results in a slight phase shift (mean phase shift of four observations on lower plot: 100.25 ms) between the sEMG signal (blue) and the angular velocity (red) so that the sEMG envelope leads the velocity modulation indicating that sEMG activation drives the assistive support of the user.

Fig. 2.10 shows the sEMG-velocity relationship for both experiments. It can be seen that smaller sEMG activity results in substantially larger velocities when assisted movements (red, Exp. 2) are compared to non-assisted movements (blue, Exp. 1). Note that the virtual mass M_{virt} and the virtual damping B_{virt} are high and necessitate an extensive effort in the non-assisted condition.

2.6 Discussion and conclusions

The current chapter presented the design of a wearable exoskeleton with sEMG-based force control for the wrist. No such wearable sEMG controlled assistive device is currently available for the wrist, despite its importance in ADL. The integration of sEMG signals in the admittance control demonstrates that it is possible to adjust assistance with respect to a proxy measurement of corticomotor drive.

The adopted actuation and transmission types allowed us to quickly design a workable prototype that fits most of our requirements and which could be easily adapted to different users. The fixation design still needs improvement, especially regarding comfort, but the offered possibility of adjusting the tension of the attachment is a real benefit for the user. Moreover, the set-up time (37.3 seconds) with healthy young participants is reasonable even though the
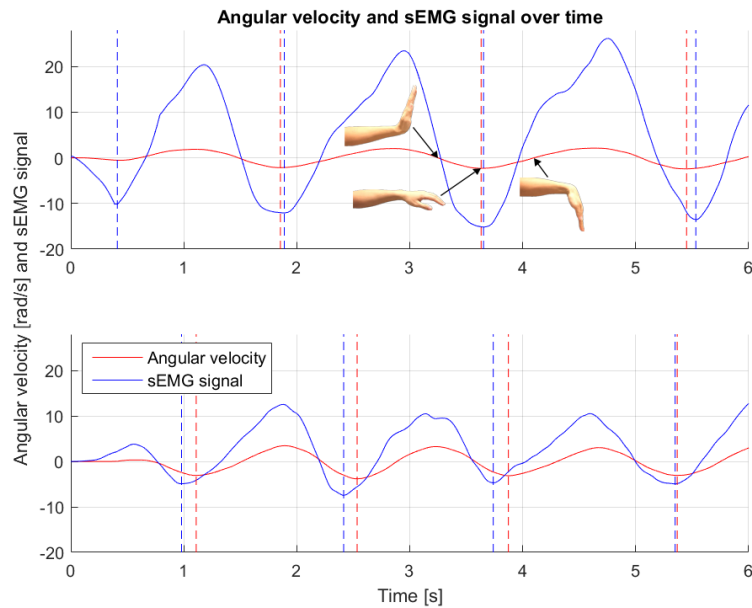
Figure 2.9: Time plots of angular velocity and sEMG signal where admittance control is used. Upper plot corresponds to non-assisted condition and lower plot to assisted condition. Figures show the wrist position during repetitive extension and flexion movements. 6'000 data samples were recorded over 6 s. Both variables were offline filtered with a moving window average of 400 data samples.

battery fixation needs improvements so that neurologically impaired patients could easily don the device. Further investigations will address how the mechanical axis of the exoskeleton can be more accurately and quickly aligned to the joint axis, thus reducing donning time.

Our measurements and analyses on healthy subjects showed the usability of the device, nevertheless, improvements regarding the weight are necessary. The extra weight on the right side of the exoskeleton caused by motor, gears and load cell (see Fig. 2.3) creates a torque around the forearm that tends to supinate the limb. This issue might be even more critical in stroke patients whose paretic arm is weak.

The Myo armband used to measure sEMG signals is a first solution, however, dry electrodes could also be directly integrated into the fixation structure of the exoskeleton, thereby reducing the number of components. It is worth noting that the quality of the sEMG signal obtained from the Myo armband has not yet been compared to a research grade sEMG system. Further, while the Myo armband sampling rate of 200 Hz is relatively low, it appears sufficient for the current use case. The battery lifetime during normal use has not been tested yet even though our measurements demonstrated that usage time is sufficient for a short exercise session even during heavy load.

Our current sEMG-based controller is a first step towards an *assist-as-needed* support strategy which can adapt to the user's impairment and voluntary control. Such strategies might lead
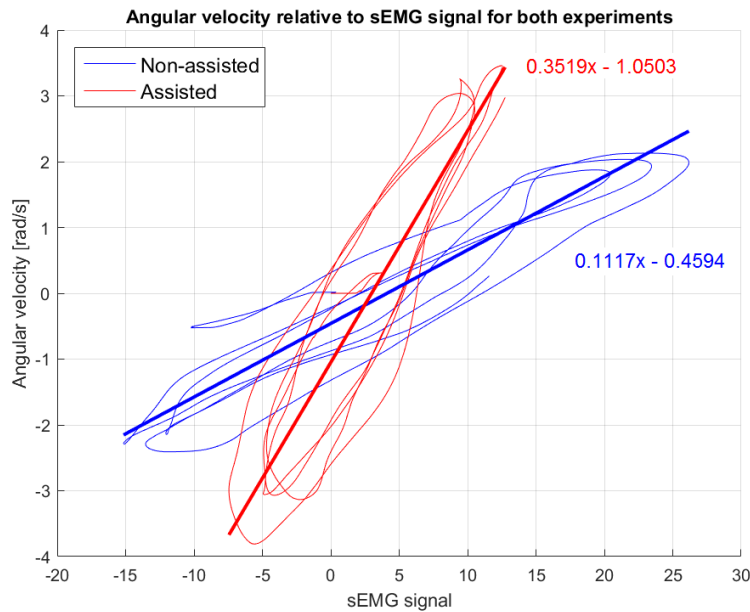
Figure 2.10: Angular velocity relative to sEMG signal for experiments 1 and 2 where admittance control is used. A linear regression was performed on both data sets.

to reduction of upper extremity spasticity and might support recovery because they enable patients to perform high repetitions of functional movements (Kwakkel et al., 2007; Prange et al., 2006).

Future work will focus on the integration of an IMU on the exoskeleton to compensate for gravity when it is worn. Moreover, abnormal sEMG patterns such as co-contraction are an important consideration for future controller development. The actual prototype must be adapted for different forearm/hand sizes as well as for the left arm. Furthermore, online monitoring of the user and an interface with the physiotherapist will be implemented.

3 Characterization and wearability evaluation of a fully portable wrist exoskeleton for unsupervised training after stroke

Charles Lambelet, Damir Temiraliuly, Marc Siegenthaler, Marc Wirth, Daniel Woolley, Olivier Lambercy, Roger Gassert, and Nicole Wenderoth

---

Chapter 3. Characterization and wearability evaluation of a fully portable wrist exoskeleton for unsupervised training after stroke

3.1 Abstract

Chronic hand and wrist impairment are frequently present following stroke and severely limit independence in everyday life. The wrist orientates and stabilizes the hand before and during grasping, and is therefore of critical importance in activities of daily living (ADL). To improve rehabilitation outcomes, classical therapy could be supplemented by novel therapies that can be applied in unsupervised settings. This would enable more distributed practice and could potentially increase overall training dose. Robotic technology offers new possibilities to address this challenge, but it is critical that devices for independent training are easy and appealing to use. Here, we present the development, characterization and wearability evaluation of a fully portable exoskeleton for active wrist extension/flexion support in stroke rehabilitation.

First we defined the requirements, and based on these, constructed the exoskeleton. We then characterized the device with standardized haptic and human-robot interaction metrics. The exoskeleton is composed of two modules placed on the forearm/hand and the upper arm. These modules weigh 238 g and 224 g, respectively. The forearm module actively supports wrist extension and flexion with a torque up to 3.7 Nm and an angular velocity up to 530 deg/s over a range of 154°. The upper arm module includes the control electronics and battery, which can power the device for about 125 min in normal use. Special emphasis was put on independent donning and doffing of the device, which was tested via a wearability evaluation in 15 healthy participants and 2 stroke survivors using both qualitative and quantitative methods.

All participants were able to independently don and doff the device after only 4 practice trials. For healthy participants the donning and doffing process took 61±15 s and 24±6 s, respectively. The two stroke survivors donned and doffed the exoskeleton in 54 s/22 s and 113 s/32 s, respectively. Usability questionnaires revealed that despite minor difficulties, all participants were positive regarding the device.

This study describes an actuated wrist exoskeleton which weighs less than 500 g, and which is easy and fast to don and doff with one hand. Our design has put special emphasis on the donning aspect of robotic devices which constitutes the first barrier a user will face in unsupervised settings. The proposed device is a first and intermediate step towards wearable rehabilitation technologies that can be used independently by the patient and in unsupervised settings.

3.2 Introduction

Stroke affects approximately 795'000 people each year in the US alone and is one of the leading causes of long-term adult disability and dependency (Benjamin et al., 2018). Traditional stroke rehabilitation options for outpatients include therapist-based treatments with hands-on physical and occupational therapy in rehabilitation centres. The treatment lasts several weeks and is composed of periodic blocked practice, but overall training time remains low

compared to the time the patient is inactive at home (Bernhardt et al., 2004; Lang et al., 2009). Moreover, stroke patients are discharged at an increasingly early stage (Hall et al., 2012; Ramirez et al., 2016) requiring new approaches for rehabilitation training in unsupervised settings. These novel approaches must be effective (Brewer et al., 2007; Pignolo, 2009), and empower patients to self-initiate rehabilitation training that will enable more distributed sessions. This is particularly important since, in the future, more rehabilitation resources will be moved to community settings and patient homes to complement conventional therapy (Chen et al., 2017; Johnson et al., 2007; Singh et al., 2019; Sivan et al., 2014).

Upper extremity hemiparesis is a common weakness following stroke and heavily impairs ADL (Ashford et al., 2008). Adequate wrist function is critical for orientating and stabilising the hand (Palmer et al., 1985), but the recovery process of this specific joint is still not well understood in stroke survivors (Veerbeek et al., 2017). It has been shown that the probability of recovering distal functions (e.g. the wrist) are closely linked with the acute state of proximal functions (shoulder or elbow) (Houwink et al., 2013). In the same vein, distal training can lead to positive effects at the shoulder and elbow (Hsieh et al., 2018; Lambercy et al., 2011; Qiuyang et al., 2019). While the hand has received a lot of attention from the research community, there remains a need to provide wrist function training.

Robot-assisted therapy for stroke patients is a promising approach (Bos et al., 2016; Maciejasz et al., 2014) and proven advantages include: 1) increasing dose and intensity of training (Kwakkel et al., 2008; Norouzi-Gheidari et al., 2012; Ward et al., 2019), 2) allowing quantitative measurements to assess performance and recovery of the patient more precisely than conventional rehabilitation training (Zollo et al., 2011), and 3) engaging the patient in a motivating and stimulating environment (Colombo et al., 2007; Maclean et al., 2002). However, a robot-mediated therapy administered in unsupervised settings implies several technical, clinical and social challenges: first of all, the technology must be safe to be deployed in such a context, its footprint acceptable to the patient, relatives and caregivers, and it should adhere to conventional therapy principles to administer appropriate treatment to the user. Moreover, the device must be adaptable to the individual and designed such that patients can use it independently and in various environmental settings (Kozlowski et al., 2015; Pezent et al., 2017; Tefertiller et al., 2017).

A myriad of devices have targeted training of the whole arm, and also more specifically the hand and fingers (Bos et al., 2016; Maciejasz et al., 2014; Stewart et al., 2017), while relatively few wearable exoskeletons have focused on the wrist (Al-Fahaam et al., 2016; Ates et al., 2016; Bae et al., 2012; Khokhar et al., 2010; Sangha et al., 2016). Unlike stationary rehabilitation devices (Gupta et al., 2008; Martinez et al., 2013; Perry et al., 2016), a fully wearable exoskeleton offers the possibility to use (i.e. to train) the paretic limb during functional everyday tasks (Brewer et al., 2007; Bützer et al., 2019; Gasser et al., 2017) where higher training dose could more conveniently be achieved. Exoskeletons interact at the level of individual joints and enable joint specific kinematic assessments (Patel et al., 2010; Rose et al., 2018). Moreover, it has been shown that training isolated individual joint movements facilitates learning complex

multi-joint movements (Klein et al., 2012; Penalver-Andres et al., 2019). Practically, this means that through the *"part-whole transfer paradigm"* simple low degree of freedom (DoF) robotic devices could facilitate the training of more complex movements. In an unsupervised training context, simplicity is paramount (Micera et al., 2005), therefore, simple wearable technologies might provide an interesting add-on to a conventional therapy where complex movements are trained.

We have previously presented a first prototype version of the *eWrist* (Lambelet et al., 2017). Here we present further developments which focussed on improving portability, independence of use and adaptability in view of unsupervised use of the system. The *eWrist* is a fully wearable single DoF sEMG-based force controlled wrist exoskeleton that actively supports extension and flexion. We put special emphasis on the attachment mechanisms that facilitate the donning and doffing of the device so that a hemiparetic patient could mount the device independently with a single hand. Among the vast amount of published work on rehabilitation devices for in-home therapy, few have addressed the fixation issue, which constitutes the first barrier a user would have to overcome in order to use the device independently (Hasegawa et al., 2015; Miranda et al., 2015). Currently the *eWrist* is intended to be used as a training device rather than as an assistive exoskeleton during ADL. However, our long term design goal is to fuse training and assistance with the aim of increasing movement of the affected arm in daily life via technology that modulates assistance in order to improve upper arm function. This requires an exoskeleton that is fully wearable, easy to use, and especially simple to don and doff. The *eWrist* is our first wearable prototype that is capable of assisting wrist flexion and extension, the latter being particularly relevant for post stroke recovery (Squeri et al., 2013).

Here we briefly describe the previous *eWrist* version, we then outline requirements for a fully wearable wrist exoskeleton and present an advanced *eWrist* device where we focussed on wearability improvements. We first characterize the current implementation based on standardized haptic and human-robot interaction metrics for rehabilitation devices. Secondly, we present the results of a wearability study which evaluates the donning/doffing procedure in healthy and stroke participants. Finally, limitations of the current work and potential future use of the *eWrist* are discussed.

3.3   Methods

3.3.1   Previous version of the eWrist

We previously introduced the *eWrist* (Lambelet et al., 2017), an exoskeleton actuated by a DC motor via bevel gears that actively supports wrist extension/flexion movements, measures force exerted on the handle, absolute angular position and velocity at the wrist axis via a Hall sensor integrated on the motor shaft. This prototype had several shortcomings, the major one being the overall weight of the exoskeleton (505 g total weight, of which 340 g was located on the forearm and hand). The current version of the *eWrist* includes the following improvements: (i)

lowering the weight of the forearm module and reducing its physical profile by implementing a lighter and smaller motor, and by moving as many components as possible to more proximal areas, (ii) increasing the durability of the *eWrist* by implementing metal gears and an absolute angular Hall encoder, (iii) integrating an improved electronic design to simplify debugging and interaction with the device, and (iv) facilitating the overall donning/doffing via a completely redesigned mechanism for the upper arm module.

3.3.2 Design requirements

Our aims were to reduce the distal weight of the *eWrist* and most importantly to develop user-friendly mechanisms that allow one-handed donning and doffing of the whole exoskeleton. In the following sections we establish the requirements.

Transmission type

Three general transmission types are commonly seen in wearable exoskeletons, namely: pneumatic, cable-driven and linear actuators (DC motors) (Gopura et al., 2016). Pneumatic systems are compliant and adapt their shape to the human body but accurate control is difficult to implement because of non-linearities. Moreover, several components such as pump, reservoir, regulator and valves are inherent to these systems which make the integration into fully wearable solutions tedious (Al-Fahaam et al., 2016; Koeneman et al., 2004; Morales et al., 2011). Cable-driven systems offer high compliance and low physical profile at the distal extremity while requiring less supplementary components then pneumatics. However, backlash and transmission losses make such systems challenging to control (Borboni et al., 2016; Mauricio Ochoa et al., 2009; Nycz et al., 2016). Linear actuators and direct DC motor actuation are straightforward to implement and allow high controllability of position, speed and torque. Nevertheless, special attention to weight and backdrivability must be paid when placed distally and directly mounted to the paretic limb (Arata et al., 2013; Ho et al., 2011; Sangha et al., 2016; Webb et al., 2012).

Actuation output torque, velocity and RoM

A minimal RoM of 140° (70° in flexion and extension) and an output torque at the wrist up to 3 Nm were chosen as design criteria based on previous work (Palmer et al., 1985; Rose et al., 2015; Yoshii et al., 2015). An angular velocity up to 180 deg/s (3.14 rad/s) was considered appropriate in a rehabilitation context, and subsequently in a daily life assistive context.

Sensing

When backdrivability of a transmission mechanism is not ensured, i.e. force (torque) cannot be assessed in the reverse direction (i.e. from limb to motor) by measuring the motor's current

draw, a common solution is to implement a force/torque sensor (load cell) serially connected with the joint kinematics (Nef et al., 2006). Moreover, the absolute angular position of the wrist joint is needed and can either be achieved through initialization of motor encoders or with an additional absolute angular sensor.

Anatomical positioning

Compliant exoskeletons adapt to the biological joint and therefore do not require precise positioning (Al-Fahaam et al., 2016; Kline et al., 2005). Rigid exoskeletons on the other hand, although much easier to control, need their mechanical axes to be aligned to the anatomical joint in order to not hinder movements or cause discomfort (Sangha et al., 2016; Schiele, 2009; Webb et al., 2012).

Fixation

Attachment systems play a major role in the ergonomics and usability of wearable devices (Hasegawa et al., 2015; Miranda et al., 2015). Velcro and straps are a common, quickly implemented and therefore favoured solution to attach exoskeletons to the human body (Arata et al., 2013; Schabowsky et al., 2010). However, these fixation techniques can be highly challenging if the user has to perform them with a single hand. For that reason, novel techniques need to be implemented to ensure that the whole exoskeleton attachment can be performed with a single hand and in reasonable time (< 2 min) (Kim et al., 2018b; Meuleman et al., 2015). Furthermore, the fixation systems must fulfil certain requirements in term of attachment strength and stability, and should also remain compliant to changes in body shape during movements (Gemperle et al., 1998).

Weight, size and ergonomics

Stroke survivors are highly sensitive to mechanical loads applied on their paretic limb, and even more so when the load is located distally (Beer et al., 2007; Beer et al., 1999). Moreover, an acceptable weight for a wrist exoskeleton is subjective and essentially patient specific (Aubin et al., 2013; Gasser et al., 2015). According to a previous study (Nycz et al., 2016), an ideal upper benchmark weight for a wrist exoskeleton placed distally is 250g. This is often achieved by moving parts that are not directly required for actuation (e.g. battery, controller and others) to more proximal body parts (Bützer et al., 2019; Nycz et al., 2016; Randazzo et al., 2017).

In order to limit the creation of shear forces and pressure on the skin, a short fixation structure is preferred for the forearm part of the exoskeleton. In this way, the pronation and supination of the forearm is less hindered and ergonomics enhanced (Reimer et al., 2014; Schiele, 2009). Regarding fixation to the hand, a palm free of attachments is desired to promote hand interaction with the environment (Al-Fahaam et al., 2016; Nycz et al., 2016).

Finally, for the sake of ergonomics, the donning process and ultimately set-up time, the wearable device should be entirely located on the arm or in a position that does not hinder any movements of other joints (e.g. elbow/shoulder) or actions (e.g. sitting on a chair or lying on a bed) of the user (Gemperle et al., 1998).

3.3.3 Design implementation

Based on the requirements, the design of the *eWrist* focussed on lowering its physical profile and weight, enhancing wear comfort, and increasing usability of the fixation system for the exoskeleton, battery and electronics. To reduce weight on the distal part of the arm, the battery and electronics have been placed on the upper arm (upper arm module) while the actuated part of the exoskeleton is on the forearm and hand (forearm module) as depicted in Fig. 3.1a. Except for the motor, the motor drive, the worm drive and the Myo armband, all components are low-cost and widely available.

Structure and fixation

All structural parts of the *eWrist* are 3D printed in PLA[1] which is a rigid and lightweight polyester. Parts requiring high flexibility are 3D printed in TPU[2] which is a soft and elastic polymer allowing for more compliance around limbs and comfort on the skin. 3D printing techniques offer highly iterative design processes which facilitate the mechanical development, and allow adaptation of the *eWrist* to different user sizes.

Forearm module: The forearm module weighs 238 g and is attached to the forearm and hand (with the handle) (see Fig. 3.1b). The design imposes 1 DoF at the wrist, which actively supports flexion/extension while preventing radial and ulnar wrist deviation. It allows a mechanical RoM in extension and flexion up to 103° and 112°, respectively (i.e. 215° overall), but it has been limited to ±77° (i.e. restrained RoM = 154°) based on the average wrist RoM (Kim et al., 2014). Pronosupination of the forearm is not actively supported, but is also not hindered. The procedure to don the forearm module requires the user to (i) place the hand inside the loop formed by the palm support and position the device on the forearm and hand, (ii) pass the fastening cable around the forearm and lock the hooks, (iii) adjust the placement of the exoskeleton along the forearm by aligning the biological joint and mechanical axis, (iv) press on both ratchet wheels and adjust tension by turning them clockwise to secure the *eWrist* around the forearm and hand. To release the cable tension and ultimately remove the exoskeleton, the wheels have to be pulled.

---

[1] Polylactic acid
[2] Thermoplastic polyurethane
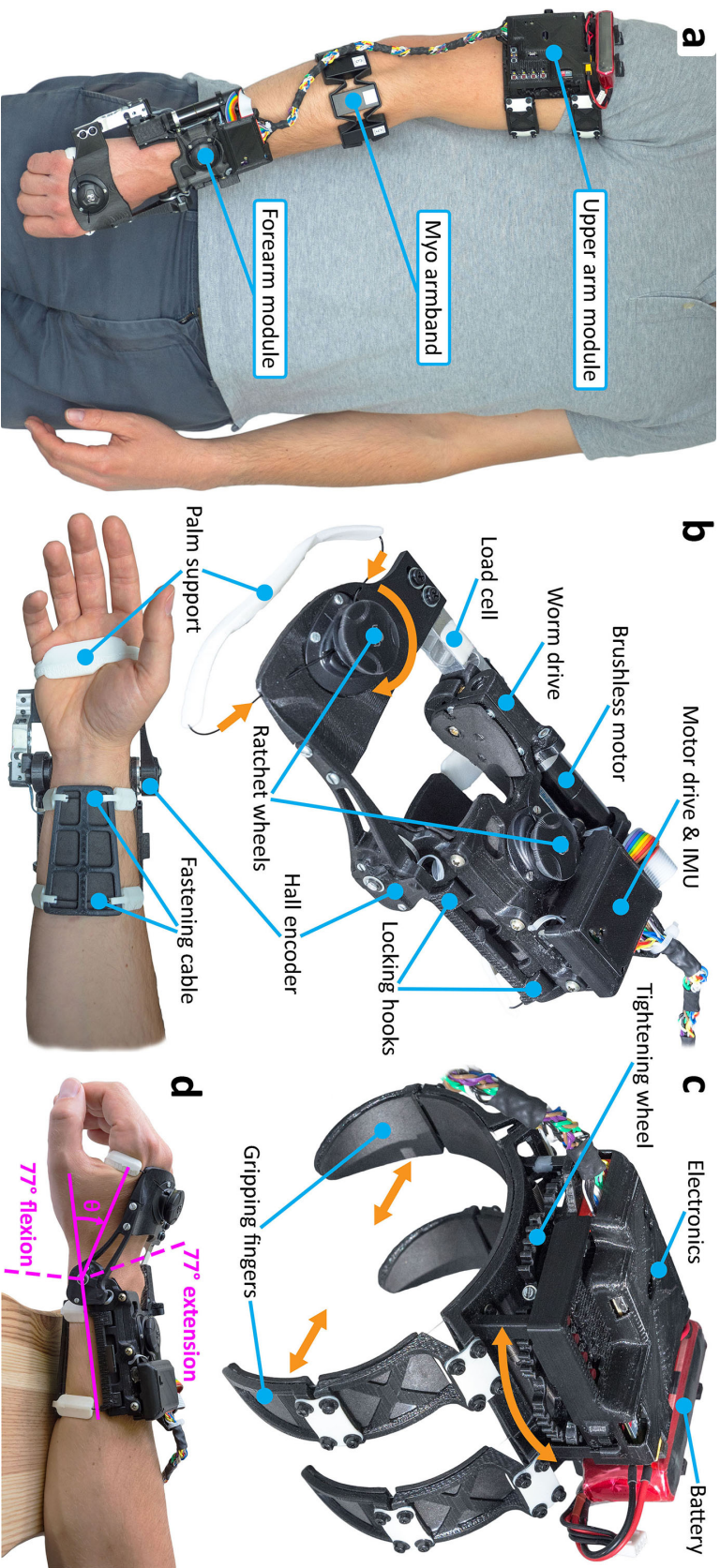
Figure 3.1: a The current version of the *eWrist* mounted on the right arm of a user. It is composed of three modules, namely, the forearm module, the upper arm module and the Myo armband. **b** The forearm module of the *eWrist* with two ratchet wheels (on the handle and on the forearm) to adjust the tightening tension. The locking hooks are equipped with two guiding magnets to ease the fixation. **c** The upper arm module of the *eWrist* and the four compliant gripping fingers that move inwards when the tightening wheel is turned. With the press of a button fixed to a ratchet (not shown on the picture) the tightening wheel unwinds and the fingers move outwards. **d** The restrained RoM from 77° in flexion to 77° in extension.

Upper arm module: The upper arm module weighs 224 g and is attached on the proximal part of the arm (see Fig. 3.1c). In order to fulfil our one-handed donning approach, a new spider-like mechanism has been developed. It consists of four gripping fingers and a tightening wheel. When the wheel is turned, wires running through the fingers wind around the wheel axis, which closes the fingers inwards as depicted by the orange arrows in Fig. 3.1c. Spring slats placed at each finger joint tend to constantly open the fingers outwards and unwind the wires around the wheel axis. A ratchet with a push button prevents the wires from automatically unwinding. To be donned, the system just needs to (i) be slightly pressed against the upper arm, (ii) held in place with the hand palm and (iii) tightened using the fingers. The gripping force can be adjusted by simply turning the wheel and therefore increasing the tension in the wires. As one side of the wires is attached to a spring, each finger can still extend outwards and thus remains compliant to changes in body shape (e.g. during biceps contraction). To release the mechanism and the tension in the wires, the ratchet needs to be disengaged by pushing a button, which will unwind the wheel.

Actuation

A DC motor (Maxon EC 16, ⌀16 mm, brushless, 30 Watt) with a reduction ratio of 19:1 drives a worm drive. The motor with incorporated gearhead weighs 63 g and is placed along the forearm which minimizes impediment (see Fig. 3.1b). Mechanical backdrivability is not ensured because of the high reduction ratio, nevertheless, partial-transparency is rendered through active control. The worm drive is composed of the worm screw (in steel) and the worm wheel (in bronze), and exhibit a low friction coefficient and a high strength. The ratio of the worm drive is 25:1 leading to a total reduction ratio between the motor and the wrist axis of 475:1 (19x25). This reduction combined with the nominal torque of the motor (7.85 mNm) gives a continuous torque output at the handle up to 3.7 Nm. Moreover, the backlash between the worm screw and worm wheel can be reduced by slightly adjusting their relative position thanks to oblong fixations on the motor support. It also acts as a fail-safe in case of a high torque applied on the wrist joint and ultimately on the worm drive. In such a case, the worm screw would simply shift up and jump gears.

Sensors and electronics

Wrist joint velocity is computed by the motor drive, which is connected to a Hall sensor integrated within the motor together with a 128 CPT (count per turn) magneto-resistive encoder (tachometer) on the motor shaft. The current drawn by the motor is monitored by the motor drive and can be used for torque estimation and power analysis. Absolute wrist position is given by a durable Hall sensor (rotational life: up to 50M cycles) placed directly on the wrist rotational axis (see Fig. 3.1b) with an angular position resolution of 0.058°. Wrist joint torque is measured with a load cell mounted between the worm drive and the handle (see Fig. 3.1b). The load cell is rated for a maximum force up to 50 N and has been calibrated with forces up to 30 N in both directions (extension and flexion) with a resolution of 0.0073 N. The

Myo armband (Thalmic Labs) is used to record sEMG signals, which can be used in parallel with the admittance controller to trigger proportional mechanical support similar to (Lipovská et al., 2015; Lyu et al., 2019). Finally, an IMU (MPU 6050) is located on the forearm module to evaluate the spatial orientation of the *eWrist*, which is required to adapt the mechanical support if the user is moving (Moubarak et al., 2010). The processing and use of sEMG signals and IMU data within the controller are not discussed in the current study, which focuses on the characterization of the *eWrist*. However, the wearability evaluation included the Myo armband together with the *eWrist*.

The electronics consists of two custom-made shields, namely, the upper arm shield and the forearm shield (see Fig. A.1 in the Appendix). The upper arm shield includes the real-time micro-controller (Teensy) and a micro-computer (Raspberry Pi Zero or RPi0). The Teensy collects: force signals, absolute wrist angle, angular velocity, current consumption, battery voltage and IMU data, and runs the motor control by sending speed (or current) commands to the motor drive. The RPi0 collects sEMG data and serves as a general purpose unit to select different control algorithms or store recorded data. The forearm shield incorporates the motor drive and the IMU. The motor drive is placed close to the motor to limit the creation of electromagnetic interference (EMI) due to high commutating currents.

Motor and electronics are powered from a 11.1 V, 1000 mAh (11.1 Wh) lithium-ion polymer battery. The complete system architecture is depicted in Fig. 3.2a.

Control

Since the *eWrist* is not backdrivable and force is measured at the wrist joint, admittance control is a logical, simple and commonly applied controller for real-time control (Kilic, 2017; Lee et al., 2017). It receives a force input and outputs a motion in response. With admittance control (Eq. 4.1), the dynamic behavior of the exoskeleton can be tuned with two parameters, namely virtual inertia M [$Nm \cdot s^2/rad$] and virtual damping B [$Nm \cdot s/rad$]. Eq. 4.1 expresses the equation of motion in the time domain and its conversion to the Laplace domain with respect to angular velocity.

$$M\ddot{\theta} + B\dot{\theta} = F \cdot L \quad \xrightarrow{\mathscr{L}(\cdot)} \quad \omega = \frac{L}{Ms + B} \cdot F \tag{3.1}$$

where $\ddot{\theta}$ and $\dot{\theta}$ are the angular acceleration and angular velocity of the wrist in the time domain, respectively, ω the angular velocity in the Laplace domain, L the distance between the mechanical axis and the average pressure point of the hand on the handle (set at 8 cm), and F the force applied on the handle.

A discretized version of the admittance controller (Eq. 3.2) is implemented in the Teensy micro-controller with the Tustin transformation, which is known to preserve stability (Vinagre

et al., 2003).

$$\dot{\theta}_{ref,n} = \frac{T_s \cdot L \cdot (F_{ref,n} + F_{ref,n-1})}{2M + BT_s} + \frac{(2M - BT_s) \cdot \dot{\theta}_{ref,n-1}}{2M + BT_s} \tag{3.2}$$

The current angular velocity $\dot{\theta}_{ref,n}$ depends on the past angular velocity $\dot{\theta}_{ref,n-1}$, and on the current and past force measurement $F_{ref,n}$ and $F_{ref,n-1}$, respectively. T_s is the sampling time interval. Both $\dot{\theta}_{ref}$ and F_{ref} are low-pass filtered in real-time with a moving average of window length N=20 (i.e. $f_{co} \approx 21.1$ Hz at f_s=1 kHz). The admittance controller depicted in Fig. 3.2b as a block diagram is the default controller of the *eWrist* used during human-robot interaction.

3.3.4 Device characterization

Different aspects of the *eWrist* affecting its final performances as a rehabilitation device have been evaluated and are presented in the following section. All aspects but impedance rendering have been assessed without the exoskeleton being mounted on a forearm. Table 3.1 gives an overview of the main characteristics of the *eWrist*.

Peak velocity and acceleration

Since the *eWrist* is not backdrivable, mechanical transparency (i.e. low interaction forces during human-*eWrist* interaction) can only be rendered through active control. To achieve optimal transparency, the handle should ideally move and accelerate as fast as a human wrist can. Therefore, peak angular velocity and acceleration of the handle were assessed by deriving offline filtered angular velocity measurements recorded at 1 kHz during a maximum current impulse of 6 A (Hayward et al., 1996). Peak velocities and accelerations were measured in both directions (extension and flexion). The angular acceleration estimate was calculated from the angular velocity via FDM (finite difference method or backward Euler method) described in Eq. 3.3.

$$\ddot{\theta}_n = \frac{\dot{\theta}_n - \dot{\theta}_{n-1}}{T_s}, \quad n = \{1,2,3,...\} \tag{3.3}$$

where $\dot{\theta}_n$ and $\dot{\theta}_{n-1}$ are the current and previous angular velocity measurements, n the control loop counter and T_s the sampling time interval of 0.001 s.

The discrete differentiation amplifies the quantization and discretization noise of the encoder reading such that $\dot{\theta}$ and $\ddot{\theta}$ were low-pass filtered offline with Butterworth filters[3].

---

[3] $\dot{\theta}$ and $\ddot{\theta}$ with a 2nd order 10 Hz and 20 Hz cut-off frequency, respectively.
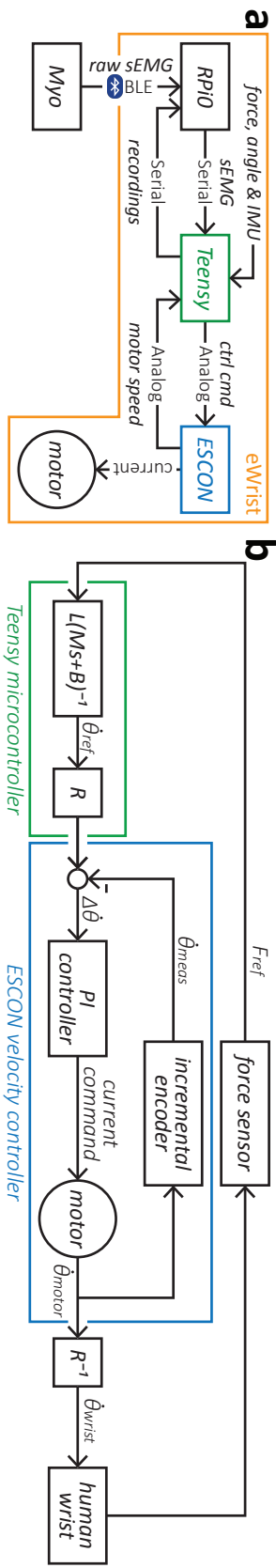
Figure 3.2: Block diagrams. **a** System architecture. **b** Admittance controller with inner velocity control loop running at 5.36 kHz on the motor drive (ESCON). The Teensy computes the reference angular velocity $\dot{\theta}_{ref}$ according to the measured force F_{ref} applied by the user on the handle and transmits it to the motor drive. The motor drive records the angular velocity $\dot{\theta}_{meas}$ of the motor shaft, combines it with the reference angular velocity $\dot{\theta}_{ref}$ reflected at the motor shaft and computes the current command for the motor thanks to an integrated PI (proportional-integral) controller. R is the reduction ratio of the gear stage (i.e. 475:1).

Table 3.1: Summary of the technical characteristics of the *eWrist*

Performance metrics	Obtained values
Forearm module weight [g]	238
Upper arm module weight [g]	224
Myo armband weight [g]	94
Total weight [g]	**556**
Forearm module dimensions[1] [mm]	$200 \times 120 \times 80^2$
Upper arm module dimensions[1] [mm]	$120 \times 160^3 \times 125^3$
Output max. torque [Nm]	3.7
Output max. velocity [deg/s]	$530^4/520^5$
Output max. acceleration [deg/s^2]	$6'510^4/7'570^5$
Force/torque range[6] [N]/[Nm]	0-50/0-4
Force/torque resolution [mN]/[mNm]	7.3/0.58
Angular position resolution [deg]	0.058
Angular velocity resolution [rpm]	configurable
Restrained RoM [deg] (see Fig. 3.1d)	±77
Static friction[7] [Nm]	$<\lvert \pm 0.1 \rvert$
Dynamic friction[8] [Nm]	$0.00198\dot{\theta} \pm 0.0135$
Position control bandwidth [Hz]	1.74
PD steady-state error [deg]	<0.12
Autonomy[9] [min]	125
Battery capacity [Wh]	11.1

[1] for a 1m83 tall user
[2] with palm support and fastening cable
[3] with module fingers fully extended
[4] in extension and in restrained RoM
[5] in flexion and in restrained RoM
[6] measurable by the load cell in both directions
[7] in restrained RoM
[8] for $\dot{\theta}$ up to 250 deg/s, $R^2 = 0.995$
[9] in normal use

From the average of five executions, $\dot{\theta}$ and $\ddot{\theta}$ were assessed at 530 deg/s and 520 deg/s, and 6'510 deg/s^2 and 7'570 deg/s^2 in extension and flexion directions, respectively, as shown in Table 3.1.

Static and dynamic friction

Static friction is the motor torque (reflected at the wrist) required to move the handle at different starting angles. Static friction was identified by progressively increasing motor current in steps of 10 mA until an output movement (larger than the encoder noise) was detected. It was evaluated every 5° in both directions, i.e starting from 87° in flexion and going up to 93° in extension, and in the opposite direction. Similarly, dynamic friction was evaluated in both directions by recording mean current consumption at different angular velocities (at the wrist) ranging from 30 to 584 deg/s.

Over the restrained RoM (i.e. ±77°), static friction remained below ±0.1 Nm. Variations in static friction could arise either from the worm drive, or the coupling between the motor and the worm screw. For dynamic friction, a linear relationship between angular velocity and torque ($y = 1.98 \times 10^{-3} x \pm 1.35 \times 10^{-2}$, $R^2 = 0.995$) was identified for velocities up to 250 deg/s, as presented in Table 3.1 (see Fig. A.4 in the Appendix for further details).

Autonomy

The autonomy of a fully wearable exoskeleton is a significant aspect of its usability and is a common performance metric for electronic equipment. In our case, considering non-spastic stroke survivors, the autonomy was defined as the time during which the device can continuously move a passive hand in extension and flexion when it is placed horizontally (see Fig. 3.1d) and a given battery (11.1 Wh) is used. A total electrical energy of 2'800 J (i.e. 0.78 Wh) was used to move the passive hand of a 1m83 tall user during 10 min at a constant speed of 25.7 deg/s.

To assess our on-board energy measurement and the practical battery capacity, we simulated a whole autonomy trial (i.e. from battery fully charged until fully discharged) by actuating the *eWrist* in water. To this end, the *eWrist* was equipped with a paddle fixed at the end of a lever and constantly immersed into water. The lever was directly fixed to the load cell (see Fig. A.2 in the Appendix). The lever length, the paddle surface area and the angular velocity (set at 35.4 deg/s) were adjusted to yield maximal mechanical resistance while staying within the device's capability. Following this trial, a total electrical energy consumption of 35'060 J (i.e. 9.75 Wh) was measured, which is reasonably close to the theoretical capacity of the battery (i.e. 11.1 Wh) considering its state of use.

The practical autonomy of the *eWrist* was inferred with the aforementioned conditions to 125 min (i.e. 10*35'060/2'800) as shown in Table 3.1.

Position bandwidth

The closed-loop position bandwidth evaluates the dynamics of the system and shows how quickly the device can react to fast and small changes in direction. In this assessment, the handle was PD controlled to follow a sinusoidal trajectory with a constant amplitude of 5° and increasing frequency from 0.1 to 6 Hz. The PD controller was implemented specifically for this assessment and was tuned to render maximum dynamic performance while remaining stable under these specific conditions.

The position bandwidth was evaluated at 1.74 Hz (at -3 dB) as presented in Table 3.1. At that frequency, the phase shift was 61.6° (see Fig. A.5 in the Appendix for further details).

Steady-state error

The steady-state error evaluates how precisely the handle can be controlled to reach a given angular position. For this assessment, a PD controller was implemented and step impulses from 40° in flexion to 40° in extension, and vice-versa, were executed in an alternating manner. Once the handle stabilized, the error was determined and the process repeated over seven trials for averaging. The PD controller was tuned to reach the target position as fast as possible without overshooting.

The steady-state error was on average lower than 0.12° as shown in Table 3.1. We also estimated steady-state error with the same PD controller used for assessing position bandwidth (i.e. identical tuning parameters K_p and K_d), which yielded an error lower than 0.31° on average.

Impedance rendering

The admittance controller described in Eq. 3.2 can be tuned with two parameters, namely virtual inertia M_{virt} and virtual damping B_{virt} to render various mechanical impedance ranging from transparent to resistant. The ability of our device to render a low and a medium impedance behaviour was assessed through impedance planes. A low impedance plane (or transparency plane) captures the lower apparent impedance boundary of the device based on measurements during human-robot interaction. It indicates visually, through its flatness, whether the device is transparent or resists the movements of the user (Metzger et al., 2015; Tagliamonte et al., 2011). The steeper the plane, the more resistant the interaction.

Impedance planes were generated with the *eWrist* worn on the forearm and while performing extension and flexion movements repetitively during 1) transparent rendering and 2) resistive rendering. In the transparent rendering, M_{virt} and B_{virt} were set as low as possible to allow a stable human-robot interaction, while for the resistive rendering they were set so that the torque applied by the experimenter would remain in an acceptable range for the *eWrist*. The ratio between M_{virt} and B_{virt} was also adjusted to optimize the stability of the human-robot interaction. Angular acceleration $\ddot{\theta}_{int}$ was calculated via FDM from the angular velocity $\dot{\theta}_{int}$. Interaction force F_{int}, $\dot{\theta}_{int}$ and $\ddot{\theta}_{int}$ were low-pass filtered offline with Butterworth filters[4]. The recordings and estimates were then fitted with a multiple linear regression model presented in Eq. 3.4.

$$F_{int} = M_{app} \cdot \ddot{\theta}_{int} + B_{app} \cdot \dot{\theta}_{int} \tag{3.4}$$

where M_{app} and B_{app} are the apparent inertia and damping felt by the user during human-robot interaction.

---

[4] F_{int}, $\dot{\theta}_{int}$ and $\ddot{\theta}_{int}$ with a 2nd order 5 Hz, 10 Hz and 20 Hz cut-off frequency, respectively.

The force-motion recordings (F_{int}, $\dot{\theta}_{int}$ and $\ddot{\theta}_{int}$) and the fit model are then plotted as points and as a plane, respectively, in a 3 dimensional plot (see Fig. 3.3). To validate the assumed linearity of the impedance plane model, the residuals of the multiple linear regression must be small, i.e. the trajectory points must lie close to the fitted plane. The axes of the 3 dimensional plot are scaled up to the peak angular velocity and acceleration found previously during maximum current impulse. If velocity/acceleration recordings were to reach the limits of the axes, the motor of the *eWrist* would have been driven into saturation (Metzger et al., 2015). In any case, the limits of the axes cannot be crossed since the actuation system is not backdrivable.

The two different dynamic behaviors of the admittance controller during human-*eWrist* interaction are shown in Fig. 3.3. In Fig. 3.3a (transparent rendering), where inertia (M_{virt}=0.23 kg) and damping (B_{virt}=0.26 mNm/deg/s) were set low, the flatness and large spread of the plane indicate that the user could freely (i.e. with low interaction torques up to 0.34 Nm) and rapidly (i.e. with high angular velocities and accelerations up to 456 deg/s and 7016 deg/s^2, respectively) execute movements while wearing the device. Whereas in Fig. 3.3b (resistive rendering), the user experienced a rather large inertia (M_{virt}=7.81 kg) with high damping (B_{virt}=8.73 mNm/deg/s) when performing extension and flexion movements. Therefore, a steep plane with high interaction torques (up to 1.59 Nm) and low velocities (up to 157 deg/s) can be observed.

In both conditions, the apparent inertia M_{app} (0.34 kg and 11.88 kg) felt by the user are about 50% larger than the virtual inertia M_{virt} (0.23 kg and 7.81 kg) set in the controller. Interestingly, the apparent damping B_{app} (0.15 mNm/deg/s and 8.32 mNm/deg/s) remained lower than the virtual damping B_{virt} (0.26 mNm/deg/s and 8.73 mNm/deg/s) in both conditions. Moreover, in both conditions, low residuals (16.0 mNm and 25.2 mNm) and high R^2 (0.933 and 0.998) indicate that the human-*eWrist* interaction remained linear over the whole RoM.

3.3.5   Functionality and wearability testing

The independent donning and doffing of the *eWrist* was tested via a wearability evaluation in healthy participants and stroke survivors by means of needed time to execute the tasks, and questionnaires.

Subjects

Fifteen healthy subjects (7 females and 8 males, mean age: 26±3.4, ranging: [22, 33] years) and two stroke survivors S1 and S2 were recruited (both males, age: 68 and 52 years, FM-UE: 44 and 41, both left-arm impaired and both suffered a haemorrhagic stroke 167 and 113 months ago, respectively). In the healthy participants, eight were identified as right-handed, five as left-handed and four as ambidextrous according to the Edinburgh inventory (Oldfield, 1971). Both stroke survivors were identified as right-handed. The study was approved by the

a **Admittance control with inner velocity control loop**
(desired: M_virt = 0.23 [kg], B_virt = 0.26 [mNm/deg/s])

M_app = 0.34 [kg]   B_app = 0.15 [mNm/deg/s]   Avg. residual = 16.0 [mNm]

fitted points = 950   R² = 0.933   Max. residual = 139.7 [mNm]

b **Admittance control with inner velocity control loop**
(desired: M_virt = 7.81 [kg], B_virt = 8.73 [mNm/deg/s])

M_app = 11.88 [kg]   B_app = 8.32 [mNm/deg/s]   Avg. residual = 25.2 [mNm]

fitted points = 1191   R² = 0.998   Max. residual = 152.3 [mNm]

Figure 3.3: Impedance planes obtained during human-*eWrist* interaction (repetitive extension and flexion movements) for two different sets of virtual inertia M_{virt} and damping B_{virt}. **a** Low mechanical resistance (i.e. high transparency) where M_{virt} and B_{virt} were set to 0.23 kg and 0.26 mNm/deg/s, respectively. **b** High mechanical resistance to movements where M_{virt} and B_{virt} were set in the admittance controller to 7.81 kg and 8.73 mNm/deg/s, respectively.

institutional ethics committee of the ETH Zürich. All subjects gave signed, written informed consent in accordance with the Declaration of Helsinki before participating in the experiment.

Experimental protocol

The experiment consisted of donning and doffing the *eWrist* exoskeleton, independently, with a single hand, on the right arm for the healthy participants, and on the left arm for the two stroke survivors. The donning procedure consisted of placing: 1) the Myo armband, 2) the forearm module and 3) the upper arm module. During the experiment, the participants were asked to speak out their thoughts aloud, i.e. to explain what they were doing while they were doing it. This so called *"Think Aloud Method"* (Charters, 2003; Nielsen et al., 2002), encourages the verbalisation of mental processes and enhances the feedback collection by the two experimenters who were present during the whole session. To familiarize the participants with the *Think Aloud Method,* they were asked beforehand to take the dimensions of their forearm and upper arm with a ruler, while explaining what they were doing. They were then introduced to the purpose and working principle of the *eWrist,* and donning and doffing were demonstrated. They were given two trials to fully don and doff the *eWrist.* Then the time needed to don and doff the *eWrist* was recorded for two subsequent trials marked as 1st and 2nd trial in Table 3.2. For both the donning and doffing, time was started once the participant touched the device (*eWrist* or Myo armband) and stopped when he/she released it. During the trials, participants were asked not to rush, but simply to execute the task at normal speed. Finally, they had to fill in questionnaires assessing the donning/doffing usability of the device.

Questionnaires

Three different questionnaires were completed by the participants just after the test to quantify their subjective opinion on the donning/doffing procedure.

The first questionnaire is a standard System Usability Scale (SUS), which is a quick, simple and reliable tool for measuring usability (Bangor et al., 2008; Lewis et al., 2009).

The second questionnaire (called SUS customized) has been customized for our device evaluation and is based on the same scoring scheme as the SUS but incorporates 32 questions instead of 10. The questions were orientated around five different aspects of usability, which are typically assessed in such evaluations (Liljegren, 2006; Resnik, 2011), namely: learnability, efficiency, memorability, errors and satisfaction. Each of these aspects were evaluated independently.

The last questionnaire is the Raw NASA-Task Load Index (RTLX) (Hart, 2006), which is a six-dimensional scale designed to assess the workload experienced during a task with the following aspects: mental demand, physical demand, temporal demand, performance, effort, and frustration (Hart, 2006; Rubio et al., 2004). In its full version (i.e. not raw), the NASA-Task Load Index (TLX) incorporates a weighting procedure of these 6 aspects, however, for the

sake of simplicity, we omitted this procedure and weighted all aspects equally. The RTLX has been shown to be highly correlated with the TLX (Moroney et al., 1995; Nygren, 1991). In our analysis, each aspect was considered individually.

Moreover, all participants could leave written comments at the end of the questionnaires.

3.4 Results

A positive and promising outcome from the wearability evaluation is that all participants (healthy and stroke) were able to don and doff the device independently, with a single hand, and after only two practice trials.

3.4.1 Donning/doffing time

Table 3.2 summarizes the average time healthy participants needed to don and doff the *eWrist* during their 1st and 2nd trial, and the individual time performance of the two stroke survivors S1 and S2. A significant time improvement can be observed between the two subsequent trial in both donning (paired t-test: p<0.001) and doffing (paired t-test: p<0.01) with healthy participants. With stroke survivors, participant S1 was remarkably fast and consistent over the two trials, performing better than most of the healthy subjects. On the other hand, S2 was much slower but improved his time performance during the donning over the two trials.

Table 3.2: Donning and doffing time

Participant	Donning		Doffing	
	1st trial	2nd trial	1st trial	2nd trial
Healthy	79.3±25.9	61.5±15.1	27.7±7.0	24.0±6.2
S1 (FM: 44)	54	54	22	22
S2 (FM: 41)	127	113	31	32

The average time, in seconds and per trial, the healthy participants required to don and doff the *eWrist*, and the individual time of the two stroke survivors S1 and S2.

No significant time difference could be observed between right-handed, left-handed and ambidextrous participants both in donning and doffing.

3.4.2 Questionnaires

The average score of the SUS questionnaire is 82.0±7.1 for healthy participants, and 97.5 for S1 and 80 for S2, with a score over 68 being considered above average (Brooke, 2013).
In Fig. 3.4a are shown the scores of each aspect of the customized SUS questionnaire for both healthy and stroke subjects. Generally, all subjects found it simple to learn how to execute the tasks (*Learnability* score: 90.6±7.7), i.e. how to correctly place and tighten/untighten

the forearm and upper arm fixations. They also found the fixation systems efficient and secure (*Efficiency* score: 84.8±13.9), and they could easily remember how to perform the overall donning/doffing procedure (*Memorability* score: 92.7±8.7). On the other hand, some participants found they were likely to make errors when donning the device (*Errors* score: 81.9±14.8), and were not fully satisfied with the exoskeleton (*Satisfaction* score: 68.6±13.9) because it was hindering their forearm/hand movements. Aesthetics, physical proportions and weight also received low scores.
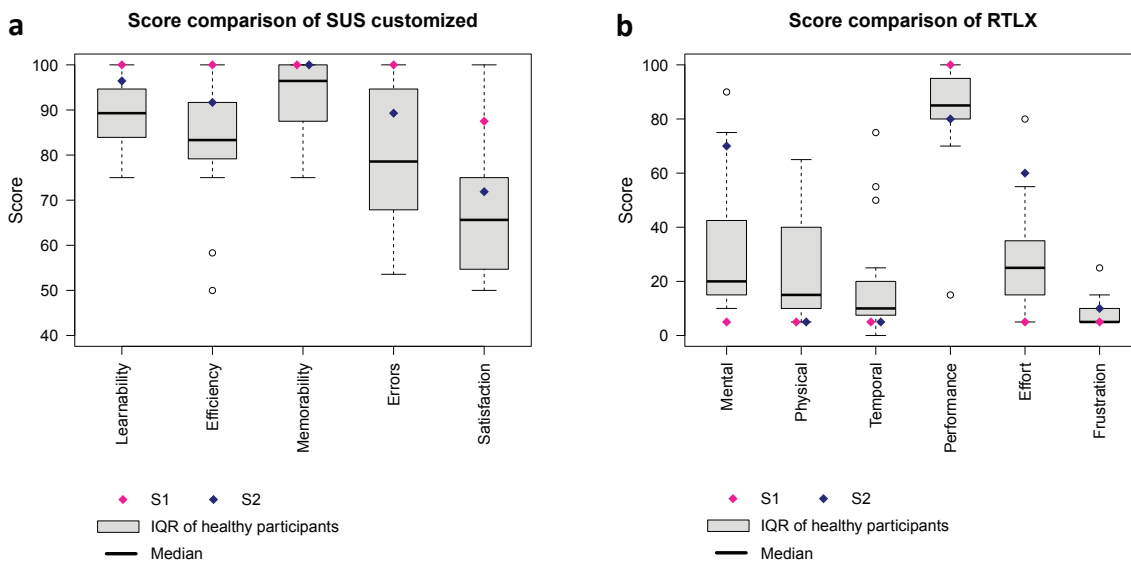
Figure 3.4: Scores comparison derived from questionnaires for all participants (healthy and stroke). **a** Scores from the customized SUS questionnaire. The average score over all aspects is 83.1±8.2. **b** Scores from the RTLX questionnaire. The average workload score excluding *Performance* (Grier, 2015) is 22.3±9.5.

Fig. 3.4b depicts the scores of the RTLX questionnaire issued to the participants right after the trials. The score ranges from 0 to 100 and reflects the workload of each aspect. A low score indicates that perceived workload was low. A high score in *Performance* means that the participants found they were successful in accomplishing the task. Mental and physical workload (score: 32.6±26.1 and 24.1±19.9, respectively) exhibit a large variability for both healthy and stroke participants where the mental demand was much higher for S2 (score: 70) than for S1 (score: 5). In the same vein, the effort required to execute the task was perceived much differently by S2 (score: 60) than S1 (score: 5). Other than that, all participants found they could accomplish the task rapidly without being rushed (*Temporal* score: 18.2±21.4), they found they were successful (*Performance* score: 84.7±20.2) and not frustrated during the donning and doffing (*Frustration* score: 8.2±5.3).

3.4.3 Subjective feedback

Below are subjective feedback and observations collected during the donning/doffing which are to be considered for future prototype versions:

- During their first trials, participants were struggling to appropriately place the forearm module so that both the mechanical axis and biological joint are aligned.

- The donning phase of the forearm module where the hooks must be locked was sometimes problematic since the device must be balanced on the forearm while it tends to fall towards the side of the actuator.

- Some discomfort appeared (tightening cable lacerating the skin, blood vessels blocked, skin squeezed) because of size mismatch. Also, for users with small hands, turning the rather large wheel of the tightening system on the upper arm module was difficult.

- The forearm fixation tends to generate stress on the skin during pronation and supination movements.

- Some female users found it tedious to turn and pull the ratchet wheels on forearm and handle fixations.

- The stroke survivors experienced slight difficulties to pass their fingers through the loop formed by the palm support if the latter was not completely loose (see Fig. 3.1b).

In the comments left by the participants, positive feedback was given regarding the ease of use and comfort of the device. On the other hand, some commented size mismatches, excessive perceived weight (especially because they were holding their arm above the table), movement constraints and a need for design improvement especially in terms of aesthetics.

3.5 Discussion

In this paper we have presented the development, characterization and wearability evaluation of a fully portable, powered one DoF wrist exoskeleton designed for independent and unsupervised training. The results of the characterization showed that the current prototype fulfils the technical requirements of output torque (up to 3.7 Nm), angular velocity (up to 530 deg/s) and RoM (154° or up to 215° if required), distal weight (238 g for forearm module) and autonomy (125 min) as previously specified in the literature. Furthermore, the wearability evaluation revealed that all participants (healthy and stroke) embraced the device and were able to don and doff it independently and quickly after a few practice trials.

3.5.1   Design choices and performance characterization

Our approach of directly integrating the actuator and its drive locally at the wrist has the advantage of a rather simple implementation and good control of the wrist joint (PD steady-state error <0.12°). However, the motor alone (69 g) accounts for about 29% of the forearm module weight (238 g) and is therefore a major contributor of the weight placed distally on the arm. Fixing the second module on the upper arm reduces the weight distally and facilitates donning with the other hand, but still impacts arm motion in patients. This could be avoided by moving it to the back or less affected body side (Nilsson et al., 2012; Polygerinos et al., 2015; Randazzo et al., 2017), however, the further the exoskeleton is removed from accompanying modules, the more difficulties arise for donning and doffing independently. Thus, our solution is a compromise between good usability for donning/doffing and reducing the weight attached distally to the affected arm. The weight of the forearm module is comparable or lower than for other similar devices (Choi et al., 2019; Higuma et al., 2017; Sangha et al., 2016).

The dynamics assessment has demonstrated that the angular velocities and accelerations achievable with the *eWrist* in the restrained RoM are comparable to those observed in healthy skilled workers which perform typical manual activities (Marras et al., 1993). High achievable velocities and accelerations are necessary to render transparency. Despite a rather low position bandwidth of 1.7 Hz our impedance planes show that the implemented admittance controller can stably (i.e. high R^2 and low residuals) provide transparent or resistive dynamic behaviour, which is important for accommodating different rehabilitation training settings (Proietti et al., 2016). The capacity to provide all of these training modalities is important for haptic rehabilitation devices (Gupta et al., 2006; Vallery et al., 2009) for (i) training a wide range of impairments (i.e. from plegic to moderately impaired function), and (ii) quantitatively assessing the patient's ability to perform movements without being disturbed by the device dynamics (Tagliamonte et al., 2011).

PD controllers were implemented in both steady-state error and position bandwidth assessments and were tuned for maximum performance in each case. Although proportional K_p and derivative K_d tuning parameters were set to different values for each assessment, their ratio was kept the same to preserve stability (K_p/K_d=10 in both cases). Moreover, K_p and K_d were 45% larger for the position bandwidth assessment compared to the steady-state error assessment in order to exhibit a more dynamic behavior. The two PD controllers were implemented for the sole purpose of performing these assessments and tuned independently to demonstrate the best capability of the device in each experimental context. Only the admittance controller is used during human-robot interaction, and dictates the experience of the user with the device.

Our autonomy assessment is comparable to other studies (Bützer et al., 2019; Nycz et al., 2016; Sangha et al., 2016) and would provide an extensive training dose for the user. However, the obtained autonomy must be interpreted with caution because it depends on the movement regime, for example, higher interaction velocities or higher interaction forces might arise if the

hand is not completely passive. Surprisingly, we observed during the autonomy assessment that for a given time and with a substantially larger angular velocity (+42%), the energy consumption was reduced (-5%), revealing a non-linear effect which decreases with increasing velocity. This observation could partially explain the large disparity (-42%) between the desired virtual damping B_{virt} and the measured apparent damping B_{app} seen in Fig. 3.3a but not in Fig. 3.3b. With larger velocities this non-linear effect is lower, leading to a lower apparent damping felt by the user.

In the same vein, the large discrepancies (about +50%) observed in both renderings (i.e. transparent and resistive) between the virtual inertia M_{virt} and the apparent inertia M_{app} can be mainly explained by the intrinsic mechanical feature of our design, which requires that an interaction force needs to be applied first in order to illicit a motion. In the time delay (due to processing) between the force measurement and the handle motion, the force increases. And stronger forces will cause stronger friction between the gears and eventually resistance to the movement, thus leading to a larger apparent inertia experienced by the user compared to the one initially set in the controller. The steel-bronze combination for the worm drive is a fair compromise between low friction coefficient and high strength (Merritt, 1935). Nevertheless, special attention must be given to optimising the manufacturing of these parts to keep their weight low. Moreover, the first-order characteristics of Eq. 4.1 also introduces a time lag in the control command which is directly linked to the inertia term. It would thus be tempting to minimize or even suppress this term to decrease time lag, however, we observed empirically that both terms (inertia and damping) are required to stabilize the exoskeleton during human-robot interaction. More specifically, stability was enhanced when the ratio between inertia and damping remained constant, as shown in other studies (Dimeas et al., 2016; Landi et al., 2017). Finally, since the worm screw can shift up relative to the worm wheel due to the oblong fixation points, thus uncoupling the motor from the handle, our experience showed that the safety of the user's wrist and the mechanics are preserved in case of unexpected high torque.

3.5.2 Wearability evaluation and general considerations

The effort directed towards the development of adjustable attachment systems which ease the donning and doffing procedure of the *eWrist* was positively received by the participants according to the scores obtained in our questionnaires. Although not standardized, the customized SUS questionnaire allowed us to get a better understanding of which specific aspects were favored and which were disliked. Encouragingly, the majority of participants quickly endorsed the mechanisms and found them efficient in terms of gripping force and adjustability. Generally, the doffing was found more straightforward than the donning. Stroke survivors judged wearability similar to healthy participants in the customized questionnaire. However, one clear limitation of our study is that we tested only two patients with moderate to minor impairment. In order to generalize our results to stroke patients, it would be valuable to also test wearability in more severely impaired patients. One important difference between the two cohorts was that healthy participants, but not stroke survivors, found their movements to

be hindered by the device, most likely reflecting a difference in the perceived benefit of motor assistance via the exoskeleton.

As mentioned in the design review and also clearly expressed in the feedback, a critical phase during the donning is the correct placement of the forearm module to match the biological joint and mechanical axis of the *eWrist*. Most of the participants struggled with this aspect during the first four trials. During this phase, the forearm module must be balanced on the forearm and the hooks of the attachment system locked. However, the combined weight of the actuator, the gear drive and the load cell, all located on the same side of the module, tends to tip the device over. Nonetheless, our experience suggests that with slightly more practice both of these phases can easily be mastered.

According to a survey of 22 studies scoring mechanical tasks with the TLX (Grier, 2015), the obtained score of 22.3 in the RTLX questionnaire (average workload score without considering *Performance*) is below the 25th percentile of the scores (i.e. better than 75% of all scores). Nevertheless, despite this encouraging result, the scores comparison in Fig. 3.4b reveals that stroke survivors perceived mental and physical demands of donning/doffing much differently from healthy participants. This disparity, and more generally the wearability evaluation, should be further assessed by testing the device with more stroke survivors of different impairment levels and over several sessions. Nonetheless, it has been shown that the most critical usability problems are likely to be detected in the first few subjects, and that the likelihood of uncovering new problems decreases as more and more subjects participate (Virzi, 1992). In our usability study, we consistently observed that difficulties encountered by healthy participants affected stroke subjects in a similar manner.

The weight of the exoskeleton was found to be acceptable. The rating was sometimes biased when participants would hold their whole arm over the table during the donning instead of laying it down, thus increasing their weight perception. Unfortunately, some participants felt discomfort mainly due to size mismatch. This can be addressed by tailoring the device to the individual user. For this study, two *eWrist* of different dimensions were built, one for the right arm and one for the left. Based on anthropometric measurements (width, length and circumference) of the forearm, the wrist and the hand, an individualized exoskeleton can be printed. Tailor-made manufacturing with 3D printing techniques has already been adopted in community settings to offer simple prosthetics for impaired children and could potentially be applied for powered and more complex robots (Liarokapis et al., 2014). Nevertheless, although the structure and 3D printed parts can be adapted, the electronics, load cell and actuator remain the same and would not properly suit small patients (i.e. < 1m60 tall).

There were a number of general limitations to the wearability assessment. First, introducing the concept of the device before its assessment might have biased the participants towards higher ratings regarding functionality. Second, certain participants might have evaluated their own performance rather than the actual wearability of the device. Third, the wearability assessment was also limited in its design since participants were only evaluating the device

during a single session. For instance, it would have been worthwhile to evaluate whether participants had memorized the procedure by retesting them after a week. Finally, the use of the *Think Aloud Method* conjointly with the observations of the two experimenters allowed identification of where participants were experimenting difficulties in the task. However, even though participants were given preparation in verbalizing their thoughts, the use of this method with naive users had a tendency to slow down the execution time, especially with S2. Additionally, one has to keep in mind that we only evaluated the donning and doffing of the device but did not yet test its usability within a rehabilitation setting. Even though wrist extension/flexion function is highly relevant for post stroke recovery (Squeri et al., 2013), only supporting this movement in such a setting might limit some activities.

In its current form, the *eWrist* is an important preliminary step towards a rehabilitation technology that could be donned, used and doffed independently by the patient in unsupervised settings, and which would complement a conventional therapy. Target patients would ideally start training with this device in the acute or sub-acute phase post stroke. The main inclusion criterion is low spasticity (i.e. MAS < 3). However, patients who will likely benefit the most are those that have some remaining EMG activity in the forearm muscles and suffer from impaired hand and/or wrist function. In the initial phase, patients would use the device in a supervised manner, but as rehabilitation progresses and their impairment decreases, they would use the device more independently in daily life settings. As currently envisioned, rehabilitation training with the *eWrist* will be in the form of a visuomotor task where the wrist angle of the exoskeleton is visualized as a cursor on a computer display and the patient performs wrist extension and flexion movements to move the cursor to different targets (Lyu et al., 2017), with an adaptive level of mechanical support from the exoskeleton based on sEMG amplitude. The control of robotic devices with sEMG signals have been extensively studied and one of the most preferred approach is to proportionally match sEMG to position (Lyu et al., 2019) or force (Khokhar et al., 2010; Lenzi et al., 2012). We believe that a visual feedback combined with the mechanical support can not only reinforce sensorimotor loops and enhance the recovery process, but perhaps more importantly, boost motivation. Moreover, the wearable aspect of the device gives more freedom to the user and could easily be combined with a smartphone or a tablet.

3.6 Conclusion

In the context of a robotic-directed therapy in unsupervised settings, donning a medical device is the very first barrier a patient will have to face if he/she were to train independently. Therefore, it is essential that this first step is straightforward and keeps the user's motivation high. In this paper, we have demonstrated that the performance of our device is similar or better than other fully wearable exoskeletons for wrist training, but more specifically, we have drawn attention to the problem of the independent donning/doffing of an upper limb exoskeleton and have brought new insights on possible user-friendly and innovative mechanisms which ease this procedure.

4 Variable admittance control with sEMG-based support for wearable wrist exoskeleton

Charles Lambelet, Melvin Mathis, Marc Siegenthaler, Jeremia Held, Daniel G. Woolley, Olivier Lambercy, Roger Gassert, and Nicole Wenderoth

In preparation

Chapter 4. Variable admittance control with sEMG-based support for wearable wrist exoskeleton

4.1 Abstract

Wrist function impairment is common after a stroke and heavily impacts the execution of daily tasks. Robotic therapy, and more specifically wearable exoskeletons, have the potential to boost training dose in relevant-context scenarios, promote voluntary effort through motor intent detection, and mitigate the effect of gravity. Portable exoskeletons are often non-backdrivable and it is challenging to make their control safe, reactive and stable. Admittance control is often used in this case, however, this type of control can become unstable when the supported biological joint stiffens. Variable admittance control adapts its parameters dynamically to allow free motion and stabilize the human-robot interaction. In this study, we implemented a variable admittance control scheme on a one degree of freedom wearable wrist exoskeleton. Besides the admittance control scheme, sEMG-based and gravity compensation controllers were implemented, characterized, optimised on ten healthy participants and tested on six stroke survivors. The results show that 1) the variable admittance control scheme could stabilize the interaction but at the cost of a decrease in transparency, and 2) the sEMG-based controller enhanced wrist functionality of stroke survivors in the most extreme angular positions.

4.2 Introduction

Upper limb paresis is a common impairment poststroke affecting 75% of stroke survivors (Rathore et al., 2002). This manifests not only during whole arm movements but also during tasks that require well-coordinated hand and wrist actions. Wrist function in particular is essential in many activities of daily living (ADL) for orientating and stabilizing the hand (Palmer et al., 1985), and recovery of this function can have a meaningful impact on the quality of life poststroke (Squeri et al., 2013). Robotic-mediated rehabilitation has the potential to provide intensive, repetitive, and task-specific training in a motivating environment (Colombo et al., 2007; Norouzi-Gheidari et al., 2012). Moreover, by supporting movements with the impaired limb, robotic training promotes voluntary effort and enhances proprioceptive feedback, which stimulates neuroplasticity in the neural circuitry that generates skilled movements (Ghez et al., 1990; Hasan, 1992; Miall et al., 2018). One limitation of most robotic rehabilitation devices to date is that they are stationary and require supervision from trained professionals. This could be overcome by portable exoskeletons that support the impaired limb based on the movement intention of the user (Lenzi et al., 2012), or by reducing the effect of gravity (Moubarak et al., 2010; Wu et al., 2016). The putative advantage of portable exoskeletons is that they would allow the integration of rehabilitation training into functional everyday tasks, which would provide a high training dose via distributed sessions in task-relevant contexts (Brewer et al., 2007; Bützer et al., 2019; Gasser et al., 2017).

Currently, there are only a few active wearable devices targeting wrist function that could be used as portable rehabilitation tools (Al-Fahaam et al., 2016; Andrikopoulos et al., 2015; Bartlett et al., 2015; Choi et al., 2019; Dragusanu et al., 2020; Higuma et al., 2017; Khokhar

56

et al., 2010; Sangha et al., 2016), and none of these solutions are fully portable and mobile. Existing wearable wrist exoskeletons fall into two main categories. The first includes designs that use highly flexible and compliant structures with pneumatic, cable-driven, or spring blades transmissions. However, controlling these devices is challenging so they usually only provide relatively basic support, e.g. via pre-programmed (Andrikopoulos et al., 2015; Bartlett et al., 2015; Dragusanu et al., 2020) or remotely triggered (Higuma et al., 2017) movement sequences. The second category includes designs that use rigid structures which are less comfortable to wear but allow the implementation of more precise and continuous control schemes that incorporate physiological signals such as force myography (FMG) (Sangha et al., 2016) or surface electromyography (sEMG) (Khokhar et al., 2010). Control schemes based on physiological signals afford some level of voluntary effort from the stroke survivor, which is believed to be more beneficial for neural reorganization and recovery (Lotze et al., 2003; Perez et al., 2004). Moreover, precise and proportional control of the mechanical support enhances the rehabilitation of coordinated movements (Ghez et al., 1990; Lotze et al., 2003). These assumptions motivated the development of new interactive robotic-based treatments that require active participation (Hu et al., 2015; Lenzi et al., 2012; Song et al., 2013).

One challenge when designing wearable actuated exoskeletons for poststroke rehabilitation is the development of an appropriate controller. sEMG is a technique that has been used extensively for the control of upper-limb robotic devices by decoding the user's movement intention (Farina et al., 2014). This method is non-invasive, easy to apply, and contains rich information about motor intentions. Moreover, the occurrence of the sEMG signal starts about 20-50 ms before the overt movements take place (Norman et al., 1979), which can be exploited to compensate for the limited bandwidth of the robot actuation system. However, the signal varies substantially across subjects and electrode placement, requiring a calibration after the device has been donned (Fleischer et al., 2007; Hashemi et al., 2014). Typically, the signal is heavily filtered to extract its envelope, which is suitable for robotic control (Lyu et al., 2020). From there, the amplitude of the envelope is extracted to proportionally control joint velocity (Corbett et al., 2011), pressure (Sawicki et al., 2009) or torque of the assistive device. Torque mapping is by far the most common and straightforward approach to obtain a natural motion (Hu et al., 2015; Lenzi et al., 2012; Song et al., 2013), but precise control can be challenging due to the non-linear sEMG-torque relationship with respect to movement velocity and joint position (Farina, 2006; Solomonow et al., 1991).

An alternative control strategy that does not attempt to decode the user's movement intention is gravity compensation. By definition, a wearable exoskeleton moves with its user, and thus the mechanical support it provides to the limb is altered by the effect of gravity. One solution that takes this effect into account is evaluating the spatial orientation of the exoskeleton and adjusting the mechanical support accordingly. This can be done by implementing an inertial measurement unit (IMU) on the device. Gravity compensation has mostly been implemented on stationary exoskeletons that support shoulder and elbow joints to compensate for the weight of the arm (Hsieh et al., 2015; Spagnuolo et al., 2015). Anti-gravity support benefits upper-limb rehabilitation primarily by reducing the amount of fatigue experienced by acute

and sub-acute patients, thus enabling an increase in the quality and dose of training (Kwakkel et al., 2013). It is also effective for improving motor control and decreasing spasticity (Brewer et al., 2007; Prange et al., 2006).

Wearable exoskeletons featuring a rigid structural design with a direct implementation of the actuation system (i.e. DC motors) usually lack backdrivability. This results from the implementation of small actuators with high gear ratios in order to minimize weight. In this context, a natural and smooth physical human-robot interaction (pHRI) cannot solely be mediated through physiological signals or gravity support. The pHRI must be safe, but also reactive and compliant to the user's movement intentions (De Santis et al., 2008). To that end, a straightforward approach is to measure interaction forces with sensors serially connected with the joint kinematics (Nef et al., 2006). Admittance control is an appropriate and commonly adopted force-based control to actuate the robot (Kilic, 2017; Lee et al., 2017; Zeng et al., 1997). However, admittance control is prone to instability, especially when the human joint becomes stiffer during pHRI (Landi et al., 2017; Wang et al., 2015). For instance, oscillations of the end-effector can arise during a reaching task when the wrist needs to stiffen to stabilize the hand for a grasp. A possible strategy to prevent oscillations and instability is to dampen the system by adjusting the parameters of the admittance controller. A simplistic approach is to set these parameters sufficiently high in order to constantly dampen the pHRI, however, the transparency of the robotic system, i.e. its capacity to not apply resistance or assistance to free motion (Proietti et al., 2016), is then affected. The capability of haptic rehabilitation devices to provide transparent behaviour is important for quantitatively assessing the patient's ability to perform movements without being disturbed by the device dynamics (Tagliamonte et al., 2011). Thus, in order to allow free motion, but at the same time stabilize the pHRI, the parameters of the admittance control needs to be adapted dynamically. A variable admittance controller adapts its parameters either by detecting the instability (Dimeas et al., 2016; Landi et al., 2017) or by estimating the stiffness of the human limb (Castellini et al., 2014).

The present work investigates the benefit of variable admittance control for sEMG-based and gravity-based support implemented on a wearable and non-backdrivable wrist exoskeleton. In this context, we test whether 1) the variable admittance control will stabilize the pHRI while allowing transparent motion, and 2) the sEMG-based and gravity-based controllers will enhance wrist functionality and promote voluntary effort. For this purpose, we performed a proof of concept study and implemented different control strategies using a 1 DOF device actively supporting wrist extension and flexion movements (Lambelet et al., 2017; Lambelet et al., 2020). The controllers were assessed in a visuomotor goal-directed task which required participants to move their wrist to different target positions. The variable admittance scheme and both controllers were optimised in a group of ten healthy participants and then tested in six stroke patients.

4.3   Materials and methods

First, this section describes the implementation on the exoskeleton of the variable admittance scheme and the controllers. A short characterization of the variable admittance scheme is provided, followed by a description of how we evaluated the controllers in a behavioural task with healthy and stroke participants.

4.3.1   Apparatus

The *eWrist*

The *eWrist* depicted in Fig. 4.1a is a fully wearable 1 DOF force controlled wrist exoskeleton that actively supports extension and flexion movements (Lambelet et al., 2017; Lambelet et al., 2020). It actuates the wrist with a torque up to 3.7 Nm, an angular velocity up to 530°/s over a range of motion (ROM) of 215°. A load cell measures the force applied by the user on the handle. Absolute angular position and velocity are measured with a Hall encoder placed at the wrist axis and a Hall sensor integrated on the motor shaft, respectively. An inertial measurement unit (IMU) measures the orientation of the exoskeleton. Because of high reduction gear ratios, the transmission mechanism of the device is not backdrivable. The *eWrist* is fixed on the forearm and hand of the user as shown in Fig. 4.1c. The variable admittance scheme is implemented in a real-time microcontroller (Teensy 3.2[1]) and actuates the handle of the exoskeleton based on interaction forces as shown in Fig. 4.2. During the visuomotor task the Teensy collects and transmits force, angular position/velocity and IMU data to a host computer via serial communication (USB) (see Fig. 4.4).

The Myo Armband

The Myo armband was[2] a commercially available device from Thalmic Labs. It measures sEMG activity on the forearm and consists of eight dry sEMG sensors. It has a sampling frequency of 200 Hz for raw sEMG data and communicates via Bluetooth Low Energy (BLE) making it easy to connect to other devices wirelessly. The raw data ranges from -128 to +128 and is unitless. The Myo armband can be easily donned, doffed, and adjusted to many forearm size thanks to its expandable flex (see Fig. 4.1b).

4.3.2   Control

The core control of the *eWrist* used during pHRI is based on a variable admittance scheme that uses measured interaction forces to generate a motion. The sEMG-based and gravity-based controllers produce a mechanical support that is either based on the sEMG signal measured on the forearm with the Myo armband or based on the spatial orientation of the forearm

---

[1]MK20DX256 32 bit ARM Cortex-M4 72 MHz
[2]The Myo armband was discontinued in October 2018.
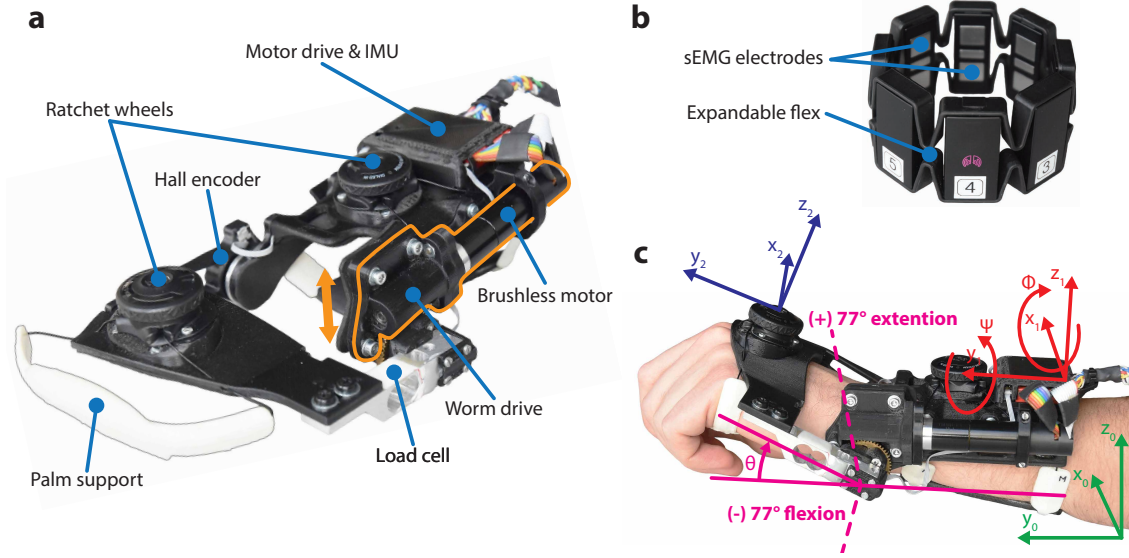
Figure 4.1: a The forearm module of the *eWrist*, where the motor and worm drive can be shifted up in order to uncouple the handle from the motor (see orange arrow). **b** The Myo gesture control armband from Thalmic Labs. **c** Illustration of the wrist angular position θ and the referentials used to compute F_{grav}, i.e. the earth referential $\mathfrak{R}_0$ in green, the forearm module referential $\mathfrak{R}_1$ in red, and the hand referential $\mathfrak{R}_2$ in blue.

module measured with an IMU. Both controllers generate a fictive additional force that is added to the input of the variable admittance scheme as shown in Fig. 4.2. This additional force can be fine tuned with gains. The two controllers were always used separately.

Variable admittance scheme

Admittance control receives a force input and outputs a motion in response as shown in Eq. 4.1. Two parameters, namely virtual inertia M [$Nm \cdot s^2/rad$] and virtual damping B [$Nm \cdot s/rad$] can be tuned to change the dynamic behavior of the exoskeleton. Eq. 4.1 expresses the equation of motion in the time domain and its conversion to the Laplace domain with respect to angular velocity.

$$M\ddot{\theta} + B\dot{\theta} = F \cdot L \quad \xRightarrow{\mathscr{L}(\cdot)} \quad \omega = \frac{L}{Ms + B} \cdot F \tag{4.1}$$

where $\ddot{\theta}$ and $\dot{\theta}$ are the angular acceleration and angular velocity of the wrist in the time domain, respectively, ω the angular velocity in the Laplace domain, L the distance between the mechanical axis and the average pressure point of the hand on the handle (set at 8 cm), and F the force applied on the handle.
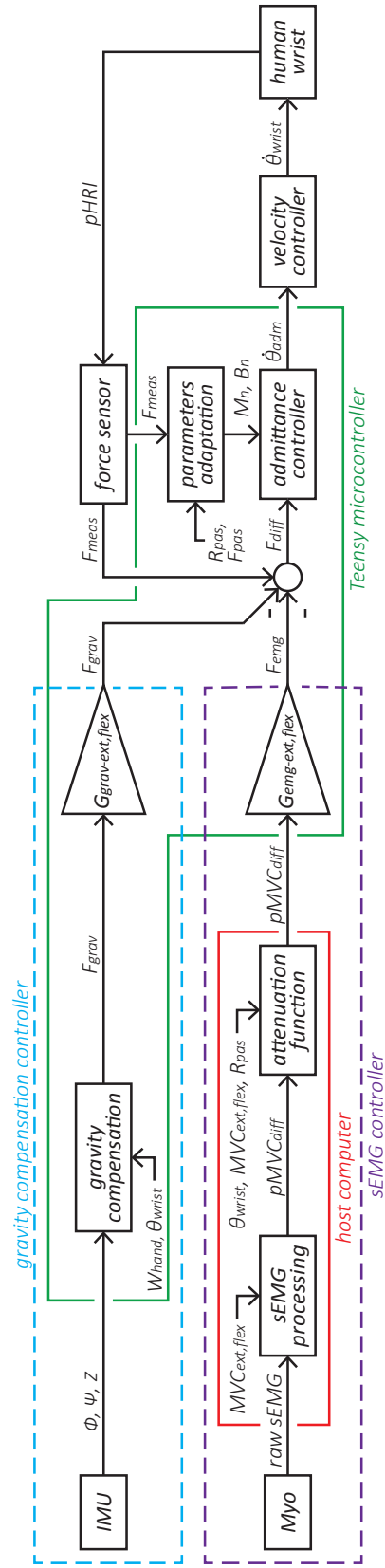
Figure 4.2: Block diagram of the variable admittance scheme and the two controllers. The elements within the purple dotted line form the sEMG-based controller, and the elements within the blue dotted line form the gravity compensation controller. The elements within the green line are implemented in the Teensy microcontroller and run at 1 kHz, while the elements within the red line run on the host computer at 60 Hz.

Chapter 4. Variable admittance control with sEMG-based support for wearable wrist exoskeleton

A discretized version of the admittance scheme is implemented in the Teensy microcontroller with the Tustin transformation (Lambelet et al., 2020). A variable admittance scheme is used to both reject disturbances in the pHRI, but also to render low inertia and transparent behaviour of the device. To that end, B is dynamically adjusted either to dampen the system in case of instabilities or to free it during smooth motion (Bian et al., 2018; Dimeas et al., 2016; Grafakos et al., 2016). The adaptation of B is represented by the block *parameters adaptation* in Fig. 4.2 and is described in Eq. 4.2.

$$
\begin{aligned}
B_n &= B_{min} + G_{stif}(\theta) \cdot I_{s,n}, \quad n = \{1, 2, 3, ...\} \\
M_n &= M_{min}
\end{aligned}
$$

(4.2)

where B_n and M_n are the current damping and inertia values, respectively. B_{min} and M_{min} are the minimal damping and inertia values set at 0.04 $[Nm \cdot s/rad]$ and 0.004 $[Nm \cdot s^2/rad]$, respectively, which render maximal transparency during smooth human-robot interactions. $G_{stif}(\theta)$ is a non-linear gain depending on the angular position of the wrist θ, $I_{s,n}$ the current index of instability, and n the control loop counter. In our implementation of the variable admittance scheme, M_n was kept constant and only B_n was dynamically adjusted (Dimeas et al., 2016).

$G_{stif}(\theta)$ expresses the change in passive stiffness of the wrist joint according to its angular position. The passive stiffness increases close to the limits of the joint's ROM (i.e. more likely to generate oscillations in the pHRI) and is the lowest around a straight wrist position. Therefore, $G_{stif}(\theta)$ dampens the system faster (i.e. to dissipate energy and attenuate oscillations) for large wrist angles than for small wrist angles. $G_{stif}(\theta)$ is subject-dependent and is set during a calibration phase (see Eq. B.1 in the Appendix for more details on $G_{stif}(\theta)$). $I_{s,n}$ is a recursive index which varies according to both the frequency and the magnitude of the oscillations measured in the force signal as shown in Eq. 4.3.

$$
I_{s,n} = I_{freq,n} \cdot I_{mag,n} + \lambda \cdot I_{s,n-1}
$$

(4.3)

where $I_{freq,n}$ is the current frequency index, $I_{mag,n}$ the current magnitude index, λ a parameter set at 0.7 that controls the frequency and magnitude parameters of the output $I_{s,n}$, and $I_{s,n-1}$ the previous index of instability.

I_{freq} encodes the frequency of oscillations, whereas I_{mag} encodes the magnitude of these oscillations as shown in Eq. 4.4 and Eq. 4.5. Both indexes are computed online on the Teensy over a moving window of length m=200 samples. The moving window moves in increments of

eight samples.

$$I_{freq,n} = \frac{\sum_{i=1}^{m} signChange_i}{\#signChange_{max}} \tag{4.4}$$

where $signChange_i$ is a boolean value and indicates whether the sign of the force changed at sample i in the moving window, and $\#signChange_{max}$ the maximum number of sign changes of the force in the moving window, which normalizes $I_{freq,n}$ between 0 and 1, and which was determined empirically.

$$I_{mag,n} = \frac{\sqrt{\frac{1}{m}((f_{h,n})^2 + \cdots + (f_{h,n-m})^2)}}{f_{max}} \tag{4.5}$$

where $f_{h,n}$ is the latest force sample, $f_{h,n-m}$ the oldest force sample, and f_{max} the maximum value of the force which normalizes $I_{mag,n}$ between 0 and 1, and which was determined empirically.

The dynamic adaptation of B_n was evaluated in a setup where the *eWrist* was exposed to various stiffnesses. For this purpose, the forearm part of the device was firmly fixed and its handle linked to a rod. This rod was fixed to a rotating lever to which a spring of constant k=698 N/m was attached as shown in Fig. 4.3a/b. The spring could be moved along the lever in order to modulate the stiffness experienced by the exoskeleton from 0.5 Nm/rad to 20 Nm/rad. This range of stiffnesses is typical during active stiffening of the wrist joint (Halaki et al., 2006; Kuchenbecker et al., 2003; Leger et al., 2000). In Fig. 4.3c, the handle was initialized to 10° in flexion and released to analyse the evolution of the movement when (1) B_n was kept constant at B_{min} and (2) B_n was adjusted dynamically as described in Eq. 4.2. In (3), the handle was manually excited first with high frequency and low magnitude oscillations, and then low frequency and high magnitude oscillations.

In Fig. 4.3c1, one observes that without a dynamic adaptation of B_n, the device enters a resonant mode and cannot stabilize when the stiffness was set to 10 and 20 Nm/rad. However, the oscillations attenuate with lower stiffnesses. On the other hand, when B_n is dynamically adjusted, the system stabilizes for all stiffnesses as shown in Fig. 4.3c2. Fig. 4.3c3 shows how $I_{\omega,n}$ and $I_{f,n}$ respond to high frequency and high magnitude oscillations, respectively. Moreover, it takes about 2 s for both indexes to come back to their initial level once the excitation terminates.
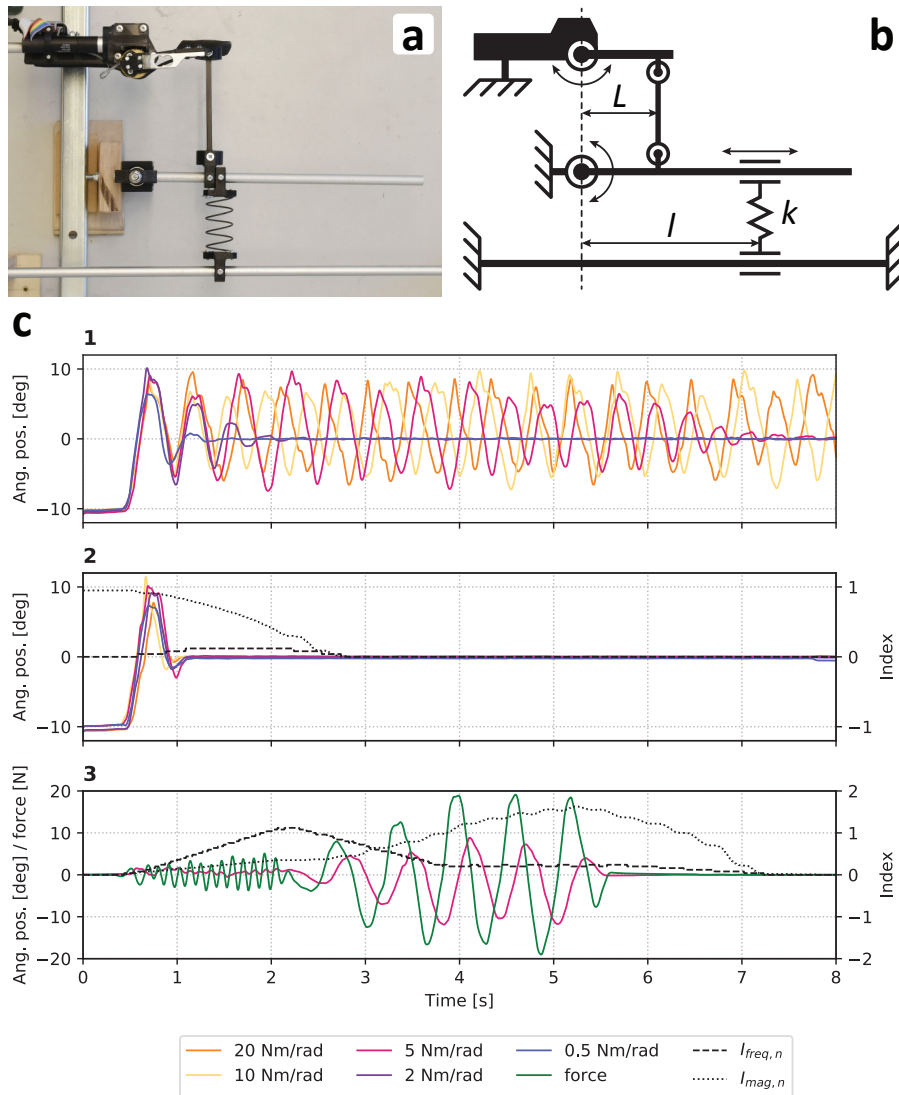
Figure 4.3: a Picture and **b** schematic of the experimental setup where stiffnesses perceived by the *eWrist* can be modulated by moving the spring k along l. **c** Results from the evaluation where in (1) B_n was kept constant, and in (2) B_n was adjusted dynamically. In (3), the system was manually excited with high frequency and magnitude oscillations.

sEMG-based controller

The sEMG controller inputs an additional force F_{emg} to the variable admittance scheme as shown in Fig. 4.2. First, raw sEMG data from the Myo armband are rectified and processed with a moving average filter[3] followed by a Kalman filter[4] to extract the envelope of the signal (cf. *sEMG processing* block in Fig. 4.2). Two electrodes are assigned to measure the activity of extensor muscles, and another two electrodes assigned to measure the activity of

---

[3]The window length was set to 40 samples.
[4]*KalmanFilter* from the Python library *pykalman* was used.

flexor muscles. A weighted sum of the signals from each of these groups of two electrodes is performed and then normalized to the maximum voluntary contraction (MVC) (Corbett et al., 2011) separately for extension MVC_{ext} and flexion MVC_{flex}. Then the difference between the normalized extension and flexion sEMG signal $pMVC_{diff}$ is computed.

Secondly, $pMVC_{diff}$ is attenuated by a non-linear gain $G_{att}(\theta)$, which is function of the wrist angle θ (cf. *attenuation function* block in Fig. 4.2). Similar to $G_{stif}(\theta)$, as the wrist angle reaches the limit of the joint's ROM, the passive stiffness increases and requires extensive muscle contractions to further move the wrist or simply hold the position. Therefore, the sEMG signal, and ultimately the supportive force F_{emg}, needs to be attenuated for high wrist angles (i.e. higher than 80% of ROM_{pas}). Consequently, $G_{att}(\theta)$ boosts movement initiation for small wrist angles, but prevents excessive mechanical support close to the joint's limit. $G_{att}(\theta)$ is subject-dependent and is determined during the calibration phase. It relies on MVC_{ext}/MVC_{flex} and ROM_{pas}, and two separate gains are used for extension and flexion (see Eq. B.2 in the Appendix for more details on $G_{att}(\theta)$).

Finally, a constant gain G_{semg} (different for extension and flexion) transforms the unitless sEMG signal $pMVC_{diff}$ into a force F_{emg}. The decision to use one of the two gains is based on the sign of $pMVC_{diff}$. A positive difference represents extension, whereas a negative difference represents flexion. G_{emg} was adjusted to provide appropriate mechanical support. The *sEMG processing* and *attenuation function* blocks within the red line in Fig. 4.2 are processed online at 60 Hz by the host computer. The time delay between the generation of raw sEMG and movement onset was evaluated over two separate measurements including 32 trials each to 0.188 s, which is generally considered acceptable (Farrell et al., 2007).

Gravity compensation controller

Similar to the sEMG controller, the gravity compensation controller inputs an additional force F_{grav} to the variable admittance scheme as shown in Fig. 4.2. This controller continuously compensates the weight of the user's hand in extension or flexion based on the spatial orientation of the forearm module (ϕ, ψ, and Z) and the angular position of the wrist θ. Measurements from the IMU and the wrist angular encoder are used to compute z_{hand}, the z-component of the normal vector to the hand z_2 expressed in the Earth's referential $\mathfrak{R}_0$ (x_0, y_0, z_0), as depicted in Fig. 4.1c. First, spatial orientation of the hand referential $\mathfrak{R}_2$ relative to $\mathfrak{R}_0$ is calculated via the multiplication of $R_{x1}(\phi)$, $R_{y1}(\psi)$, and $R_{x2}(\theta)$. These three matrices encode for the rotation (relative to $\mathfrak{R}_0$) around the pitch (x_1) and roll (y_1) axes of the exoskeleton, and for the rotation (relative to the exoskeleton's referential $\mathfrak{R}_1$) around the wrist axis (x_2), respectively. The result is then multiplied by z' to extract the normal vector z_2 as shown in Eq. 4.6.

$$R_{x1}(\phi) = \begin{bmatrix} 1 & 0 & 0 \\ 0 & \cos(\phi) & -\sin(\phi) \\ 0 & \sin(\phi) & \cos(\phi) \end{bmatrix}, \quad R_{y1}(\psi) = \begin{bmatrix} \cos(\psi) & 0 & -\sin(\psi) \\ 0 & 1 & 0 \\ \sin(\psi) & 0 & \cos(\psi) \end{bmatrix},$$

$$R_{x2}(\theta) = \begin{bmatrix} 1 \\ \sin(\theta - 77) \\ \cos(\theta - 77) \end{bmatrix}, \quad z' = \begin{bmatrix} 0 \\ 0 \\ 1 \end{bmatrix}$$

$$z_2 = R_{x1}(\phi) \cdot R_{y1}(\psi) \cdot R_{x2}(\theta) \cdot z' = \begin{bmatrix} -\sin(\psi) \\ -\sin(\phi)\cos(\psi)\sin(\theta - 77) \\ \cos(\phi)\cos(\psi)\cos(\theta - 77) \end{bmatrix} \tag{4.6}$$

z_{hand} is the z-component of z_2 and varies between 0 and 1 according the hand's orientation as shown in Eq. 4.7.

$$z_{hand} = z'^T \cdot z_2 = \cos(\phi)\cos(\psi)cos(\theta - 77) \tag{4.7}$$

The gravity compensation force F_{grav} applied by the exoskeleton on the user's hand is computed as a fraction of the hand's weight W_{hand}, as illustrated in Eq. 4.8.

$$F_{grav} = z_{hand} \cdot W_{hand} = \cos(\phi)\cos(\psi)cos(\theta - 77) \cdot W_{hand} \tag{4.8}$$

Finally, a gain G_{grav} (different for extension and flexion) is used to fine-tune and adjust the mechanical support. When $\dot{\theta}$ is positive the extension gain is used, and when $\dot{\theta}$ is negative the flexion gain is used. The *gravity compensation* block within the green line in Fig. 4.2 is processed online at 1 kHz by the Teensy microcontroller.

4.3.3 Subjects

Ten healthy participants (7 males, mean age: 27.7±3.8, ranging: [22, 33] years) and ten stroke survivors were recruited. In the healthy participant group, eight were identified as right-handed and two as ambidextrous according to the Edinburgh inventory (Oldfield, 1971). In the stroke survivor group, one withdrew for reasons unrelated to the study, one had very little

sEMG activity, and two had very high co-contraction levels, which left six stroke survivors (4 males, mean age: 57.3±12.7, ranging: [40, 70] years) that performed the task. Details about stroke participants can be found in Table 4.1. The study was approved by the institutional ethics committee of ETH Zurich. All subjects gave signed, written informed consent in accordance with the Declaration of Helsinki before participating in the experiment.

4.3.4 Experimental setup

The experimental setup includes a host computer (see Fig. 4.2) for data processing/recording and displaying the visuomotor task, the *eWrist* for actively supporting the wrist and measuring interaction force, angular position/velocity and IMU data, and the Myo armband for collecting sEMG signals on the forearm as depicted in Fig. 4.4. Participants were seated on a chair in front of a screen with the *eWrist* and Myo armband mounted on their left forearm/hand for healthy participants and on their impaired forearm/hand for stroke participants. The forearm was placed on an armrest whose height was adjusted so that the shoulder was at 45° of abduction and the elbow formed an angle of 90°. Moreover, the hand protruded from the armrest so as to allow extension/flexion wrist movements.
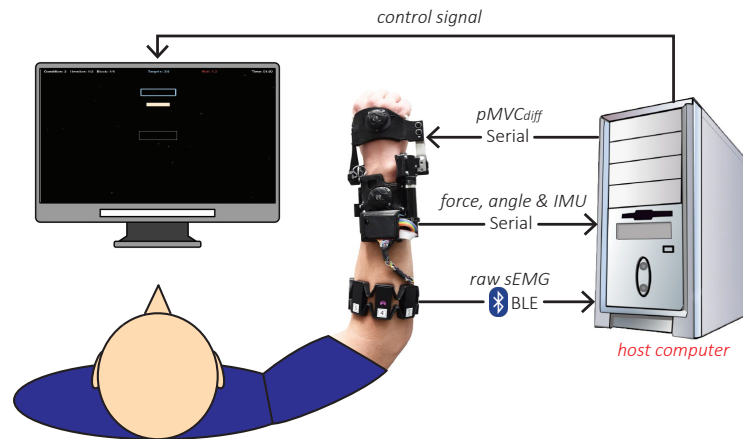
Figure 4.4: Experimental setup of the visuomotor task.

4.3.5 Visuomotor task

To assess the functionality of the variable admittance scheme and the controllers, a goal-directed experiment was developed in the form of a visuomotor task (VMT). The goal of the VMT was to reach targets with a cursor whose position is directly mapped in real-time to the angular position θ of the exoskeleton. The targets were placed at different positions on the screen (i.e. different θ) and required the participants to perform extension ($\theta > 0$) and flexion ($\theta < 0$) wrist movements to reach them (see Fig. 4.1c). Once a target appeared, participants had 5 s to acquire it. When the cursor was in the target, the latter started to turn green as an indication of correct positioning. The target was acquired if the cursor remained 1 s within

Table 4.1: Details on stroke participants (N=6)

Subject	Age [yrs]	Sex	Time PS [mth]	Stroke type	Impaired side	Handedness	FM-UE	ROM_{act} [°]	ROM_{pas} [°]
S1	70	male	167	haem.	left	right	44	-33 / 42	-58 / 76
S2	54	male	144	haem.	left	right	43	-50 / 54	-68 / 74
S4	64	male	162	haem.	right	ambidextrous	52	-31 / 34	-71 / 60
S6	70	male	52	isch.	left	right	23	-45 / 11	-71 / 72
S7	40	female	36	haem.	right	left	22	-57 / 56	-77 / 78
S10	47	female	59	isch.	right	left	26	-52 / 22	-68 / 62

Note: PS = poststroke, FM-UE = Fugl-Meyer for upper extremities, haem. = haemorrhagic, and isch. = ischemic.

the target's boundaries. Once a target was acquired or 5 s elapsed, the target disappeared and the cursor was moved back into the home rectangle (see Fig. 4.5b). The VMT was performed by both healthy and stroke participants, but the testing profile for each cohort was different. Before each testing session, a calibration phase was performed for each participant. The VMT was designed in Python 3.6 and implemented on the host computer running Ubuntu 18.04 LTS[5].
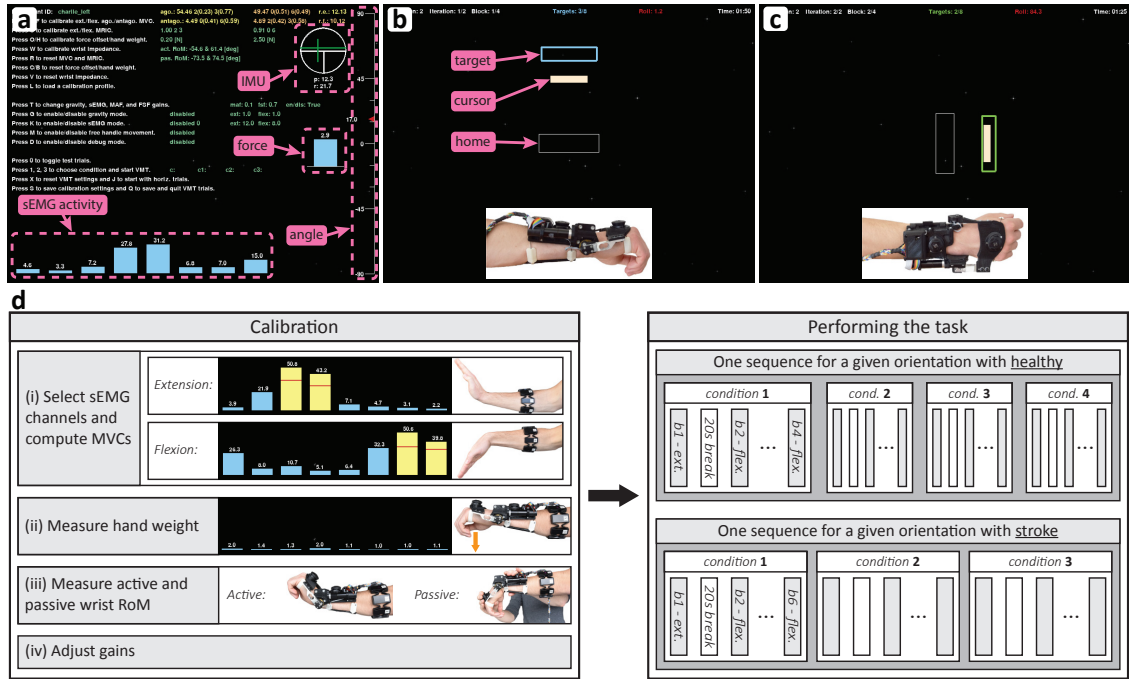
Figure 4.5: a Calibration window of the VMT where sEMG activity, force, wrist angle and IMU readouts are displayed in real-time. **b** VMT during vertical and **c** horizontal movements. **d** *Left:* calibration phase where in (i) MVC (indicated with a red bar) is measured on the two selected electrodes (in yellow) for extension and flexion separately, in (ii) low sEMG activity is required to assess W_{hand}, in (iii) active and passive (with the help of the experimenter) ROM is assessed, and in (iv) the gains are adjusted. *Right:* description of the two different sequences for healthy and stroke participants.

Calibration phase

The calibration phase depicted in Fig. 4.5d consisted of (i) manually selecting two channels for extension and two channels for flexion, and determining the maximum voluntary contraction (MVC), (ii) assessing the weight of the user's hand, (iii) evaluating the active and passive ROM of the wrist joint, and (iv) adjusting the sEMG and gravity gains G_{emg} and G_{grav}, respectively (see Fig. 4.2).

---

[5]Processor: Intel(R) Core(TM) i7-4710MQ CPU @ 2.50GHz, RAM: 16GB

Chapter 4. Variable admittance control with sEMG-based support for wearable wrist exoskeleton

(i) Selection of channels and MVCs   In order to obtain the largest sEMG difference $pMVC_{diff}$ during extension (positive diff.) and flexion (negative diff.) movements, a compromise was made between selecting the channels with the highest sEMG activity for a given movement, but also the lowest agonist/antagonist overlap with the channels of the opposite movement. MVC was measured as the maximum sEMG activity that can be sustained for 1 s over an epoch of 5 s. MVC is computed for each channel individually and a weighted average is performed to obtain a single MVC value for extension MVC_{ext} and flexion MVC_{flex}. Thereafter, sEMG signals are normalized to MVC_{ext} and MVC_{flex}. During calibration, participants received real-time visual feedback of the activity of all 8 channels as shown in Fig. 4.5a.

(ii) Assessment of the hand's weight   The hand's weight W_{hand} was measured by the load cell when the participant was wearing the exoskeleton, the forearm placed horizontally, and θ set at 17° in extension (see Fig 4.1c). During the measurement, participants were asked to fully relax their wrist joint, which could be verified by checking sEMG activity.

(iii) Evaluation of the wrist's ROM   First the active ROM ROM_{act} was assessed, and then the passive ROM ROM_{pas}. The participant was wearing the device (which was uncoupled to allow a free wrist motion) and was asked first to fully flex and then fully extend the wrist. Maximal angles reached in extension and flexion were obtained from the real-time angle readout depicted in Fig. 4.5a. For the passive ROM assessment, the wrist of the participant was manually flexed and extended by the experimenter until discomfort was reported.

(iv) Adjustment of sEMG and gravity gains G_{emg} and G_{grav} were adjusted to provide adequate mechanical support to the participant. A balance was found between increasing the normal excursion of the wrist and keeping good control of the device.

Assessment of variable admittance scheme with healthy participants

The functionality of the variable admittance scheme was evaluated with healthy participants performing the VMT. For this purpose, the task was performed with and without adaptation of the damping parameter B_n (damping factor). Both the sEMG and gravity controllers were evaluated (controller factor). In order to assess the influence of gravity, the task was executed in two different orientations, i.e. during vertical and horizontal wrist movements (see Fig. 4.5b/c). The testing profile depicted in Fig. 4.5d consisted of two sequences, one for each orientation. The first sequence was always performed in the vertical orientation followed by the horizontal orientation. A sequence was composed of 4 conditions in which the controller and damping factors were interchanged and the order of these factors was pseudo-randomized across participants. Each condition was composed of 4 blocks. A block included 8 trials (i.e. 8 targets to acquire), where the height of targets were set to 40% and 80% of ROM_{pas} (i.e. 4 targets per height). The order of targets was pseudo-randomized. The first block of a condition

was always extension trials followed by flexion trials, and continued in an alternating manner. Blocks were separated by a 20 s break.

Assessment of controllers with stroke participants

The sEMG and gravity controllers were evaluated with stroke survivors performing the VMT. Both controllers were compared to a control condition named transparent mode. In the transparent mode, the motor is physically uncoupled from the handle (see orange arrow in Fig. 4.1a), which allows the latter to move freely in extension and flexion directions. Only the angular position of the wrist θ and IMU data are recorded. In this assessment, the testing profile was similar to the previous experiment (see Fig. 4.5d) except for the following points: 1) the adaptation of B_n was always enabled, 2) a sequence consisted of 3 conditions, one for each control mode (i.e. sEMG, gravity, and transparent), and the order of the control modes was pseudo-randomized across participants, 3) a condition was composed of 6 blocks, and 4) a block consisted of 8 trials with the height of targets set to 20%, 40%, 60%, and 80% of ROM_{pas} (i.e. 2 targets per height).

4.3.6 Evaluation metrics

During the VMT, all data generated by the *eWrist* and the Myo armband were continuously recorded and saved. To quantitatively assess the variable admittance scheme and the controllers, the following metrics were investigated:

- Maximal angular velocity $\dot{\theta}_{max}$

- Maximal angular acceleration $\ddot{\theta}_{max}$

- Normalized integrated interaction torque $\hat{T}_{int}$

- Normalized integrated jerk (NIJ)

- Number of acquired targets

Maximal angular velocity and acceleration

$\dot{\theta}_{max}$ and $\ddot{\theta}_{max}$ reflect the transparency of the device. The higher the velocity and acceleration, the more transparent the device. $\dot{\theta}_{max}$ and $\ddot{\theta}_{max}$ were calculated offline from θ via FDM (finite difference method) described in Eq. 4.9.

$$\dot{\theta}_n = \frac{\theta_n - \theta_{n-1}}{\Delta t}, \quad \ddot{\theta}_n = \frac{\dot{\theta}_n - \dot{\theta}_{n-1}}{\Delta t}, \quad n = \{1, 2, 3, ...\} \tag{4.9}$$

where θ_n / $\dot{\theta}_n$ and θ_{n-1} / $\dot{\theta}_{n-1}$ are the current and previous angular position / velocity measurements, respectively, n the control loop counter, and $\Delta t = t_n - t_{n-1}$ the time difference between the current and previous timestamp. As the sampling time interval of the VMT, Δt is not constant and varies around 0.017 s (60 Hz).

Before the discrete differentiation to obtain $\ddot{\theta}_n$, $\dot{\theta}_n$ was low-pass filtered with a Butterworth filter[6]. Both metrics were computed over the movement initiation and rise phases of the trial, and for trials where the target was reached (see Fig. 4.6).

Normalized integrated interaction torque

$\hat{T}_{int}$ defined in Eq. 4.10 is another indicator of the transparency of the device. The lower the interaction torque, the more transparent the device. $\hat{T}_{int}$ was computed over the movement initiation and rise phases of the trial, and for trials where the target was reached (see Fig. 4.6).

$$\hat{T}_{int} = \frac{1}{\Delta t_{mir}} \cdot \sum_{i=n_{start}}^{n_{end}} T_{int,i} \Delta t \tag{4.10}$$

where $\Delta t_{mir} = t_{n_{end}} - t_{n_{start}}$ is the duration of the movement initiation and rise phases, n_{start} the starting sample point of the movement initiation phase, n_{end} the ending sample point of the rise phase, $T_{int,i}$ the current interaction torque, and $\Delta t = t_i - t_{i-1}$ the time difference between the current and previous timestamp.

Normalized integrated jerk

The NIJ defined in Eq. 4.11 is an empirical measurement of movement smoothness. The smaller the jerk, the smoother and less fragmented the movement (Hogan et al., 2009). NIJ was computed over the whole trial, and for trials where the target was reached (see Fig. 4.6).

$$NIJ = \sqrt{\frac{\Delta t_{trial}^5}{2 \cdot s_{trial}^2} \cdot \sum_{i=n_{start}}^{n_{end}} jerk_i^2 \Delta t} \tag{4.11}$$

where $\Delta t_{trial} = t_{n_{end}} - t_{n_{start}}$ and s_{trial} are the duration and path length of the trial, n_{start} and n_{end} the starting and ending sample points of the trial, $jerk = d^3\theta/dt^3$ the 3rd derivative of the angular position θ, and $\Delta t = t_i - t_{i-1}$ the time difference between the current and previous timestamp. $\frac{\Delta t_{trial}^5}{2 \cdot s_{trial}^2}$ is a normalizing factor to obtain a unit-free measure (Teulings et al., 1997).

---

[6] 2nd order 2 Hz cut-off frequency

$\ddot{\theta}$ was low-pass filtered with a Butterworth filter[6] before the discrete differentiation to obtain $jerk$.

Number of acquired targets

The overall performance of stroke participants in the task is assessed via the number of targets they could acquire.
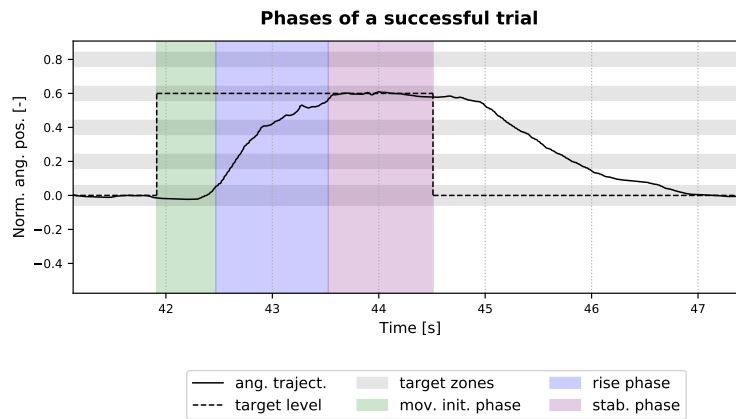
Figure 4.6: The three phases of a successful trial. The plain curve is the normalized (to ROM_{pas}) angular trajectory $\hat{\theta}$, the dotted line is the target level, and the gray horizontal bars are the targets zones and the home zone. A successful trial (i.e. target acquired) is composed of the movement initiation phase (in green), the rise phase (in blue), and the stabilization phase (in purple). A target is reached when the cursor enters the corresponding gray zone.

4.3.7 Data analysis

A repeated measures ANOVA ($\alpha = 5\%$) was used to analyse data from healthy participants. The general model consisted in five factors with 2 levels each, namely: direction (extension/flexion), orientation (vertical/horizontal), controller (sEMG/gravity), height (40%/80%), and damping (with/without dynamic damping). Data were tested for normality. Moreover, the median across all trials of a given condition and subject was entered into the model. The median of these medians is then reported at the group level in the figures. The statistical analysis was performed on four sub-models, where a sub-model only considers a given direction and orientation. The rationale for this approach is that: 1) based on the orientation, gravity influences both controllers differently, 2) the different posture of the forearm in each orientation can influence the sEMG readout (due to different position of muscles relative to electrodes) and the ROM of the wrist joint, and 3) while the gravity controller supports the hand in the extension-vertical condition, it resists movement in the flexion-vertical condition. No statistical analysis was performed on stroke data because of the small sample size and high variability across participants, therefore, the results are descriptive.

4.3.8 Qualitative evaluation

Stroke participants completed two questionnaires during the testing session to quantify their subjective opinion of the different control modes and the visuomotor task in general. The first questionnaire is based on a 5 point Likert scale (Joshi et al., 2015) and assesses the mechanical support provided by both sEMG and gravity controllers. The questions were orientated around seven different aspects of the mechanical support, namely: force, speed, stability, consistency, lag, accuracy and ROM. Each of these aspects were evaluated independently. The second questionnaire is the Raw NASA-Task Load Index (RTLX) (Hart, 2006), which assesses the workload experienced during the VMT with the following aspects: mental/physical/temporal demands, performance, effort and frustration (Hart, 2006; Rubio et al., 2004). Each controller (sEMG and gravity) was assessed separately with both questionnaires, whereas the transparent mode was only evaluated with the RTLX. Finally, all participants could provide further comments at the end of the questionnaires.

4.4 Results

This section presents the behavioural results from healthy and stroke participants performing the VMT with the implemented controllers. The subjective evaluation of the controllers is also presented.

4.4.1 Assessment of variable admittance scheme with healthy participants

First, the results from the evaluation of the variable admittance scheme with healthy participants are presented. We predicted that adaptive damping would reduce jerk without generating higher interaction torques in the pHRI. We also predicted that adapted damping would not decrease maximal movement velocity and acceleration compared to the non-adaptive condition.

Fig. 4.7a presents the NIJ results at the group level. A significant main effect of damping (df=1, F≥50.569, p≤0.001) and height (df=1, F≥71.632, p≤0.001) factors is observed across all models. A strong interaction effect (df=1, F≥51.823, p≤0.001) between damping and height was also observed across all models, which is clearly driven by increased jerk at the higher target level when B_n was not dynamically adapted. However, when B_n was actively adapted, jerk remained consistently low across all conditions. Moreover, while there was not a significant difference in jerk between the sEMG controller and the gravity controller for vertical orientations (df=1, F≤0.844, p≥0.382), there was a significant difference for horizontal orientations (df=1, F≥5.115, p≤0.050).

In Fig. 4.7b, $\hat{T}_{int}$ varies substantially across conditions. Note that for a given direction, a negative interaction torque indicates that the device was supporting the movement, while a positive torque means that the hand was driving the movement. In the flexion-vertical-
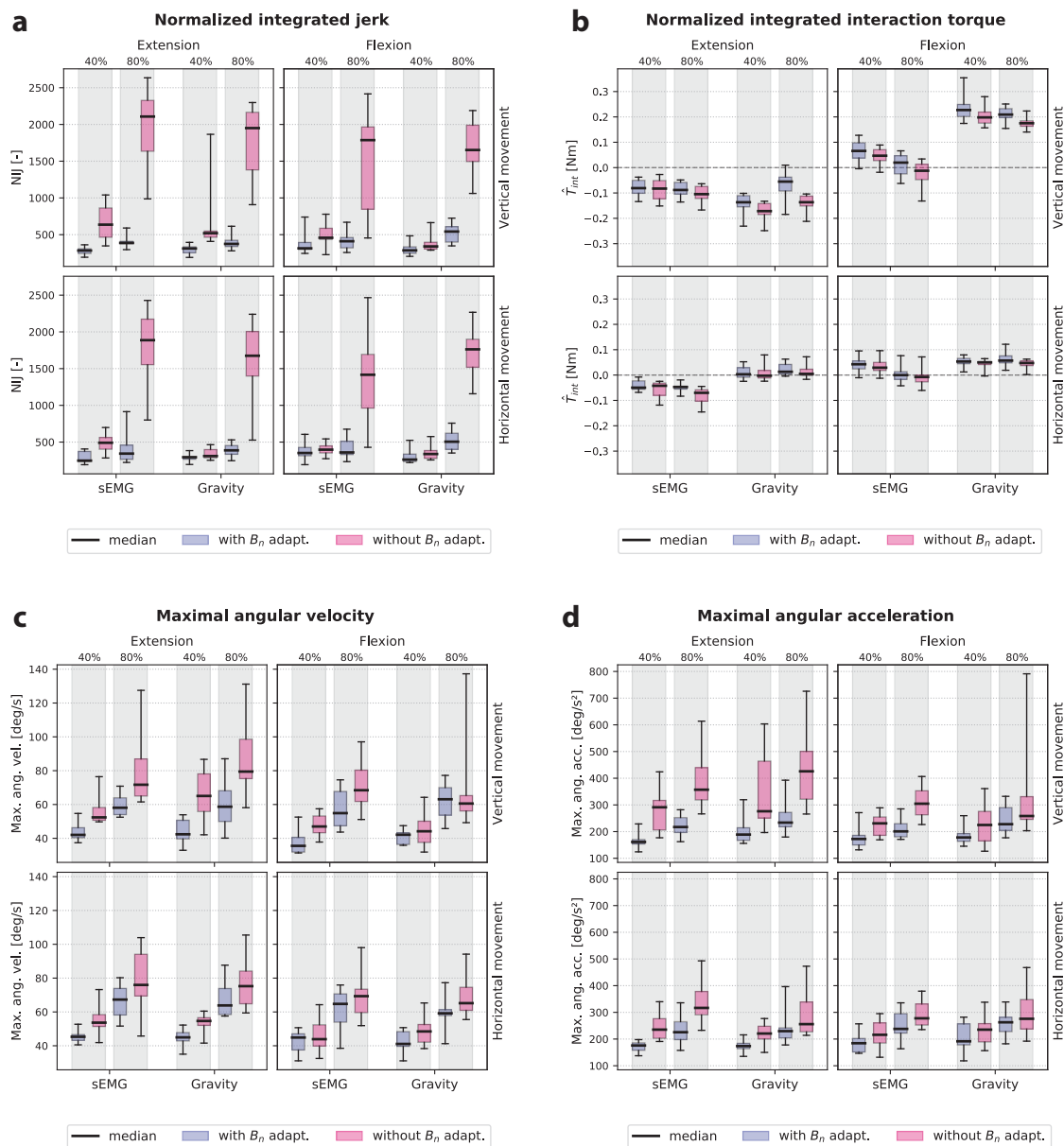
Figure 4.7: The boxplots show the median, interquartile range (IQR), and min./max. values of ten healthy participants for all factor permutations. The adaptive damping condition is shown in blue and the non-adaptive damping condition in pink. **a** Normalized integrated jerk (NIJ) and **b** interaction torque $\hat{T}_{int}$. **c** Maximal angular velocity $\dot{\theta}_{max}$ and **d** acceleration $\ddot{\theta}_{max}$.

gravity condition, $\hat{T}_{int}$ is largely positive since participants had to counteract the upward supporting force imparted by the gravity controller. In all four models, $\hat{T}_{int}$ was significantly more positive in the adaptive damping condition (df=1, F≥5.298, p≤0.047). This suggests that the user was slightly more supported (or less hindered) by the device when the damping was not dynamically adapted.

In Fig. 4.7c, $\dot{\theta}_{max}$ was significantly greater at higher target levels compared to lower target levels in all models (df=1, F≥36.275, p≤0.001), and was significantly greater when damping was not adaptive compared to adaptive damping (df=1, F≥6.455, p≤0.039). The same pattern of results was observed for $\ddot{\theta}_{max}$ (see Fig. 4.7d), main effect of target height: df=1, F≥10.160, p≤0.015; main effect of damping condition: df=1, F≥8.391, p≤0.023). Both the maximal angular velocity and acceleration results are inconsistent with our prediction that adaptive damping would not alter transparent rendering. In both metrics, the pHRI was consistently faster and more reactive when B_n was not dynamically adapted. Based on these results, we conclude that the implemented controllers offer a trade-off between faster but more jerky movements versus slower but more stable movements. For stroke rehabilitation, stability is more important than speed, therefore, we favoured the former for the assessment with stroke participants.

4.4.2 Assessment of controllers with stroke participants

Fig. 4.8 presents the percentage of acquired targets during the VMT for all stroke participants. Generally, the benefit of the device with the implemented controllers remains limited. In the transparent mode, participants had difficulties to reach the 80% targets especially in the extension-vertical condition since they had to move against gravity. This problem is somewhat less severe for the flexion-vertical condition and for both horizontal conditions. Whereas most participants benefited from the sEMG and anti-gravity support in the extension-vertical condition for the higher targets (especially S2, S4 and S7), less benefit was observed in other conditions. In particular, the anti-gravity controller negatively affected flexion movements since participants had to overcome the upward supporting force.

Although both controllers increased the ROM of participants and helped them to reach higher targets (see percentage of reached targets in Fig. B.1 in the Appendix), they were still unable to stabilize their wrist to acquire the target within 5 s. This is particularly true for lower targets in the horizontal orientation with the sEMG-based controller. The loss of control could be the combined effect of not being influenced by gravity and the higher sensitivity of the controller at smaller angles due to $G_{att}(\theta)$.

In the extension-horizontal-gravity condition, which requires only the variable admittance controller since no gravity compensation force was generated, participants also experienced difficulties to stabilize their wrist within the target boundaries. These instabilities could have been caused by an inability to relax the wrist joint, and could not be resolved by the dynamic damping. Moreover, as the horizontal condition was always performed after the vertical condition, fatigue and spasticity were more likely to be present during this phase, which could have resulted in increased stiffness of the joint. Nevertheless, participants S6 and S10 did appear to benefit from the mechanical support and acquired more targets compared to the transparent mode, especially in the extension-vertical condition (but also in both horizontal orientations). Interestingly, both S6 and S10 were amongst the most impaired of

our participants, with FM-UE scores of 23 and 26 respectively.

Subjective evaluation

A synthesis of the two questionnaires that stroke participants completed immediately after using a controller for the first time is presented in Fig. 4.9.

Fig. 4.9a shows the scores of the questionnaire assessing mechanical support from the *eWrist* during the VMT, which is based either on sEMG signals or on the orientation of the device. The score ranges from 0 to 100. A high score indicates that the aspect of the mechanical support being rated was appropriate. Based on the median score for each aspect, both the sEMG and gravity controllers were evaluated in a similar way. Generally, participants found that the supporting torque was too weak (*Force* median score (sEMG/gravity): 50.0/41.7), especially in the flexion-vertical-gravity condition where the device resisted the movement. However, they did rate the assistive movements as sufficiently fast (*Velocity* score: 83.3/95.8). Moreover, the sEMG controller was found to be less stable than the gravity controller (*Stability* score: 68.7/87.5). The support from both controllers was perceived to be consistent with the movement intention (*Consistency* score: 87.5/87.5), and the lag between the intention to move and the assistance provided by the device was sufficiently low (*Lag* score: 87.5/87.5). Because of a low supportive torque, participants tended to undershoot higher targets, and because of the high sensitivity of the controllers, they tended to overshoot lower targets, which impacted their accuracy (*Accuracy* score: 62.5/66.7). For the same reason, they found that the assistance was active across a range of motion that was too small (*RoM* score: 58.3/45.8).

Fig. 4.9b shows the scores of the RTLX questionnaire, which also ranges from 0 to 100 and reflects the workload experienced during the task. The lower the score, the lower the perceived workload. A high score in *Performance* indicates that the participants felt that they were successful in performing the task. In most cases and based on the median score for each aspect, all three control modes were evaluated equally. *Mental*, *physical* and *effort* ratings (median scores for sEMG/Transparent/Gravity: 40/40/40, 87.5/67.5/80, and 77.5/67.5/77.5, respectively) exhibit large variability across participants. Generally, they found the task very demanding mentally and physically, most likely because of its difficulty (to reach 80% of the passive ROM) and its duration (~ 1.5 hr). As a resulting of the perceived difficulty, they rated their performance to be rather low (*Performance* score: 60/50/57.5). All participants reported that they were not rushed (*Temporal* score: 17.5/12.5/17.5) during the task, nor frustrated (*Frustration* score: 7.5/7.5/10).

In the comments left by the participants, some reported that the scoring of *performance* and *effort* was mainly influenced by the difficulty of reaching higher targets. They also highlighted the resistance of the gravity controller in the vertical movement condition and stressed that it was difficult and unnatural to hold the forearm position for the horizontal movement condition. Apart from that, all participants expressed interest and motivation in the experiment, and reported that the task encouraged active participation and was challenging. None of
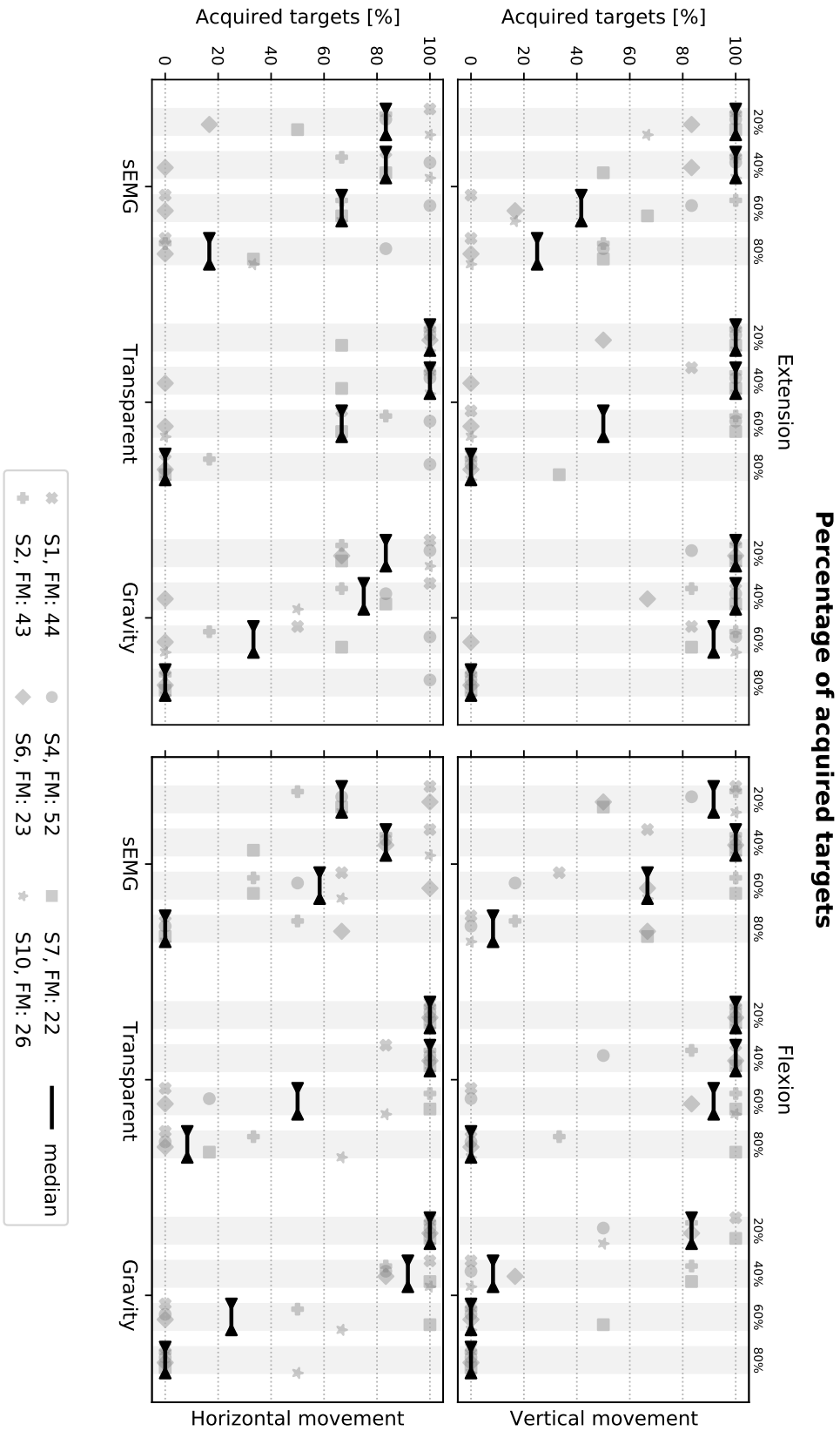
Figure 4.8: Percentage of acquired targets in stroke participants in all conditions. The median across participants is shown.
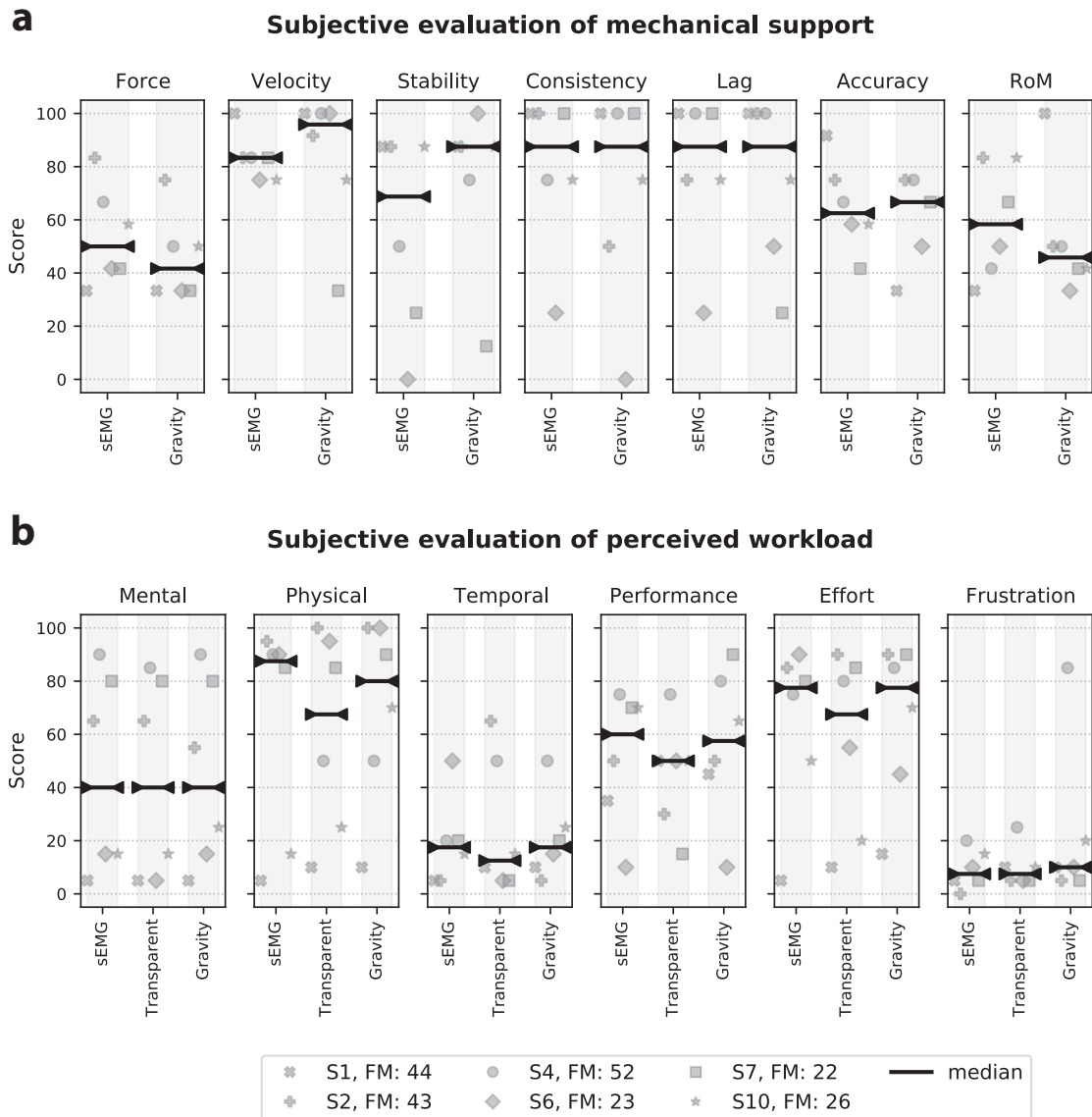
Figure 4.9: Score comparison derived from questionnaires for stroke participants where the median is shown. **a** Scores from the questionnaire assessing the mechanical support. The average score over all aspects is 66.1±12.8 for sEMG and 64.1±12.9 for Gravity. **b** Scores from the RTLX questionnaire. The average workload score excluding *Performance* (Grier, 2015) is 40.2±25.2 for sEMG, 39.0±21.4 for Gravity, and 44.8±23.2 for Transparent.

them expressed any discomfort due to the device. Generally, participants considered that the duration of the testing session was adequate, however, S7 and S10 showed clear signs of fatigue at the end of the session. Finally, participants were asked to score their most favoured (+1) and least favoured (-1) control modes. As shown in Table 4.2, the sEMG controller was favoured slightly more than the gravity controller or the transparent mode.

79

Table 4.2: Control mode preference of stroke participants

Subject	sEMG	Gravity	Transparent
S1	+1	-1	0
S2	+1	0	-1
S4	0	+1	-1
S6	0	+1	-1
S7	0	-1	+1
S10	0	-1	+1
Total	**2**	-1	-1

4.5   Discussion

This study explored the implementation of a variable admittance scheme on a non-backdrivable portable wrist exoskeleton. In addition, an sEMG-based and a gravity-based controller were implemented in order to enhance the functionality of the wrist and promote voluntary effort. The variable admittance scheme and both controllers were first optimized with ten healthy participants performing a visuomotor task, and then evaluated in six chronic stroke patients performing the same task. The results with healthy participants showed that the variable admittance scheme could successfully and significantly improve the stability of the pHRI, but at the cost of a decrease in transparency. Furthermore, while both controllers improved the ROM of the wrist for stroke patients, the stabilization during target acquisition remained challenging. This was particularly true with the sEMG controller for the most distant targets, but also for near targets during horizontal wrist movements. Finally, the results also showed that patients with higher levels of impairment were more likely to benefit from the support provided by the *eWrist*.

4.5.1   Considerations on the variable admittance scheme

Humans are dynamic systems characterized by a time-varying impedance and their interaction with non-backdrivable haptic devices featuring admittance control can lead to instabilities. This usually occurs when the human limb stiffens to stabilize its motion. In addition, during interaction with an unstable robot limb stiffness is increased by the central nervous system in order to reduce these external perturbations (Burdet et al., 2001). As the stiffness of the user is not directly measurable, the controller cannot easily account for this issue.

In this work, the frequency and magnitude of the interaction force signal was analysed to detect instabilities and dampen the system accordingly using a variable admittance scheme. The implemented variable admittance controller acted solely on the damping parameter to attenuate instabilities. Damping is a velocity-dependent parameter that dissipates energy in the pHRI. Therefore, increased damping leads to more energy dissipation and the restoration of stable behaviour, but at the same time imposes increased resistive force during steady velocity movements. Previous studies have shown that only adapting the damping and not the inertia

parameter could unbalance the admittance dynamics and affect the usability of the robot (Lecours et al., 2012). It was suggested that adapting the inertia term (instead of damping) is more beneficial for low-effort movements, and only affects acceleration/deceleration phases (Dimeas et al., 2016). However, the optimal strategy depends on robot structural dynamics, the limitations of the actuators and sensors, and the implementation of the admittance controller, which highlights the need to make design decisions on a case-by-case basis (Eppinger et al., 1986).

We based our decision on initial experiments where we investigated the effect of adapting: 1) only the damping, 2) only the inertia, and 3) both terms while keeping a constant ratio between them. These experiments revealed that adjusting only the damping was most promising because it had the highest impact on stability compared to the two other options. Nevertheless, deeper consideration of the other options, especially with regard to parameter tuning, might have also revealed positive effects on both stability and transparency.

Several alternative strategies could have been considered. First, the position of the robot can be used to dissociate low frequency components of the human movement from high frequency components caused by the instability (Ryu et al., 2008). However, the admittance control described in Eq. 4.1 acts as a low pass filter for high frequency position oscillations. Consequently, the reduced magnitude in the frequency domain deteriorates the detection of instability, which is de facto not a suitable approach for admittance control (Dimeas et al., 2016). Moreover, whereas previous studies have used a fast Fourier transform (FFT) to analyse the frequency domain (Dimeas et al., 2016; Ryu et al., 2008), the present work implemented a less computationally demanding algorithm for use on a microcontroller. The algorithm simply counts the number of times the force signal changes sign in a moving window of m=200 samples, while this window moves in increments of eight samples. The window length m and the increment size were optimised to obtain sensitive and reactive damping adaptation, but also to not significantly slow down the control loop (1 kHz). These parameters were tuned on a single healthy subject and never changed for the behavioural assessments. Although user-dependent adjustment of these parameters would improve performance, the algorithm appeared to be a reliable and suitable solution for embedded systems with limited computing power as shown in Fig. 4.3c.

Second, the implemented method does not prevent instability but only eliminates the negative effects of oscillatory behaviour. Therefore, instead of acting upon the instability retroactively, other methods analysed co-activation level in the muscles in order to detect an increase of stiffness in the limb and proactively dampen the system (i.e. before the disturbance occurs) (Bian et al., 2018; Castellini et al., 2014; Gallagher et al., 2014; Grafakos et al., 2016). By comparing the co-activation level in the forearm (extensor vs flexor) between the movement initiation/rise phases and the stabilization phase of a trial (see Fig. 4.6), a higher co-activation level was observed in the latter phase (see Fig. B.2 in the Appendix). This demonstrates an increase of stiffness in the wrist joint during target acquisition. Such a strategy proved to be robust with healthy subjects manipulating end-effectors. It would be interesting to test a

similar strategy with stroke survivors who exhibit irregular sEMG patterns.

Third, our feed-forward approach of adapting the variable gain $G_{stif}(\theta)$, which is subject-dependent and dampens the system more rapidly for higher wrist angles, was motivated by the increase in stiffness of the wrist joint close to the limit of its ROM. This assumption proved to be correct as shown in Fig. 4.7a where the pHRI was significantly more jerky for the most distant targets. This gain accounts for the passive stiffness of the joint related to its biomechanical properties, however, stroke survivors may exhibit involuntary increase in stiffness over the whole ROM because of tremor or spasticity that may evolve over the course of rehabilitation. In such cases, it might be promising to explore whether a feedback approach analysing co-activation level or abnormal contractions in the muscles could improve stability of the control mechanism.

In summary, our variable admittance control strategy, which can be implemented on a microcontroller, reduced involuntary oscillations caused by changes in wrist stiffness. This was achieved at the cost of reduced transparency, which was still sufficient to allow functional movements. Nevertheless, future work might make use of muscular co-activation detected from the sEMG signals to dampen the system either proactively or via a co-activation-specific feedback mechanism.

4.5.2 Considerations on the sEMG controller

The performance of the sEMG-based controller with stroke participants was surprisingly lower for near targets in horizontal orientations compared to the other control modes as shown in Fig. 4.8. This decrease in performance results from a loss of control due to higher sensitivity of the controller (see Fig. B.3 in the Appendix where jerk is more important for the sEMG controller compared to the gravity controller in these conditions). The higher sensitivity of the sEMG controller for near targets comes from the combined effect of $G_{stif}(\theta)$ and $G_{att}(\theta)$, which confer less damping and more reactiveness to the sEMG signal for small angles. The gain $G_{att}(\theta)$ models the increase of sEMG production required to move the wrist close to the limits of its ROM, and prevent excessive mechanical support that would push the wrist beyond these limits. Although $G_{att}(\theta)$ is subject-dependent and based on the calibrated MVC and passive ROM, its combined effect with G_{semg} can result in an overly sensitive controller at small wrist angles. Moreover, since $G_{att}(\theta)$ is based on isometric contractions, it can introduce a systematic error when applied under dynamic conditions (Clancy et al., 1997). With G_{semg} a trade-off had to be found in order to increase the ROM while maintaining good controllability.

The sEMG-torque relationship is complex and is influenced by many factors such as electrode placement relative to the innervation zone, muscle length, cross talk from nearby muscles, and number of motor units recruited (De Luca, 1997; Farina et al., 2001). Moreover, several of these factors vary non-linearly with respect to movement velocity and joint position (Farina, 2006; Solomonow et al., 1991). The simple and straightforward approach adopted in this work was motivated by 1) a belief that the human central nervous system could compensate for

a less accurate torque estimate provided by the robot as long as the latter is physiologically coherent, and 2) an envisioned implementation on an embedded system with limited processing power (Lenzi et al., 2012). For optimal performance of the sEMG-based controller, the electrodes must be carefully selected in order to maximize $pMVC_{diff}$ during extension and flexion movements. Two electrodes were chosen for each direction so as to limit the effect of single electrode variations and thus to capture a more general pattern of activation. However, this strategy reaches its limits in the case of systematic co-contractions in the forearm, and consequently the activation patterns between extension and flexion movements cannot be sufficiently dissociated. In this study, the electrodes were selected by the experimenter, however, an automatic selection that minimizes overlap between extension and flexion activations could be implemented.

Finally, one assumption was that the sEMG-based controller might further excite the system in case of instabilities in the pHRI. As the user fights against the oscillations, she/he produces counterproductive sEMG patterns that are picked up by the controller and further excites the system. However, our results show that jerk is not significantly different between the sEMG and the gravity controller (see Fig. 4.7a) suggesting that this is unlikely to have occurred. An explanation could be that given our setup and filtering process, the readout of sEMG signals was too slow to pick up fast oscillating patterns in the muscle activity, and thus could not influence the controller. Nevertheless, this problem could arise in sEMG-based control system with faster sampling rates, and would further motivate the use of a variable admittance control.

4.5.3 Considerations on the behavioural evaluations

In this work, the implemented controllers were evaluated during both vertical and horizontal wrist movements in order to assess the influence of gravity on the control of a portable exoskeleton. With healthy participants, this influence can be observed in the absolute value of the interaction torque $\hat{T}_{int}$, which was generally lower for horizontal movements as for vertical (see Fig. 4.7b). This discrepancy is normal for the gravity controller but requires further explanations for the sEMG controller. In the extension-vertical condition, the hand had to be moved against gravity, which triggered more muscle activation and thus generated more support from the device (i.e. negative $\hat{T}_{int}$). This support is less pronounced in the extension-horizontal condition since less muscle activation was required to move the hand. A similar general trend is observed with $\dot{\theta}_{max}$ and $\ddot{\theta}_{max}$ (see Fig. 4.7c/d). Especially in the extension-vertical conditions, the higher muscle activation and the anti-gravity supportive torque moved and accelerated the user's hand faster. Moreover, as the MVC calibration was solely performed in the vertical orientation, the performance of the sEMG controller could have been affected when performing the task in the horizontal orientation. Indeed, the position of muscles relative to the electrodes might have shifted due to the supination of the forearm (Kim et al., 2018a). Finally, as the gravity controller depends on θ, this resulted in less support for larger angles as shown in Fig. 4.7b for the extension-vertical condition.

The fatigue of stroke patients affected significantly the sEMG controller (Kim et al., 2016). Especially for the most distant targets, the fatigue added to the difficulty of the task resulted in more pronounced levels of co-contraction that ultimately decreased the efficiency of the controller (see Fig. B.2 in the Appendix). Moreover, actively holding the forearm for the horizontal condition added an extra contribution to fatigue. To counterbalance the effect of fatigue, the order of controllers in the task was changed across participants. The width of the target, which is a critical factor of the difficulty to acquire targets, was empirically set with healthy participants performing the task. It reflects a normal ability that stroke survivors should have when using the device. Moreover, the difficulty to reach the most distant targets was largely expressed in the workload feedback with the *Physical* and *Effort* aspects (see Fig. 4.9b). In these two aspects, the transparent mode scores better (i.e. lower workload) than both controllers. This could explain a lower efficiency of the controllers for distant targets or an unsatisfied expectation towards the controllers. Finally, the large variability in some of the aspects of the workload scores may reflect a different level of involvement of participants in the task.

4.5.4 Limitations and future directions

There were a couple of limitations in our subjective evaluation of the controllers. Given our testing profile, the questionnaires for a given controller were always completed by the participant after the first sequence of vertical trials. This permits 1) to assess the condition where the controllers support the wrist the most (i.e. during vertical movements), and 2) to obtain the most accurate and vivid feedback. However, the first control mode to be assessed does not benefit from a prior comparison, and the horizontal orientation is not represented in the subjective feedback. Moreover, the assessment of the mechanical support could have been laborious for participants with somatosensory deficits. Unfortunately, this aspect of their impairment was unknown. Half of the stroke survivors tested in this study presented with moderate to low deficits in the wrist function, and therefore felt more impaired by the device than helped. We should have not only recruited more impaired patients in the acute/sub-acute phase, but also a larger sample size. The small sample size and the wide impairment range of the tested cohort explains the low statistical power and large variability in the results. Testing a larger sample size would have allowed us to determine from which level of deficit a patient could benefit the most from the device. Furthermore, the stroke survivors recruited in this study were volunteers and highly motivated, so may not be representative of the broader stroke population.

Future work could focus on combining features from both controllers in order to enhance the mechanical support. For instance, the intention of the patient could be captured through the sEMG signal to enable/disable the support of the gravity controller. This could apply when the sEMG signal is too weak and noisy for proportional control, but the intention could still be picked up via classification methods (Khokhar et al., 2010; Shahmoradi et al., 2015). In the same vein, the spatial orientation of the device could be used to adapt the gains

of the controllers (especially sEMG) to make the pHRI more stable. As envisioned in this study, the developed controllers and algorithms should remain simple and efficient enough to be implemented in embedded systems. In this regard, the host computer in this study (cf. outlined in red in Fig. 4.2) could already be implemented in the microcomputer of the *eWrist* (Lambelet et al., 2020).

4.6 Conclusion

In the context of non-backdrivable exoskeletons for rehabilitation therapy, it is important that the physical human-robot interaction remains reactive and stable. However, instabilities can occur when the limb of the user stiffens to stabilize its motion. In this paper, we implemented a variable admittance control together with an sEMG-based controller that promotes voluntary effort, and with a gravity compensation controller that supports weakness in the wrist joint. We have demonstrated that the implemented control scheme remains stable during a passive stiffening of the wrist joint, but impacted the transparency of the device. Moreover, we have shown that our controllers could enhance the capability of stroke survivors in the most extreme wrist positions even though stabilizing the device within a given target remained challenging. This may have been perceived as requiring a high physical effort, but this is not necessarily a disadvantage, as the purpose of the device is to facilitate the patient's voluntary effort to perform movements that are not possible without the support. Finally, this work has drawn attention to the influence of gravity on the proportional control of a portable exoskeleton, paving the way for further development in that field.

5 General discussion

*A common mistake that people make when trying
to design something completely foolproof is to
underestimate the ingenuity of complete fools.*
— Douglas Adams

5.1 Summary and synthesis

Often overshadowed by hand function in the scientific literature, the wrist plays a fundamental role in ADL. Impairment of the wrist heavily impacts the independence and quality of life of people with neuromotor deficits following a stroke. As one of the leading causes of long-term adult disability and dependency, stroke has an enormous economic impact on healthcare systems and society (Lapchak et al., 2017). With an increased prevalence of stroke with age, a worldwide ageing population, and improved stroke survival rates, the economic burden of stroke rehabilitation is bound to increase in the coming decades. Therefore, novel and cost-effective rehabilitation approaches need to be developed and made commonplace.

Rehabilitation treatments are most effective during the acute and sub-acute phases poststroke, which are thought to be a period of heightened plasticity in the brain. Nevertheless, neuroplasticity and motor recovery can be promoted long after a stroke onset through intensive motor learning protocols (Bowden et al., 2013). The inclusion of somatosensory feedback during the rehabilitation therapy is essential for relearning functional, coordinated, and accurate movements (Smania et al., 2003). Moreover, the promotion of internally generated voluntary movement is essential for triggering cortical reorganization and boosting motor recovery (Kitago et al., 2013; Murphy et al., 2009). Robot-assisted therapy is an ideal approach for providing all these modalities. It can complement conventional movement-based therapy in a motivating and controlled manner, deliver high intensity training stimuli, and provide proportional assistance-as-needed based on user intention and voluntary effort (Lotze et al., 2003).

So far, robot-based therapies have mainly been implemented in clinical environments under the supervision of clinicians. However, after discharge from the hospital or simply between weekly therapy sessions, the lack of training opportunities is real and needs to be addressed (Bernhardt et al., 2004). The field of home-based rehabilitation using powered wearable robotic technologies for patients with neurological injuries is still in its infancy. Despite the tremendous work accomplished in this field (Bos et al., 2016), most of the projects remain in the research domain and are therefore insufficiently accessible for daily therapeutic treatments. Moreover, among the many challenges to develop devices targeting independent use, there is, to the best of knowledge, no existing solution that meets the requirements in terms of usability, functionality, and intuitive control. In particular, usability has been overlooked in many projects targeting home-based therapy in favour of more technical considerations, but remains a critical aspect that needs to be considered in the future (Lambelet et al., 2020; Meyer et al., 2020).

Following this line of thought, the work presented in this thesis aimed to develop a fully wearable exoskeleton for active wrist support with a high degree of usability. For the sake of simplicity, which is of paramount importance in the context of unsupervised rehabilitation training, the device was designed to support a single DOF that covers most functions of the wrist during ADL (Palmer et al., 1985). Through multiple prototype iterations, a functional

solution that could be donned and doffed with a single hand was finalized and tested in healthy participants and stroke survivors. Moreover, keeping in mind a vision where the future of rehabilitation will take place in community settings, the development of this work prioritized the selection of commercially available and affordable components, in addition to the use of 3D printing techniques and open-source software. The developed platform served to investigate the feasibility and challenges of an intuitive and robust control scheme implemented on a portable device.

5.2 Thesis contributions

The contribution of this thesis can be divided into two parts. The first part consisted of the development and characterization of the *eWrist* exoskeleton, and mainly focused on the wearability and usability of a portable device for wrist rehabilitation training after stroke. The second part involved the implementation of an intuitive and robust control scheme for the *eWrist*, which was tested on healthy and stroke participants in a visuomotor task.

5.2.1 Development and characterization of the *eWrist*

The *eWrist* is a new 1 DOF fully portable exoskeleton supporting extension and flexion wrist movements. The *eWrist* is non-backdrivable, but force/torque and absolute angular sensors placed at the exoskeleton's end-effector enable the measurement of pHRI dynamics. Various metrics such as maximum output torque and angular velocity/acceleration, position bandwidth, steady-state error, and impedance rendering allowed an objective assessment of the haptic capability of the device. In particular, the renderable impedance range revealed that the *eWrist* can administer transparent and resistive dynamic behaviour, which is important in the context of rehabilitation training to assess the patient's ability to perform movements without being disturbed by the device dynamics (Gupta et al., 2006; Proietti et al., 2016; Vallery et al., 2009). Moreover, important aspects for fully portable exoskeletons, such as weight, physical profile, and autonomy, showed that the developed solution is comparable or better than other work providing similar supportive functions (Choi et al., 2019; Dragusanu et al., 2020; Higuma et al., 2017; Sangha et al., 2016). With the goal of miniaturization and low weight in mind, two custom electronic boards were developed and integrated into the design. After hundreds of hours of use, the electronics proved to be reliable and stable, although an assessment of the current consumption should be carried out in order to improve efficiency and autonomy. The weight of the exoskeleton components placed distally in the prototype presented in Chapter 2 was reduced in the version presented in Chapter 3 by splitting the exoskeleton into two modules. This modular approach has been adopted by several research projects, but also in commercially available products targeting assistance during daily living. The strategy consists of moving the weight of actuators, electronics, and battery to more proximal body parts such as in a backpack (Bützer et al., 2020) or beltpack (Polygerinos et al., 2015; Xiloyannis et al., 2016). Consequently, the most distal part of the exoskeleton is free of sensitive components

such as electronics and sensors, which improves robustness, especially in the context of daily assistance. However, the further the device is removed from accompanying modules, the more its usability is affected. In the commercially available device *NeoMano*, which is composed of a hand module and a forearm module, a trade-off was made to free the hand from as many components as possible, but at the same time not alter usability and wearability (Neofect, 2020).

Usability and wearability were important aspects of the *eWrist* design that were considered and improved throughout the development phase (Lambelet et al., 2020). In the development of the forearm and upper arm modules, novel solutions were investigated to facilitate donning and doffing, and to easily fasten the system. For that reason, solutions such as straps or Velcro, which are commonly implemented in wearable exoskeletons (Dragusanu et al., 2020; Higuma et al., 2017; Sangha et al., 2016), were discarded due to the difficulty to manipulate them with a single hand. Instead, a fixation system that requires a single hand to don and doff the entire device was favoured. This would enable hemiparetic patients to initiate unsupervised and independent training sessions with the device. The implementation of two Boa Closure Systems on the forearm module (Boafit, 2020) permitted easy fastening and placement on the forearm and hand. Given the rigid structure of the *eWrist*, the alignment of the mechanical axis with the biological joint of the user is important for comfort and accurate support (Su et al., 2019). Therefore, the size of the exoskeleton was adjusted based on anthropometric measurements of the forearm and hand. Five different sizes of specific parts of the device could be printed and assembled in a short time, for both the right and left hand/wrist/forearm. Nowadays, the flexibility of this approach can be facilitated thanks to recent advances in 3D scanning methods accessible to everyone with a smartphone (Fitzpatrick et al., 2017; Qlone, 2020). A major and novel contribution to wearability and ease of use of the *eWrist* exoskeleton lies in the upper arm module, whose conception was completely guided by the principle of one-handed donning and doffing. Following the concept of the Boa Closure System using fastening cables, the upper arm module was designed to accommodate changes in body size and volume (Gemperle et al., 1998), and to remain comfortable and efficient in terms of the grip force required for operation. When tested on fifteen healthy participants and two stroke survivors, both cohorts embraced the device and were able to don and doff it independently and quickly after a few practice trials. Nevertheless, the large number of parts that form the upper arm module, and its relative fragility makes it laborious to assemble and not yet ready for everyday use. Taken together, no such attachment mechanism for exoskeletons has been presented in the literature, and this design might trigger further development of novel fixation systems for the human body.

5.2.2 Control of the *eWrist*

Besides the mechanical development and characterization of the *eWrist*, the second part of this work investigated the implementation of a robust, proportional, and intention-based controller for a non-backdrivable wearable exoskeleton. In Chapter 2, the implementation
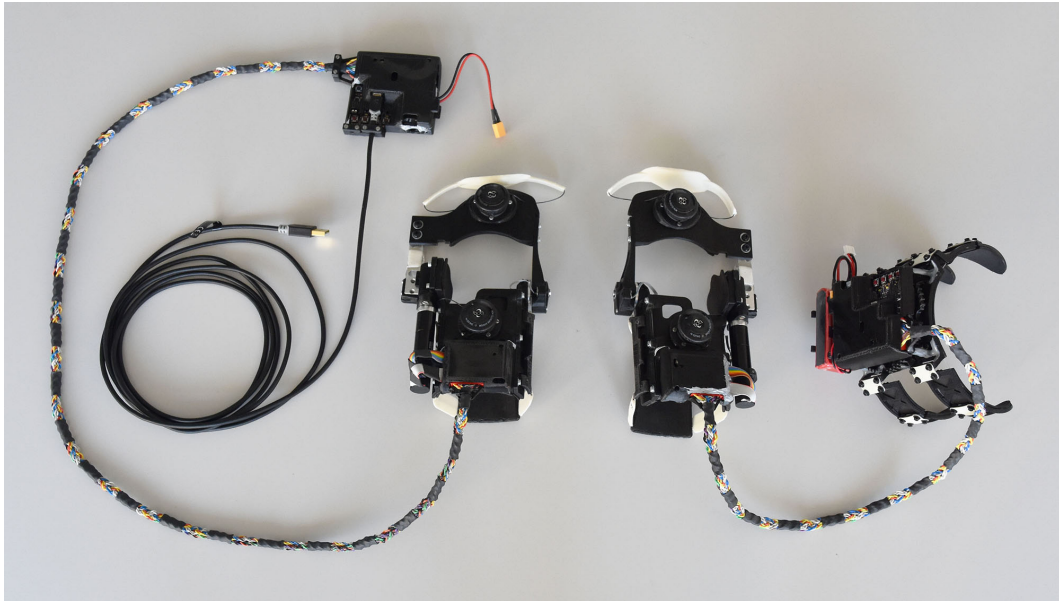
Figure 5.1: The latest versions of the *eWrist* for the left and right wrist. *Left:* Table-top solution. *Right:* Fully wearable solution.

of an admittance scheme together with an sEMG-based controller was evaluated in a single healthy subject. This first attempt confirmed the feasibility of proportional control, which actively supports extension and flexion wrist movements, based on sEMG signals measured with the Myo armband (Lambelet et al., 2017). However, further development was required to tailor the controller to the user and improve its robustness, especially in the context of a wearable exoskeleton for stroke rehabilitation training. The implementation of a variable admittance controller in Chapter 4 aimed at investigating a way to improve the pHRI both in terms of stability and reactivity (Dimeas et al., 2016). More specifically, the ability of the controller to stabilize the robot during stiffening of the joint without affecting its transparency was evaluated in healthy participants and stroke survivors. The novelty of this approach lies in the combination of the variable admittance scheme with a gravity compensation controller and an improved sEMG controller. The results showed that the variable admittance scheme could consistently improve the pHRI stability in healthy participants, but at the cost of a slight decrease in transparency. Even though the sEMG and gravity controllers enhanced wrist functionality in stroke survivors, some oscillations during stabilization of the joint could not be resolved with the current implementation and settings of the controllers.

Whereas variable admittance control has mainly been applied on stationary devices (Bian et al., 2018; Dimeas et al., 2016; Grafakos et al., 2016), implementation on a fully wearable exoskeleton such as the *eWrist* imposed constraints in terms of processing power. For the same reason, a simple and straightforward sEMG-torque mapping was considered for the sEMG-based controller. Other studies investigated different methods such as a musculoskeletal Hill-based model (Buchanan et al., 2004), nonnegative matrix factorization (Jiang et al., 2008),

neural networks and classifiers (Khokhar et al., 2010; Shahmoradi et al., 2015), and multiple fuzzy-neural controllers (Gopura et al., 2008; Hashemi et al., 2014) to produce an accurate torque estimate based on sEMG signals. However, many of these methods usually require extensive calibration, accurate electrode placement (Hargrove et al., 2008; Hwang et al., 2017) and substantial computing power. Moreover, it is believed that the human central nervous system can compensate for a less accurate torque estimate provided by the robot as long as the latter is physiologically coherent (Lenzi et al., 2012). In the study of Chapter 4, a feed-forward approach with subject-dependent gains allowed tailoring the variable admittance scheme and sEMG-based controller to the impairment level of the individual patient. The implementation of these gains within the controllers was an exploratory approach motivated by personal observations and assumptions, but further testing is required to quantitatively assess effectiveness. Integrating gravity compensation on a portable exoskeleton for the wrist joint provided beneficial support for stroke survivors in specific wrist orientations. This approach could be further enhanced by combining it with motor intent detection in order to enable or disable the anti-gravity support when needed. Moreover, the study of Chapter 4 revealed that, in the context of a wearable exoskeleton, proportional control based on sEMG signals should consider the effect of gravity to improve the pHRI stability. In particular, higher sensitivity of the sEMG-based controller was observed when the effect of gravity was reduced (i.e. for horizontal wrist movements).

Additionally, the study presented in Chapter 4 required the development of a platform in Python that reliably collects real-time data from the Myo armband and the *eWrist* exoskeleton. The execution and display of the visuomotor task, as well as the recording of data were also programmed in Python. All these aspects were performed by a host computer with sufficient processing power. The sEMG filters (moving window and Kalman) were also implemented on the host computer to ensure adequate execution time. However, the integration of these filters on a portable platform such as a Raspberry Pi with limited computing power should be further investigated. Notably the Kalman filter has been shown to be one of the most efficient filtering methods used for biosignals (Lyu et al., 2019; Menegaldo, 2017), and its implementation on a Raspberry Pi has previously proved to be feasible (Lyu et al., 2020). Finally, following the idea of promoting open-source tools, the variable admittance controller was programmed using Arduino-compatible libraries, and therefore the overall project could easily be transferred to other Arduino-based or Python-based platforms.

5.2.3   Functionality assessment in healthy and stroke participants

In Chapter 3, fifteen healthy participants and two stroke survivors were recruited to assess the wearability of the *eWrist*. In this evaluation, a significant improvement was observed in donning and doffing time over two subsequent trials, considering only four practice trials in total. The evaluation relied on subjective feedback via questionnaires, namely, the System Usability Scale (SUS) and a customized questionnaire. Whereas the SUS questionnaire portrayed an averaged representation of usability, our customized questionnaire - based on

similar aspects as the SUS - provided a deeper appreciation on points such as learnability, efficiency, memorability, errors, and satisfaction. However, the use of these questionnaires and the *Think-Aloud Method* were prone to some limitations that are worth mentioning. First, although these questionnaires highlighted a general consensus across participants that the device was easy to don and doff, the two stroke survivors were highly motivated and may not be representative of the broader stroke population. Second, as the questionnaires were completed in the presence of the experimenter, the participants might have been more likely to provide a positive evaluation. Therefore, it would have been more appropriate to conduct the evaluation with an independent team so as to avoid any influence the experimenters may have had (Rosenthal, 2005). Third, the use of the *Think-Aloud Method* during the task was a questionable approach since it tended to slow down the execution time and thus biased the experiment. Alternatively, the *Retrospective Think-Aloud Method* might have been more appropriate. This method consists of filming the task from the users' perspective so that they focus on the task itself, and then retrospectively apply the *Think-Aloud Method* while watching the recorded video (Meyer et al., 2020). Fourth, a major limitation of the wearability assessment was the small number of stroke participants recruited (i.e. 2). Although it is known that the most critical usability problems are likely to be detected in the first few participants (Virzi, 1992), the two patients tested also exhibited a low level of impairment (FM-UE: 44 and 41). More impaired patients, who may also benefit more from the *eWrist* as suggested by the results in Chapter 4, might have revealed other shortcomings of the donning and doffing process. Last, in this experiment, only donning and doffing was assessed, but a wearability assessment of the device during the performance of daily tasks might reveal other issues.

For the functionality assessment of the controllers, another ten healthy participants and ten stroke survivors were recruited. Of the ten stroke survivors, only six performed the visuomotor task. Of the four patients that were excluded, one had very little sEMG activity that was not sufficient to trigger proportional mechanical support. Two others had very high co-contraction levels, which meant that extension and flexion movements could not be differentiated based on sEMG activation patterns. This selection of patients revealed that in its current implementation, the *eWrist* fits a specific stroke population with the following characteristics: sufficiently high sEMG activity, little ability to produce overt wrist movements, and low co-contraction levels and spasticity. Although impairments following stroke vary substantially across individuals (McKenna et al., 2017; Raghavan, 2007), the profile described can be found most often in the acute and sub-acute stroke population. Based on subjective feedback, a majority of the tested stroke survivors were unsatisfied with the supportive force provided by the device. Interestingly, the results show that some of these patients clearly benefited from the support and acquired more targets during the visuomotor task. This discrepancy might have reflected their inability to feel the support due to somatosensory deficits (Carey, 1995; Kessner et al., 2016). Unfortunately, this aspect of their impairment was not assessed. Positively, all stroke participants felt challenged and encouraged to actively participate in the task. Moreover, none of them reported discomfort after wearing the exoskeleton continuously for more than 1.5 hours, which would allow extended training sessions with the device. Nevertheless, towards

the end of the session, some participants reported fatigue, which might have decreased the efficiency of the sEMG-based controller due to higher co-contraction levels and compensatory movements (Huang et al., 2019).

Generally, both studies presented in Chapter 3 and in Chapter 4 would have benefited from more direct access to stroke survivors to not only modify the setup more rapidly, but also to assess wearability and controllers over several sessions. Multiple testing sessions would have allowed better tuning of the controllers to the patients, and to potentially observe a learning effect, i.e. with more training sessions, the participants would have performed better in the visuomotor task. A reason for the limited access to patients was the global health situation in which the study of Chapter 4 was conducted, which required the experimental team to test in the patients' home. Nevertheless, despite some minor logistical complications, it showed that the current iteration of the *eWrist* could be easily deployed not only in a research environment, but also in a home-based setting. Taken together, thanks to the relative robustness of the design, both devices presented in Fig. 5.1 accumulated 6'720 extension/flexion cycles, when only considering sessions with participants and disregarding the hours of testing during development and characterization phases. This corresponds to about 40 hours of continuous training and provides evidence that in its current state, the *eWrist* could potentially be used in longitudinal studies taking place in research environments, given that both devices are still working very well.

5.2.4 Other contributions

Integration of dry electrodes

An exploratory project investigated a way to fully embed sEMG electrodes into the structure of the *eWrist* without affecting wearability and usability. To that end, super-soft, dry, and self-adhesive electrodes from IDUN Technologies (IDUN, 2020) were integrated into a flexible 3D printed support (see Fig. 5.2). Similar to the Myo armband, these electrodes do not need any skin preparation before use. Moreover, they exhibit a low skin-contact impedance that is comparable to standard gel electrodes, and lower than existing dry electrodes (Stauffer et al., 2018). The OpenBCI platform (OpenBCI, 2020) was used to read the biosignals from the electrodes. As opposed to the Myo armband that sends data via Bluetooth, the electrodes were connected to the OpenBCI board with wires allowing faster sampling rates and better resolution. Despite high sensitivity to surrounding electromagnetic noise (mainly due to the wires), preliminary results suggest that integration of this approach into the *eWrist* exoskeleton is feasible. However, further development is required to fully implement this solution and to achieve an equal or even improved level of usability offered by the Myo armband.

(a)

(b)

(c)

(d)

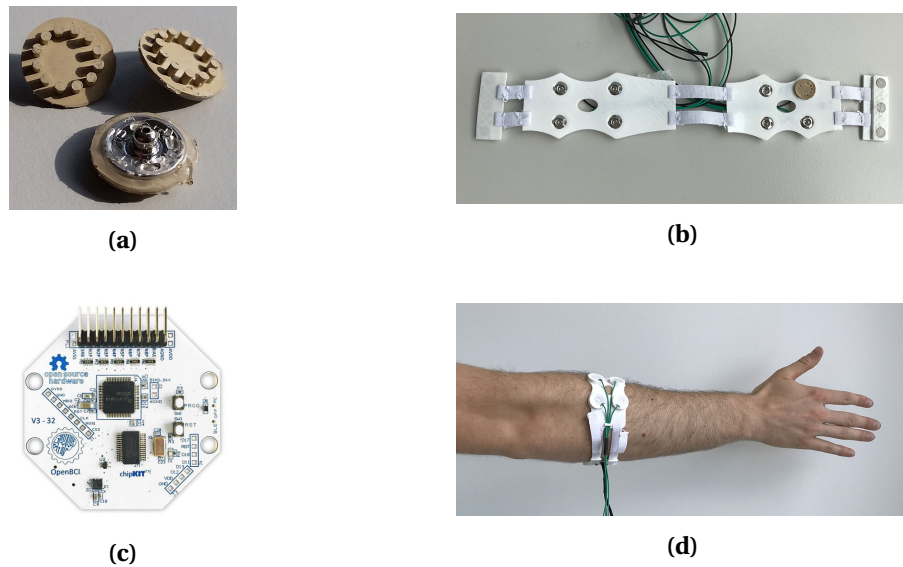**Figure 5.2:** Prototype version of an armband with a magnetic closing system that implements the dry electrodes from IDUN Technologies. **a** Three electrodes from IDUN with snap joint connectors. **b** The armband prototype with one electrode connected and 3 pairs of magnets to easily fasten the system. **c** The OpenBCI board is an open-source brain-computer interface platform. **d** The armband prototype mounted on a forearm.

Magnetic connector

A solution involving magnetic connectors was investigated in order to easily and rapidly connect the upper arm to the forearm module of the *eWrist*. The motivation for having two separate modules was to lower the weight placed distally on the arm. However, the permanent electrical connection made of braided wires between the two modules could easily be snagged and weakens the overall design, especially in a home-based setting. Three commercially available magnetic adaptors for smartphones featuring spring-loaded connectors were disassembled, glued together, and soldered to female pin headers as shown in Fig. 5.3. The resulting magnetic connector was then integrated into the exoskeleton and transferred fifteen different signals in parallel. The ground was connected to the magnets. The solution proved to be robust for transferring both analogue and TTL signals, as well as the power supply. However, the connector tended to detach when lateral forces were applied. This was particularly problematic for the electronics when occurring during high current consumption due to the motor. To prevent unintentional disconnections, a quick mechanical locking system could have been implemented to secure the connection while the device was in use.

| (a) | (b) | (c) |
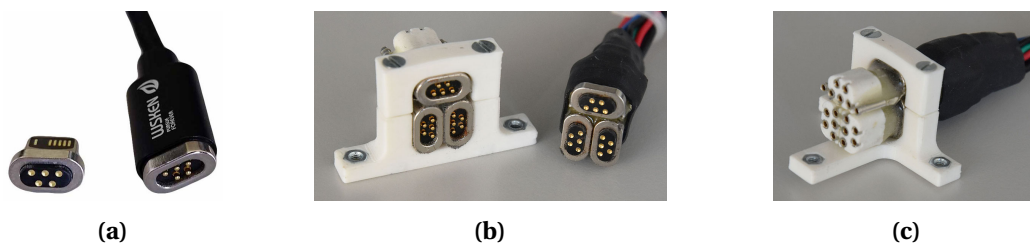
Figure 5.3: a Commercially available magnetic adaptor for smartphones. **b** Augmented magnetic connector featuring fifteen different connections and ground. **c** Female pin headers for modular wire connection.

Educational application

In the context of the practical course titled *"Methods and Concepts in Human Systems Neuroscience and Motor Control"* taught by PhD students of the Neural Control of Movement Lab, a drawing machine was developed. Driven by the desire to provide a highly motivating learning environment for students, but also by personal interest, the machine was designed to hold a pen, move it up or down to stop or start drawing, and steer it in two directions on a horizontal plane. In this specific practical class, students were introduced to the methods of recording and analysing sEMG signals. The Myo armband was used to record sEMG signals on the forearm, which were classified to detect various hand and wrist movements performed by the students. Five movements had to be classified and differentiated in order to control the drawing machine, i.e. two movements to steer it in both directions along the x-axis, two for the y-axis, and one to move the pen down or up. The final task consisted of successfully steering the pen through a maze as depicted in Fig. 5.4. Although this project was not directly related to motor rehabilitation, it showed the students the feasibility and challenges of controlling a

robot in real-time using sEMG signals measured with a fully wearable device.
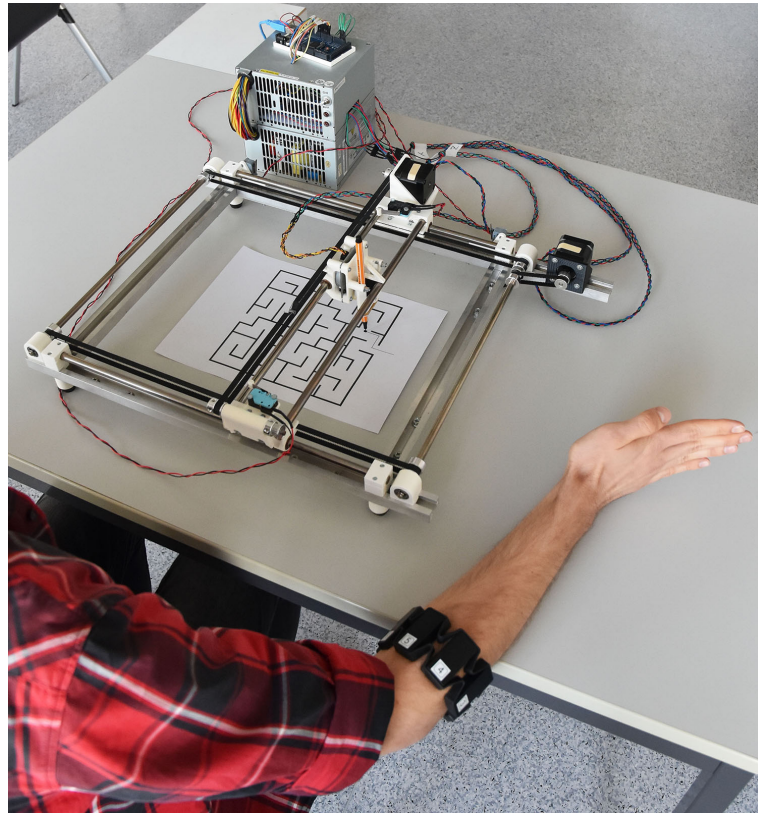
Figure 5.4: Educational drawing machine.

5.2.5 Dissemination

The research conducted in the context of this thesis resulted in the preparation and publication of three scientific journal papers and two conference papers. This thesis is based on publications 1, 2, and 3.

1. Lambelet C, Lyu M, Woolley DG, Gassert R, and Wenderoth N. "The eWrist-A wearable wrist exoskeleton with sEMG-based force control for stroke rehabilitation," in *2017 International Conference on Rehabilitation Robotics (ICORR)*. IEEE, pp. 726–733, 2017.

2. Lambelet C, Temiraliuly D, Siegenthaler M, Wirth M, Woolley DG, Lambercy O, Gassert R, and Wenderoth N. "Characterization and wearability evaluation of a fully portable wrist exoskeleton for unsupervised training after stroke," in *Journal of NeuroEngineering and Rehabilitation*, vol. 17, no. 1, pp. 1–16, 2020.

3. Lambelet C, Mathis M, Siegenthaler M, Woolley DG, Held J, Lambercy O, Gassert R, and Wenderoth N. "Variable admittance control with sEMG-based support for wearable wrist exoskeleton," in *Journal of Transactions on Neural Systems and Rehabilitation Engineering*, in preparation.

4. Lyu M, Lambelet C, Woolley DG, Zhang X, Chen W, Ding X, Gassert R, and Wenderoth N. "Training wrist extensor function and detecting unwanted movement strategies in an EMG-controlled visuomotor task," in *2017 International Conference on Rehabilitation Robotics (ICORR)*. IEEE, pp. 1549-1555, 2017.

5. Lyu M, Lambelet C, Woolley DG, Zhang X, Chen W, Ding X, Gassert R, and Wenderoth N. "Comparison of particle filter to established filtering methods in electromyography biofeedback," in *Biomedical Signal Processing and Control*. vol. 60, p. 101949, 2020.

5.3   Use case scenarios with the *eWrist*

In its current form the *eWrist* provides a suitable solution for research purposes in a supervised environment. Minor changes on the design would be required to 1) improve its accessibility so that other researchers could build it and use it independently, and 2) improve its durability for use in longitudinal studies (see "Future work and outlook" section for details). The following subsections describe two use case scenarios. The first scenario is feasible in the near term given the current state of the project and describes training strategies with the *eWrist* in supervised settings. The second scenario describes the potential future use of the *eWrist* in unsupervised settings.

5.3.1   Research and clinical settings

The most plausible scenario in which the current version of the *eWrist* can be used is within a research environment, where researchers have the technical background to build and debug

the device. In a research context, the *eWrist* can be introduced to clinicians that will conduct the therapy sessions with the patients in a supervised manner. Researchers can tailor the device to the size of the patients and their individual level of impairment (i.e. tuning the controllers). Depending on this level, different rehabilitation strategies to actively support wrist movements can be applied. For the most impaired patients who cannot generate overt movements and have little remaining sEMG activity, the strategy called "continuous passive movement" (CPM) is the most appropriate. It consists of predefined motion where the robot guides and controls the limb. This strategy has been shown to reduce muscle tone and spasticity, and subsequently improve the mobility of joint, muscle, and tendon (Bressel et al., 2002; Liebesman et al., 1994; O Driscoll et al., 2000; Wu et al., 2006). Patients with mild to moderate impairments and remaining sEMG activity would benefit the most from an active-assisted movement approach, where the robot follows the user's intention. This approach involves voluntary effort, which eventually triggers more cortical reorganization and could result in greater motor improvement than with CPM (Lotze et al., 2003; Perez et al., 2004; Volpe et al., 2005; Volpe et al., 2008). Finally, for the least impaired patients, an active-resisted movement strategy can enhance wrist strength by applying a continuous resistance to motion (Hu et al., 2009a). This approach is easily applicable with the *eWrist* by increasing the damping of the admittance controller. Nevertheless, the interaction forces should be carefully monitored in order to stay within the device's capability. As for the two other strategies, the *eWrist* is capable of providing sufficient torque (3.7 Nm) for supporting a wrist that is not spastic, and can promote voluntary effort with the sEMG-based controller.

With a close collaboration between researchers, clinicians, and patients, the device could be continuously improved based on constructive feedback. Finally, since the *eWrist* is a fully portable and lightweight solution with a low physical profile, it can easily be deployed in different clinical units, as demonstrated in our study of Chapter 4 that took place in the homes of stroke patients.

5.3.2   Home-based and community settings

From a critical standpoint, healthcare systems everywhere typically fall short when it comes to the rehabilitation of stroke survivors. There is a duty to take care of individuals who have experienced a stroke; however, they are often not equipped with the means and tools necessary to face the post-hospital phase. During their hospitalization that lasts several months, stroke survivors receive rehabilitation treatments to maximize functional recovery in order to regain independence, but unfortunately these treatments are often insufficient. After discharge from the hospital, more than 80% of stroke survivors have ongoing motor problems that affect their independence in ADL, which can put an extra burden on their family members (Ostwald et al., 2008). From stroke onset, the stay in the hospital should primarily focus on providing appropriate treatments for optimal recovery, but at the same time, should educate patients to prepare and give them the means to pursue rehabilitation treatment after discharge from the hospital. Novel wearable technologies such as the *eWrist*

could be introduced to the patients during the clinical phase so that they familiarize and train with it independently. From discharge, this would ensure a seamless transfer of patients using the device in the hospital to the community and home settings. When deployed in home and community settings, wearable robotics can deliver intensive therapy that positively influences the rehabilitation outcomes of sub-acute and chronic stroke survivors (Lee et al., 2018; Ward et al., 2019). Currently, patients are encouraged to continue rehabilitation training and are given specific goals, but usually report having difficulties meeting them (Ostwald et al., 2008). In unsupervised settings, the patient must self-initiate training sessions that require extensive motivation. Combining *eWrist* training sessions with interactive video games and adaptive goals could boost motivation (Barrett et al., 2016; Cameirão et al., 2010). These goals could be set by healthcare professionals that remotely monitor the patient and provide telerehabilitation (Lai et al., 2004; Laver et al., 2020). Longitudinal studies could then be completed by actively monitoring the training dose and subsequent functional improvements over a longer period of time (Lee et al., 2016). Moreover, given the current implementation of the *eWrist* which uses commercial and low-cost components, 3D printing techniques, and open-source software, this device has the potential to be constructed within the maker community, which would hopefully lead to increased accessibility (Dombroski et al., 2014; Enable, 2019).

5.4   Conclusion

This project took advantage of current technology to investigate the feasibility of integrating wearable assistive devices in poststroke therapy, which could be used independently by stroke survivors during unsupervised rehabilitation training. This work resulted in the development, characterization, and evaluation in healthy and stroke populations of a fully portable exoskeleton that supports extension and flexion wrist function. An important contribution is the development of a novel mechanism to facilitate independent donning and doffing. The device is controlled via interaction forces and physiological signals, which promote voluntary effort and enhances wrist functionality in stroke survivors. Furthermore, the implementation of the device favours the use of open-source software and widely available hardware in the hope of promoting broad access to such technology in the future. The work of this thesis may ultimately be a first step towards the development of novel approaches that supplement conventional therapy and encourage rehabilitation training outside clinical settings.

5.5   Future work and outlook

Throughout the testing with healthy participants and stroke survivors, several ideas and suggestions for improvements have emerged. The suggestions presented in the following two subsections target the implemented visuomotor task and technical improvements to the design. To conclude, a scenario is envisioned where the *eWrist* could be used as an assistive tool.

5.5.1 Visuomotor task

Although the visuomotor task was developed to assess the functionality of the controllers, it could be used as an initial platform for rehabilitation training. In such a case, the following suggestions and improvements should be considered.

Difficulty of the task

Currently, in the study of Chapter 4, target height in the visuomotor task was based on the passive ROM of the wrist. This criterion was primarily used in order to assess the beneficial effect of the implemented controllers on wrist functionality. Depending on the impairment level of the patient, the discrepancy between active and passive ROM can be large. Consequently, several patients reported that the task was too difficult, which might have affected their motivation. Therefore, the difficulty of the task should be carefully adjusted to the specific impairment level of the patient, which will allow for an optimal level of active participation, and thus a greater therapy intensity. Active participation is known to be an important factor that positively influences the outcome of rehabilitation (Lotze et al., 2003; Woldag et al., 2002). Moreover, it has been shown that a success level of 70% in a given task strikes the right balance between avoiding boredom on the one hand, and frustration on the other (Adamovich et al., 2009; Choi et al., 2011). In the current implementation of the task, the difficulty can be adapted either by changing the height of the targets (i.e. the excursion of the wrist joint), or by tuning the gains of the controllers (i.e. the amount of mechanical support). Both adjustments can be performed prior to or during therapy in order to train the patient at an optimal level of performance (da Silva Cameirão et al., 2011; Lambercy et al., 2011).

Calibration phase

The calibration phase, which is required before every training session, could be improved by implementing an automatic selection of the channels for the sEMG-based controller. This selection must be based on: 1) minimizing the overlap between extension and flexion activation patterns on the chosen electrodes, and 2) ensuring that the chosen electrodes will generate a physiologically coherent mechanical support. For the latter, information on the orientation of the Myo armband on the forearm is required. As long as the supportive torque is coherent, the patient can relearn how to produce physiologically normal activations and reduce co-contraction patterns in order to maximize her/his performance with the device. As for calibration of the passive ROM, it was initially performed automatically by the device. However, this approach has proven to be unreliable if the patient cannot fully relax her/his arm during the assessment, and was thus ultimately performed manually. The passive ROM should not vary extensively across training sessions and could therefore be performed once during the first training session. Moreover, this measurement was required in this study but might not be necessary in future implementations of the visuomotor task.

Visual interface

The current visual interface of the visuomotor task is very basic and has only been designed to be functional. In order to create a more immersive and motivating visual environment, other tools should be considered. *Unity* is a cross-platform game engine developed by Unity Technologies (Unity, 2020) and can be used to create 3D virtual or augmented reality games. A migration of the visuomotor task to *Unity* would require recoding in C# and addressing the issue of data collection from the Myo armband and the *eWrist*. This would also enable for an easier implementation of the task on a smartphone or a tablet.

5.5.2 Suggestions for technical improvements

In the following subsection, technical shortcomings of the current design and suggestions to make the *eWrist* an assistive exoskeleton during ADL are presented.

Transmission type and fixation

The direct implementation of the DC motor on the forearm module accounts for about 30% of its weight. The implementation of a remote actuation system based on bowden-cables as presented in (Bützer et al., 2020) could reduce the weight placed distally and improve usability of the design. Given the non-backdrivability of the *eWrist*, the force sensor and absolute angular encoder would need to be kept in order to provide accurate force-motion recordings from the pHRI. An accurate proportional controller would certainly be more difficult to implement with this actuation system due to backlash and non-linear friction in the cables, but the integration of a feed-forward friction model and additional sensors would help mitigate these concerns (Hofmann et al., 2018). Nevertheless, the durability of this new technology still needs to be proven. The worm screw from the transmission gear is guided by two normal (radial) bearings. However, due to the interaction forces applied on the handle and ultimately on the worm wheel, the latter applies longitudinal stress on the worm screw. Therefore, conical bearings should be used to guide the worm screw in order to support both radial and longitudinal stress.

The current fixation system on the forearm using Boa Closure mechanisms provides a firm and adjustable attachment, however, the locking and anchoring systems could be improved (Choi et al., 2019). For example, the current design tends to pinch the skin during donning and fastening. In addition, the area in contact with the lower part of the forearm should be increased in order to better distribute the pressure. Finally, the integration of a more flexible structure around the forearm and hand would improve comfort and adaptability of the design (Fitzpatrick et al., 2017; Graham et al., 2020). Nevertheless, structures around the motor, worm drive, and angular sensor must remain rigid for precise actuation and measurement.

Sensors

The unidirectional load cell used in the *eWrist* exoskeleton is a cheap and reliable way to measure interaction forces, which proved to work appropriately with the admittance controller. However, due to the design, a torsional torque T_{tor} (see Fig. A.3 in the Appendix) is experienced by the load cell when an interaction force F_{int} is applied to the center of the handle. This torque biases the force measurements as shown in Fig. A.6 in the Appendix. Moreover, lateral forces (i.e. not in extension/flexion directions) applied on the handle further distort the measurement. The implementation of a multidirectional load cell would help to assess the directionality of the applied force, which could be used to adapt the level of mechanical support provided. This would allow the device to only provide support when forces in extension or flexion directions are applied to the handle, and thus improve the quality of the therapy. Alternatively, to avoid the implementation of a costly multidirectional load cell, a hinge could be installed on each arm of the handle in order to allow free radial and ulnar deviation while still supporting extension and flexion wrist movements.

The readout of the IMU generates a cyclic delay in the control loop running at 1 kHz and affects the smoothness of the admittance controller. Moreover, the current IMU sensor tends to drift after a certain period of time (30 min). Therefore, a better integration of this sensor or the implementation of a new sensor needs to be considered. In the latter case, a sensor featuring a Digital Motion Processor (DMP), which processes the orientation and directly provides Euler angles, should be favoured in order to reduce the computational requirements placed on the micro-controller.

Wiring

Currently, all signals sent from the forearm to the upper arm module including power supply and ground are transmitted in parallel via 18 wires. Some of these signals are analogue, while others are digital (TTL). These signals should be serialized to simplify the connection cable that would ideally only require 4 wires, i.e. for supply, ground, and bidirectional transmission. Consequently, the cable would also be lighter. Moreover, a solution to easily connect and disconnect the forearm module should be integrated, e.g. with magnetic connectors as presented in subsection 5.2.4. The Hall encoder measuring absolute angular position is currently installed on the moving part of the forearm module (i.e. the handle). This approach simplified the initial development but presents an issue in terms of durability. The electrical cable connecting the Hall encoder to the electronic board on the forearm module (see Fig. A.1b) is subject to repetitive stress and prone to failure. Future improvements on the device should consider implementing this sensor on the static part of the forearm module, or to use special wires that can withstand a large number of bending cycles. A similar issue applies to the load cell where special wires should be implemented.

Interface with the device

During testing with the participants, the exoskeleton was permanently connected to the host computer via a USB cable. This approach works in a research context, but the usability of the device would be enhanced with a wireless (WiFi or Bluetooth) connection between the *eWrist* and the host computer. Importantly, the connection protocol should yield sufficient bandwidth for data transfer in real-time. The host computer could then be replaced by a smartphone or a tablet where a visuomotor task-like application would provide more convenient rehabilitation training in a home environment. Data could be automatically sent to a private cloud allowing longitudinal assessment of recovery by the caregivers (Pham et al., 2018).

5.5.3 Towards assistance in ADL

The ultimate goal of rehabilitation after stroke is to promote the return to productive daily activities that occur in real-world environments and not just in the clinic or laboratory. Home-based rehabilitation training using the *eWrist* would provide a way to increase training dose and ultimately improve wrist function. However, assisting the wrist during ADL might offer an even better approach to enhance functional recovery since the therapy would occur at any time and during functional wrist movements (Woldag et al., 2002). With its full portability, lightweight and low physical profile, the *eWrist* was envisioned to be used as an assistive tool during ADL. However, even with improved robustness and usability of the design as suggested in subsection 5.5.2, the *eWrist* exoskeleton does not support the grasping function of the hand. Therefore, it could not be used in a meaningful way for assistance in ADL to grasp and hold objects. One way to address this issue would be to take advantage of the tenodesis grasp that closes fingers when the wrist is extended (Mateo et al., 2013). However, since this effect mainly relies on passive tension in muscles and tendons, a limited grip force is generated. Alternatively, at the cost of a slight increase in weight placed distally, a passive mechanism that uses the same principal as the tenodesis effect could be implemented on the handle. In the ideal scenario, portable exoskeletons will be introduced to patients soon after the stroke event and continue to be used throughout therapy until sufficient functions are recovered to allow independence in ADL.

A Supplementary materials - Chapter 3

A.1 Additional information

A.1.1 Electronic boards

Two custom-made shields, namely, the upper arm shield and the forearm shield (see Fig. A.1), were developed to incorporate all the electronics in a low physical profile and lightweight solution. The upper arm shield includes the real-time micro-controller (Teensy), a micro-computer (Raspberry Pi Zero or RPi0), interactive buttons and LED indicators, an amplifier for the load cell signal (force measurement), a sensor to measure current consumption, and power supply management to supply different voltages (i.e. 3.3 V, 5 V, 12 V). The forearm shield incorporates the motor drive, the IMU, LED indicators, and receives signals from the load cell, the absolute Hall encoder, and the motor.
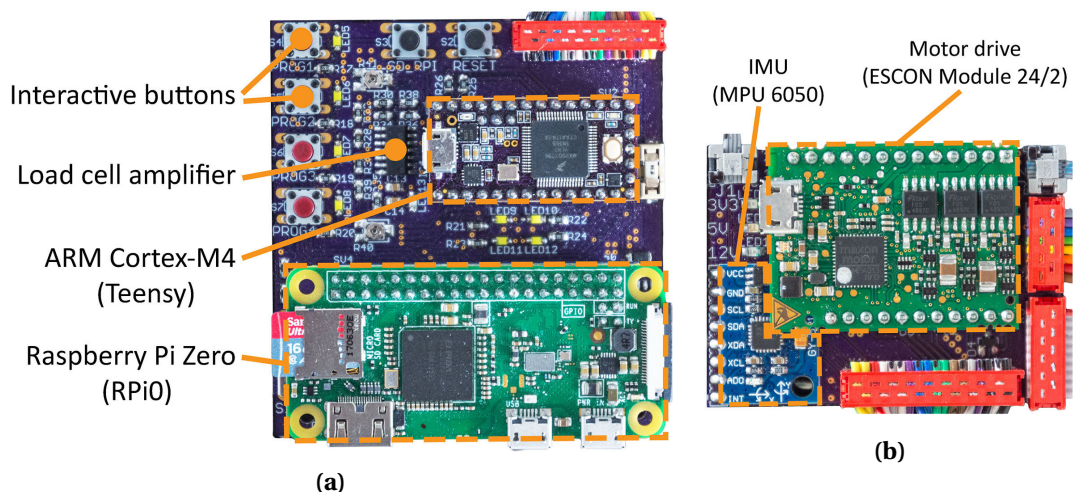
Figure A.1: a Electronic board of the upper arm module (upper arm shield). **b** Electronic board of the forearm module (forearm shield).

A.1.2   Setup of autonomy assessment

In order to assess the autonomy of the *eWrist*, the latter was equipped with a paddle fixed at the end of a lever. The lever was directly attached to the load cell so as not to generate torsional torques around the load cell (cf. Appendix A.1.3). The exoskeleton was held vertically over a basin filled with water and the paddle constantly immersed into water (see Fig. A.2). The assessment consisted in continuously actuating the *eWrist* in extension and flexion movements until the battery was fully discharged.
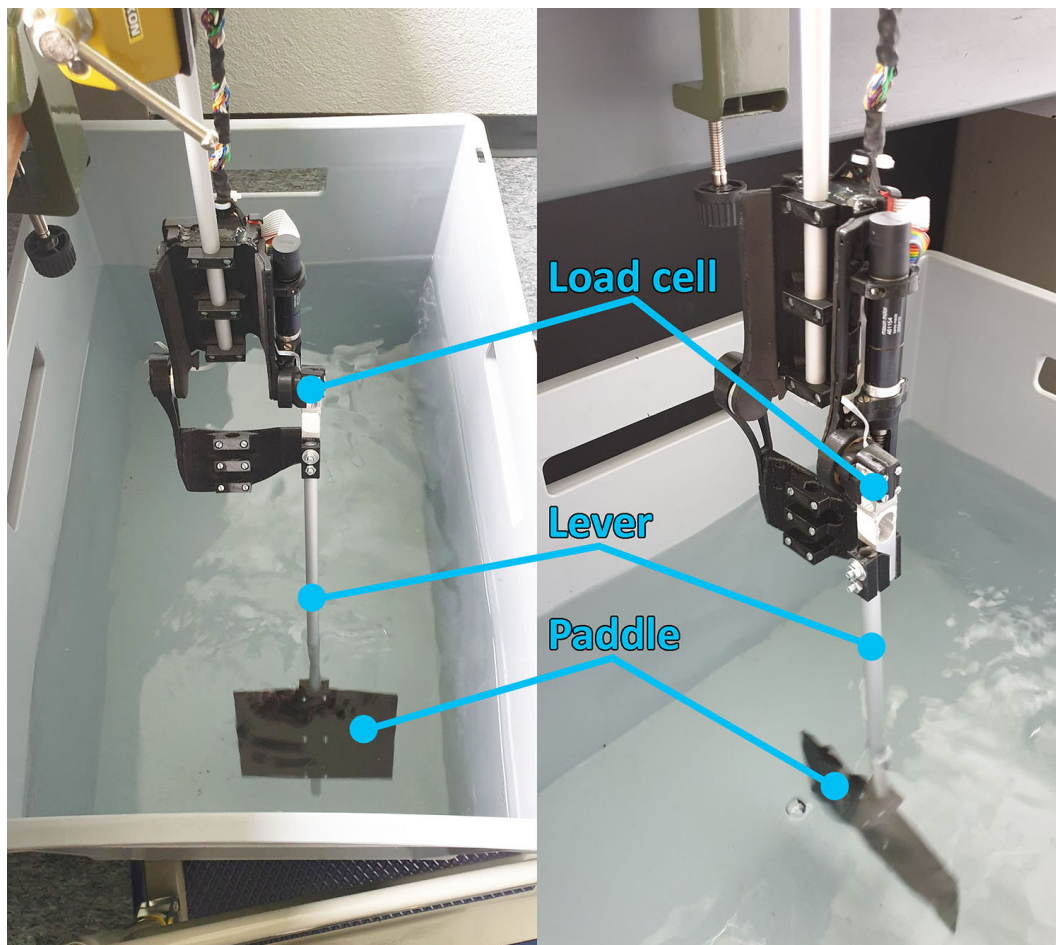
Figure A.2: Setup of the autonomy assessment where a paddle was constantly immersed into water and fixed to the load cell via a lever.

A.1.3 Torsional torque around the load cell

In the current design of the *eWrist*, torques generated during pHRI go through the load cell since the other arm of the handle (incorporating the Hall encoder) is free to move. The average pressure point F_{int} applied by the hand is located in the middle of the handle (see green dot in Fig. A.3a). Thus, a torsional torque T_{tor} is generated around the load cell that deflects the handle and biases the force measurement (cf. Appendix A.2.3).
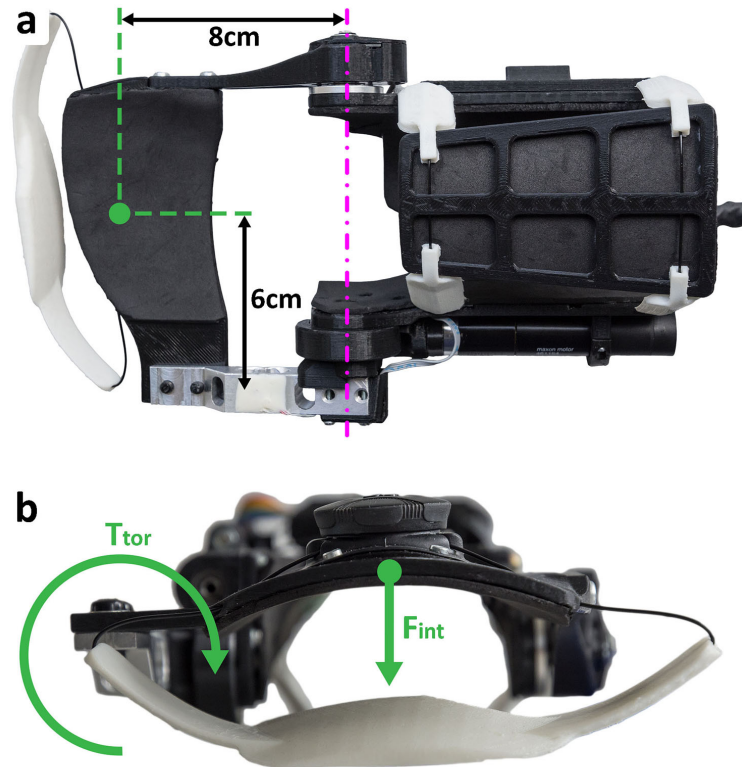
Figure A.3: Torsional torque T_{tor} experienced by the the load cell when a force F_{int} is applied to the center of the handle.

A.2 Additional results

The following figures present additional results on the characterization of the *eWrist* performed in Chapter 3.

A.2.1 Static and dynamic frictions

Static and dynamic frictions in the transmission mechanism may interfere with the proper functioning of the controller and were therefore assessed. In order to evaluate static and dynamic frictions, the *eWrist* was placed on the side (i.e. rotational axis in vertical orientation) to cancel out the effect of gravity. In addition, to assess dynamic friction at various stabilized angular velocities, the handle was removed from the device so as to allow a 360° rotation of the load cell.
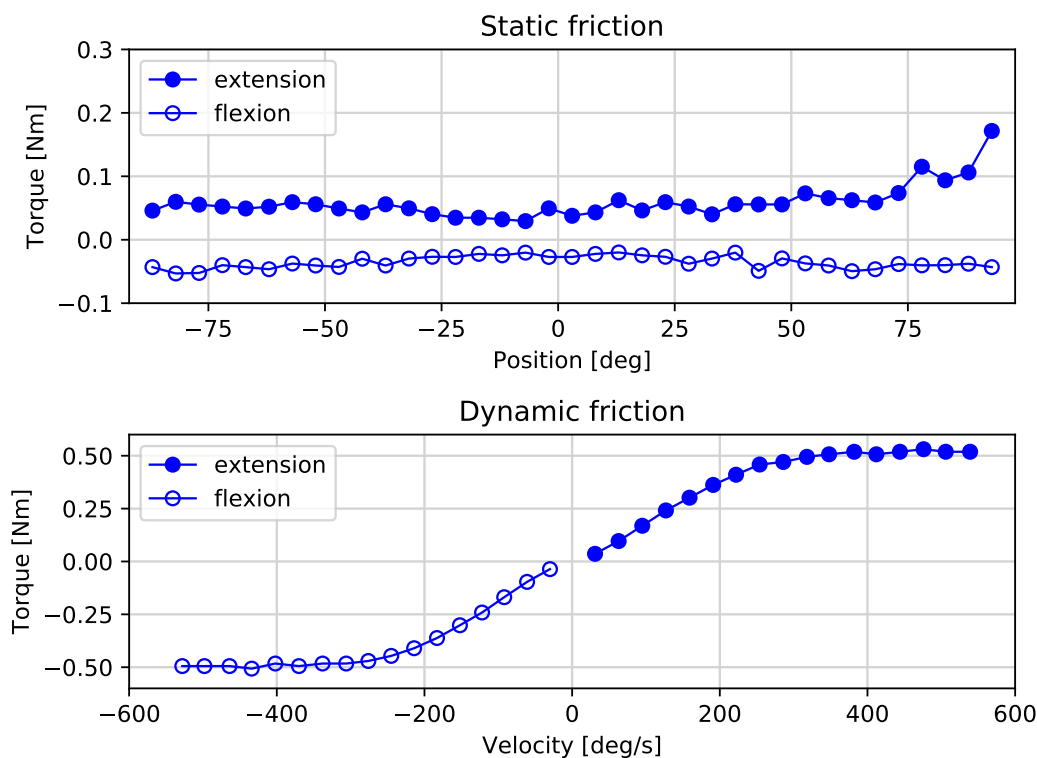
Figure A.4: Static and dynamic frictions of the *eWrist*.

A.2.2   Position bandwidth

The position bandwidth determines the reactiveness of the device to fast and small changes in direction. To that end, a sinusoidal trajectory with a constant amplitude of 5° was considered adequate. The initial oscillation frequency was set to 0.1 Hz so that the *eWrist* could easily follow it. The final oscillation frequency of 6 Hz was determined experimentally when the phase shift could not longer be evaluated. Before extracting magnitude and phase shift, the angular position was low-pass filtered offline with a 2nd order Butterworth filter with a 10 Hz cut-off frequency.
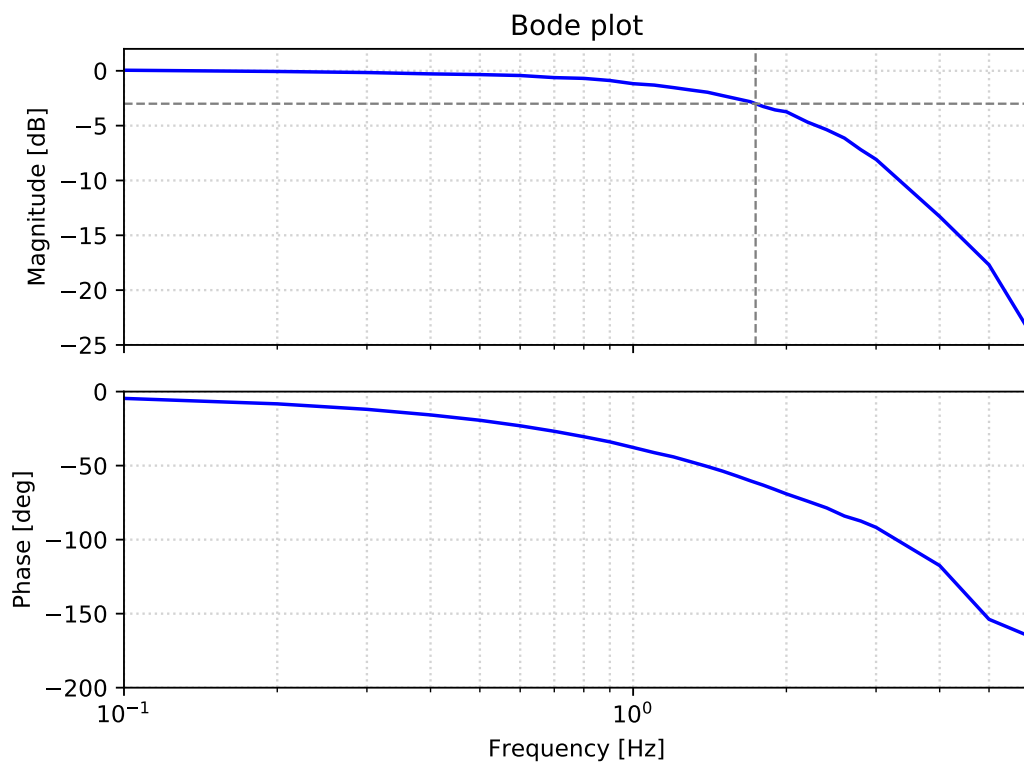
Figure A.5: Bode diagram of the position bandwidth. At -3 dB of magnitude (dotted line), the position bandwidth is evaluated at 1.74 Hz. At that frequency, the phase shift is 61.6°.

A.2.3 Handle deflection and biased force measurement

The interaction torques between the user and the *eWrist* deflects the handle and biases the force measurement (cf. Appendix A.1.3). Both the evaluation of the handle deflection and the bias in the force measurement were conducted simultaneously by hanging various weights (ranging from 100 g to 3.5 kg) in the center of the handle (see Fig. A.3). Readouts from the Hall encoder and the load cell were then recorded.
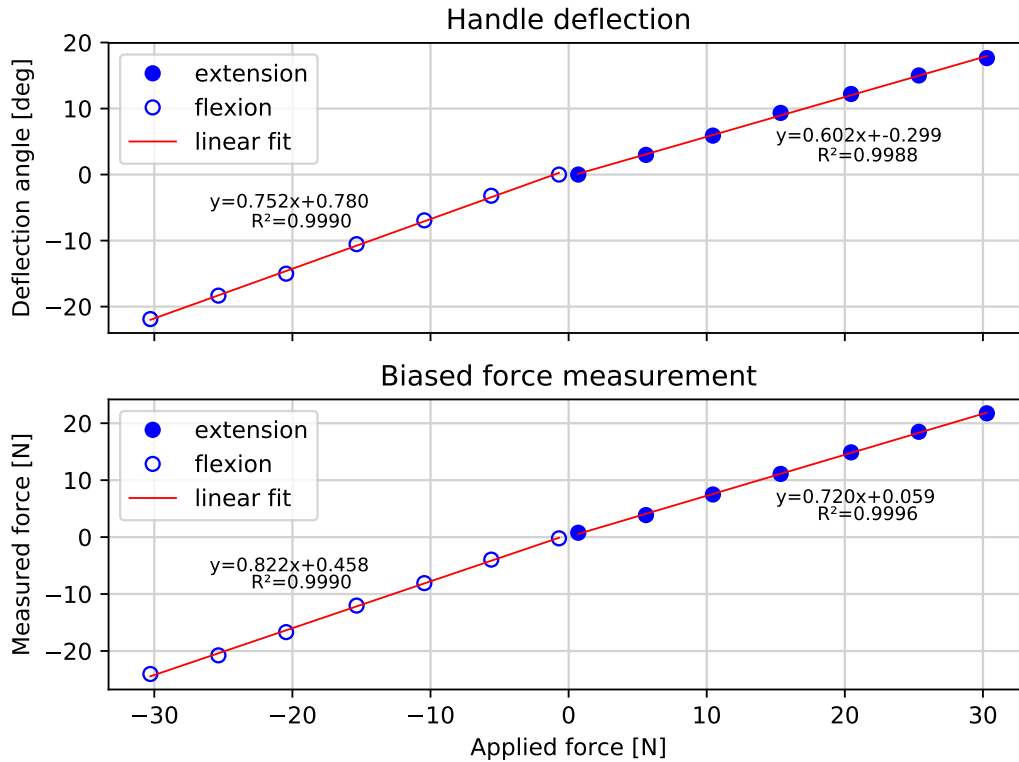
Figure A.6: Deflection angle of the handle (measured by the Hall encoder opposite to the load cell) and bias in the force measurement when a force F_{int} is applied to the center of the handle (see Fig. A.3).

B Supplementary materials - Chapter 4

B.1 Additional information

B.1.1 Details on $G_{stif}(\theta)$

$G_{stif}(\theta)$ takes into account the passive ROM of the wrist ROM_{pas} and the passive force F_{pas} applied by the hand on the handle measured at four different angular positions, namely at 20% and 80% of ROM_{pas} for extension and flexion separately. As described in Eq. B.1, $G_{stif}(\theta)$ acts linearly on the damping of the system for angles smaller than 80% of ROM_{pas}, but quadratically for larger angles.

$$
G_{stif}(\theta) = \begin{cases} \left| a_1\theta^2 + b_1\theta + c_1 \right|, & \text{if } \theta < 0.8\theta_{mpf} \\ \left| a_2\theta + b_2 \right|, & \text{if } 0.8\theta_{mpf} \leq \theta \leq 0.8\theta_{mpe} \\ \left| a_3\theta^2 + b_3\theta + c_3 \right|. & \text{if } \theta > 0.8\theta_{mpe} \end{cases} \tag{B.1}
$$

where a_1, b_1, c_1, a_2, b_2, a_3, b_3 and c_3 are based on ROM_{pas} and F_{pas}, and are determined during the calibration phase. θ_{mpf} and θ_{mpe} are the maximal passive angles reached in flexion and extension, respectively, such that $\left| \theta_{mpf} \right| + \left| \theta_{mpe} \right| = ROM_{pas}$. According to our angle convention (see Fig. 4.1c), θ_{mpf} is normally negative and θ_{mpe} positive.

B.1.2 Details on $G_{att}(\theta)$

$G_{att}(\theta)$ aims to linearize the non-linear relationship between the generation of forearm sEMG signals and the angular position of the wrist joint. $G_{att}(\theta)$ takes into account the passive ROM of the wrist ROM_{pas} and the MVC in extension MVC_{ext} and flexion MVC_{flex}. Two separate gains are used for extension and flexion, i.e. when θ is positive (extension) or negative (flexion) (see Fig. 4.1c). As described in Eq. B.2, the inverse of linear or quadratic functions is taken

based on θ to attenuate the sEMG signal.

$$
G_{att}(\theta) = \begin{cases} (a_1\theta^2 + b_1\theta + c_1)^{-1}, & \text{if } |\theta| < 0.2\theta_{mp} \\ (a_2\theta + b_2)^{-1}, & \text{if } 0.2\theta_{mp} \le |\theta| \le 0.8\theta_{mp} \\ (a_3\theta^2 + b_3\theta + c_3)^{-1}. & \text{if } |\theta| > 0.8\theta_{mp} \end{cases} \tag{B.2}
$$

where a_1, b_1, c_1, a_2, b_2, a_3, b_3, and c_3 are based on ROM_{pas}, MVC_{ext} and MVC_{flex}, and are determined during the calibration phase. θ_{mp} is the maximal passive angle reached in flexion or extension.

B.1.3 Details on the co-activation level

The co-activation level (CL) defined in Eq. B.3 was first introduced in (Frost et al., 1997). It was computed over the movement initiation/rise phases CL_{mir} and the stabilization phase CL_{stab} (see Fig. 4.6), and only for trials where the target was acquired. Thereafter, the ratio $\frac{CL_{stab}}{CL_{mir}}$ was analysed.

$$
CL = \frac{1}{\Delta t_{ph}} \cdot \sum_{i=n_{start}}^{n_{end}} A_{e-f}\Delta t \tag{B.3}
$$

where $\Delta t_{ph} = t_{n_{end}} - t_{n_{start}}$ is the duration of the movement initiation/rise phases or the duration of the stabilization phase, n_{start} the starting sample point of the phase, n_{end} the ending sample point of the phase, A_{e-f} the overlapping activity between $pMVC_{ext}$ and $pMVC_{flex}$ (i.e. the smaller of the two at a given sample point), and $\Delta t = t_i - t_{i-1}$ the time difference between the current and previous timestamp.

CL can vary from 0 (no overlapping) to 1 (full overlapping).

B.2 Additional results

The following figures present additional results on the assessment of the controllers performed in Chapter 4 with stroke participants. The figures always show the median and individual data of the six stroke survivors for all factor permutations (i.e. extension/flexion directions, vertical/horizontal orientations, sEMG/gravity controllers and no support, and 20%/40%/60%/80% target heights).

B.2.1 Percentage of reached targets
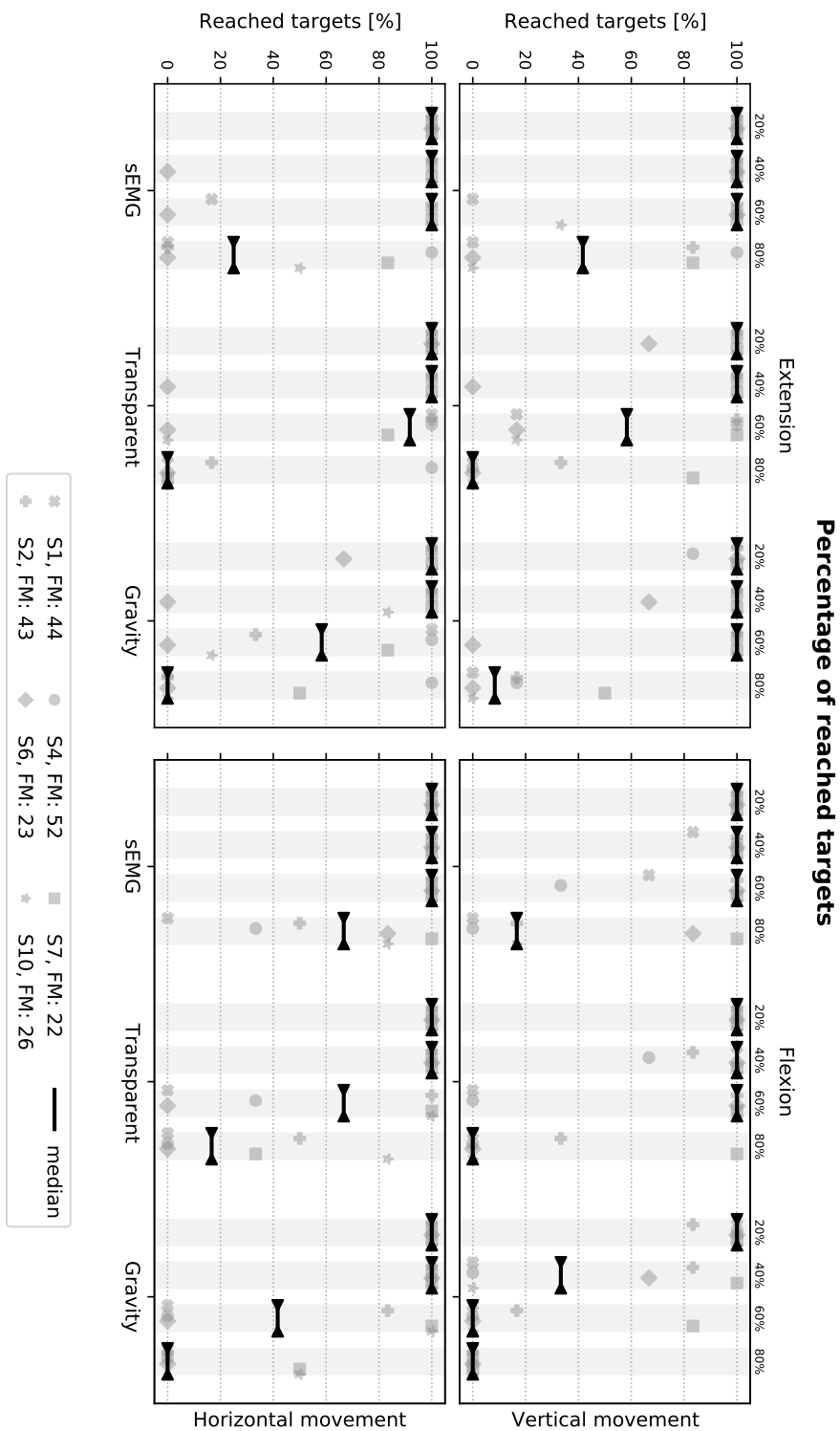
Figure B.1: Percentage of reached targets in stroke participants in all conditions. The median across participants is shown.

B.2.2 Ratio of co-activation level
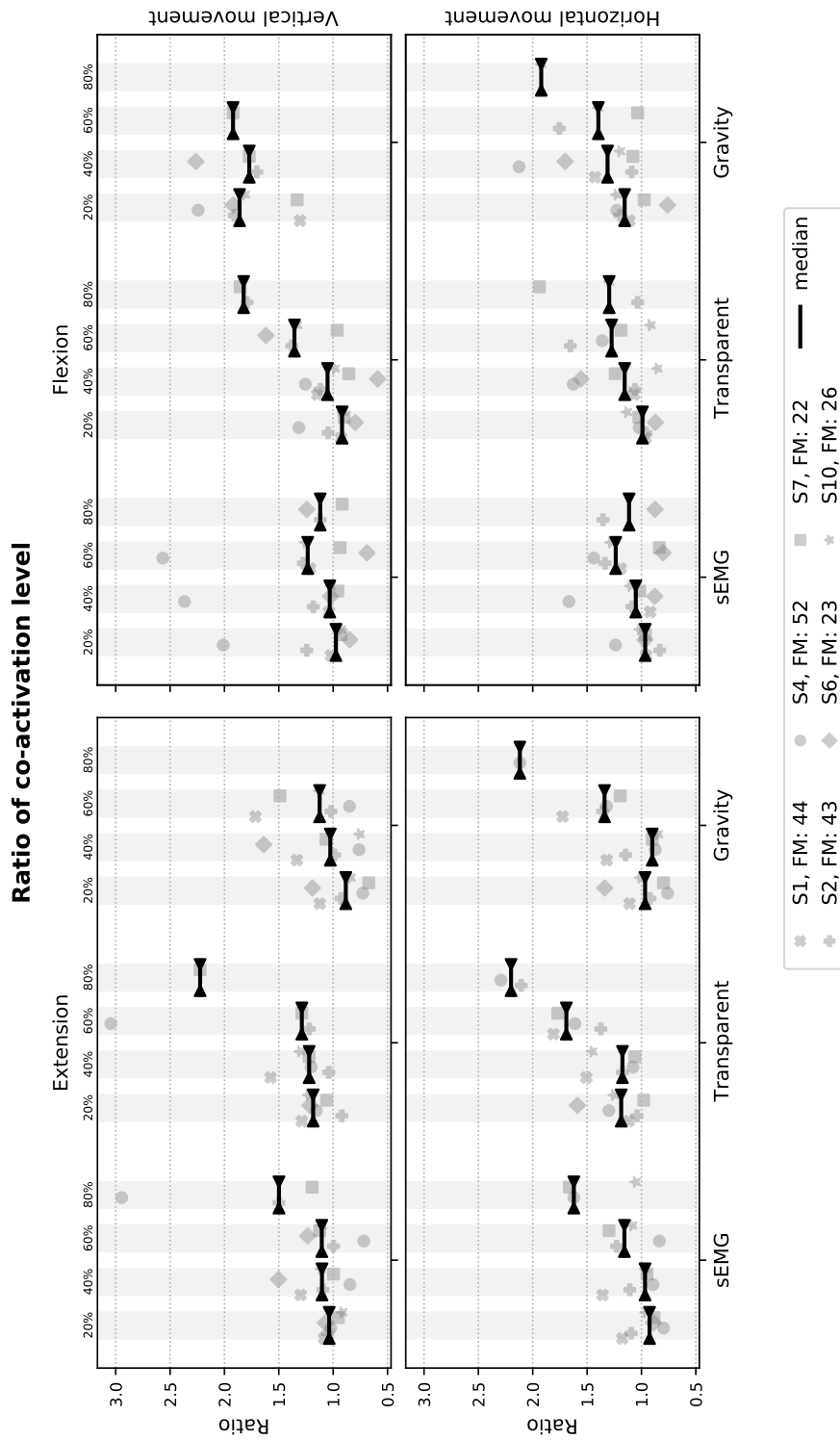
Figure B.2: Ratio of co-activation level between the stabilization phase and the movement initiation/rise phases of a trial. The median across participants is shown. The co-activation level is computed as described in Eq. B.3 and was evaluated only for trials where the target was acquired.

B.2.3 Normalized integrated jerk
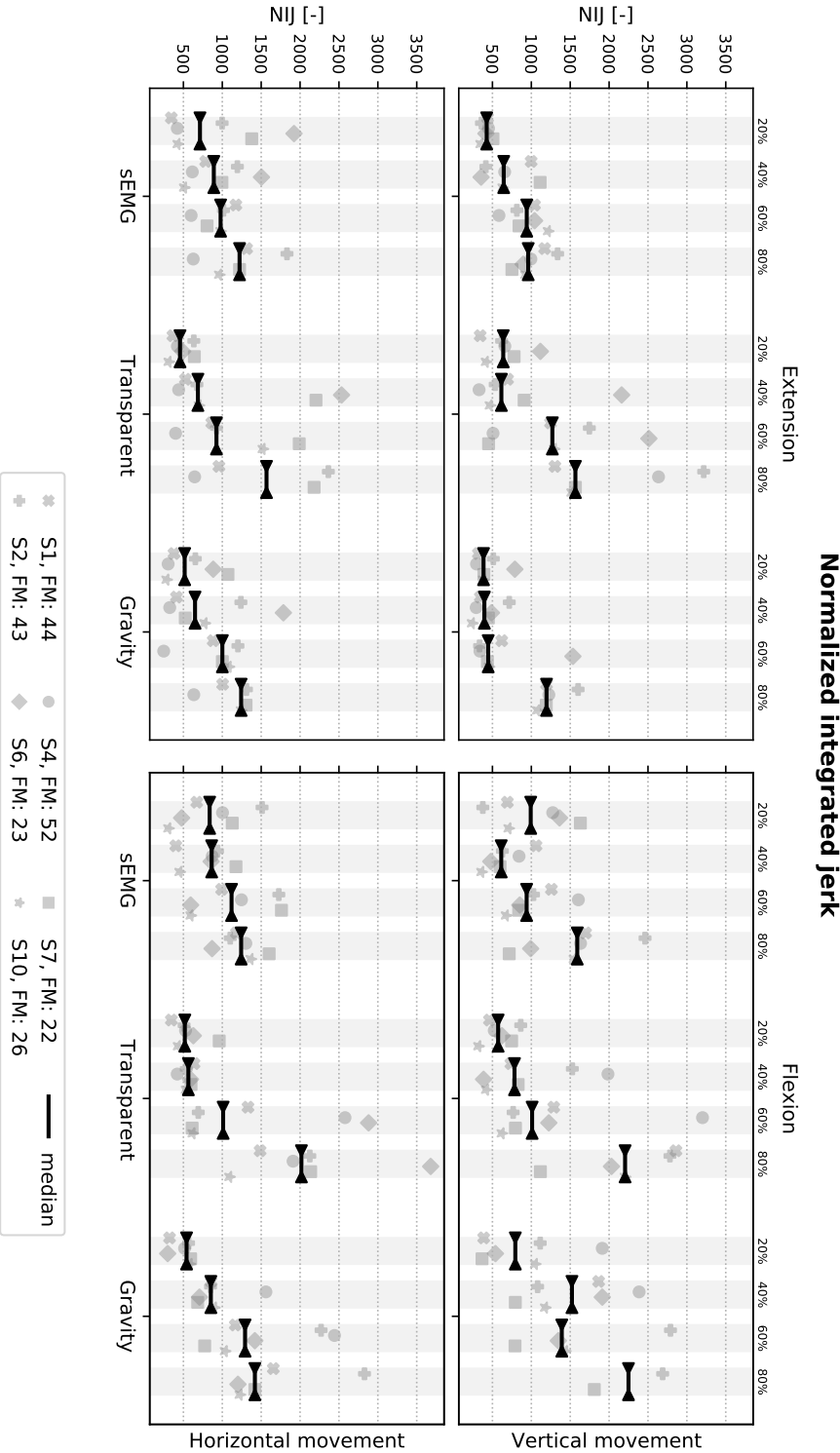
Figure B.3: Normalized integrated jerk (NIJ) in stroke participants in all conditions. The median across participants is shown. The NIJ is computed as described in Eq. 4.11 and was evaluated only for trials where 60% of the target's height was reached (in order to have more data).

Bibliography

Adamovich, S. V., Fluet, G. G., Merians, A. S., Mathai, A., & Qiu, Q. (2009). Incorporating haptic effects into three-dimensional virtual environments to train the hemiparetic upper extremity. *IEEE Transactions on Neural Systems and Rehabilitation Engineering, 17*(5), 512–520.

Al-Fahaam, H., Davis, S., & Nefti-Meziani, S. (2016). Wrist rehabilitation exoskeleton robot based on pneumatic soft actuators. *Students on Applied Engineering (ISCAE), International Conference for,* 491–496.

Andrikopoulos, G., Nikolakopoulos, G., & Manesis, S. (2015). Motion control of a novel robotic wrist exoskeleton via pneumatic muscle actuators. *2015 IEEE 20th Conference on Emerging Technologies & Factory Automation (ETFA),* 1–8.

Arata, J., Ohmoto, K., Gassert, R., Lambercy, O., Fujimoto, H., & Wada, I. (2013). A new hand exoskeleton device for rehabilitation using a three-layered sliding spring mechanism. *Robotics and Automation (ICRA), 2013 IEEE International Conference on,* 3902–3907.

Ashford, S., Slade, M., Malaprade, F., & Turner-Stokes, L. (2008). Evaluation of functional outcome measures for the hemiparetic upper limb: a systematic review. *Journal of rehabilitation medicine, 40*(10), 787–795.

Ates, S., Haarman, C. J., & Stienen, A. H. (2016). SCRIPT passive orthosis: design of interactive hand and wrist exoskeleton for rehabilitation at home after stroke. *Autonomous Robots,* 1–13.

Ates, S., Mora-Moreno, I., Wessels, M., & Stienen, A. H. (2015). Combined active wrist and hand orthosis for home use: Lessons learned. *Rehabilitation Robotics (ICORR), 2015 IEEE International Conference on,* 398–403.

Aubin, P. M., Sallum, H., Walsh, C., Stirling, L., & Correia, A. (2013). A pediatric robotic thumb exoskeleton for at-home rehabilitation: the Isolated Orthosis for Thumb Actuation (IOTA). *2013 IEEE 13th International Conference on Rehabilitation Robotics (ICORR),* 1–6.

Bae, J.-H., Kim, Y.-M., & Moon, I. (2012). Wearable hand rehabilitation robot capable of hand function assistance in stroke survivors. *Biomedical Robotics and Biomechatronics (BioRob), 2012 4th IEEE RAS & EMBS International Conference on,* 1482–1487.

Ballester, B. R., Maier, M., Mozo, R. M. S. S., Castañeda, V., Duff, A., & Verschure, P. F. (2016). Counteracting learned non-use in chronic stroke patients with reinforcement-induced movement therapy. *Journal of neuroengineering and rehabilitation, 13*(1), 74.

Bibliography

Bangor, A., Kortum, P. T., & Miller, J. T. (2008). An empirical evaluation of the system usability scale. *Intl. Journal of Human–Computer Interaction, 24*(6), 574–594.

Barrett, N., Swain, I., Gatzidis, C., & Mecheraoui, C. (2016). The use and effect of video game design theory in the creation of game-based systems for upper limb stroke rehabilitation. *Journal of Rehabilitation and Assistive Technologies Engineering, 3,* 2055668316643644.

Bartlett, N. W., Lyau, V., Raiford, W. A., Holland, D., Gafford, J. B., Ellis, T. D., & Walsh, C. J. (2015). A soft robotic orthosis for wrist rehabilitation. *Journal of Medical Devices, 9*(3).

Barzel, A., Ketels, G., Stark, A., Tetzlaff, B., Daubmann, A., Wegscheider, K., van den Bussche, H., & Scherer, M. (2015). Home-based constraint-induced movement therapy for patients with upper limb dysfunction after stroke (HOMECIMT): a cluster-randomised, controlled trial. *The Lancet Neurology, 14*(9), 893–902.

Beer, R. F., Ellis, M. D., Holubar, B. G., & Dewald, J. P. (2007). Impact of gravity loading on post-stroke reaching and its relationship to weakness. *Muscle & Nerve: Official Journal of the American Association of Electrodiagnostic Medicine, 36*(2), 242–250.

Beer, R. F., Given, J. D., & Dewald, J. P. (1999). Task-dependent weakness at the elbow in patients with hemiparesis. *Archives of physical medicine and rehabilitation, 80*(7), 766–772.

Benjamin, E. J., Virani, S. S., Callaway, C. W., Chamberlain, A. M., Chang, A. R., Cheng, S., Chiuve, S. E., Cushman, M., Delling, F. N., Deo, R., et al. (2018). Heart disease and stroke statistics-2018 update: a report from the American Heart Association. *Circulation, 137*(12), e67.

Bernhardt, J., Dewey, H., Thrift, A., & Donnan, G. (2004). Inactive and alone: physical activity within the first 14 days of acute stroke unit care. *Stroke, 35*(4), 1005–1009.

Bhatnagar, K., Bever, C. T., Tian, J., Zhan, M., & Conroy, S. S. (2020). Comparing Home Upper Extremity Activity with Clinical Evaluations of Arm Function in Chronic Stroke. *Archives of Rehabilitation Research and Clinical Translation,* 100048.

Bian, F., Li, R., Ren, D., & Liang, P. (2018). Variable Admittance Control Improving Stability in Physical Human-Robot Interaction. *2018 IEEE International Conference on Information and Automation (ICIA),* 1485–1490.

Biernaskie, J., Chernenko, G., & Corbett, D. (2004). Efficacy of rehabilitative experience declines with time after focal ischemic brain injury. *Journal of Neuroscience, 24*(5), 1245–1254.

Boafit. (2020). *Dial in to fast, effortless, precision fit.* Retrieved November 18, 2020, from https://www.boafit.com/en-gb

Bobath, B. (1978). Adult hemiplegia: evaluation and treatment London. *William Heinnemann.*

Borboni, A., Mor, M., & Faglia, R. (2016). Gloreha—hand robotic rehabilitation: Design, mechanical model, and experiments. *Journal of Dynamic Systems, Measurement, and Control, 138*(11), 111003.

Bos, R. A., Haarman, C. J., Stortelder, T., Nizamis, K., Herder, J. L., Stienen, A. H., & Plettenburg, D. H. (2016). A structured overview of trends and technologies used in dynamic hand orthoses. *Journal of NeuroEngineering and Rehabilitation, 13*(1), 62.

Bowden, M. G., Woodbury, M. L., & Duncan, P. W. (2013). Promoting neuroplasticity and recovery after stroke: future directions for rehabilitation clinical trials. *Current opinion in neurology, 26*(1), 37–42.

Boyd, L. A., & Winstein, C. J. (2003). Impact of explicit information on implicit motor-sequence learning following middle cerebral artery stroke. *Physical Therapy*, *83*(11), 976–989.

Bressel, E., & McNair, P. J. (2002). The effect of prolonged static and cyclic stretching on ankle joint stiffness, torque relaxation, and gait in people with stroke. *Physical therapy*, *82*(9), 880–887.

Brewer, B. R., McDowell, S. K., & Worthen-Chaudhari, L. C. (2007). Poststroke upper extremity rehabilitation: a review of robotic systems and clinical results. *Topics in stroke rehabilitation*, *14*(6), 22–44.

Brooke, J. (2013). SUS: a retrospective. *Journal of usability studies*, *8*(2), 29–40.

Brunnstrom, S. (1970). Motor behavior of adult patients with hemi-plegia. Movement therapy in hemiplegia.

Buchanan, T. S., Lloyd, D. G., Manal, K., & Besier, T. F. (2004). Neuromusculoskeletal modeling: estimation of muscle forces and joint moments and movements from measurements of neural command. *Journal of applied biomechanics*, *20*(4), 367–395.

Buongiorno, D., Sotgiu, E., Leonardis, D., Marcheschi, S., Solazzi, M., & Frisoli, A. (2018). WRES: a novel 3 DoF WRist ExoSkeleton with tendon-driven differential transmission for neuro-rehabilitation and teleoperation. *IEEE Robotics and Automation Letters*, *3*(3), 2152–2159.

Burdet, E., Osu, R., Franklin, D. W., Milner, T. E., & Kawato, M. (2001). The central nervous system stabilizes unstable dynamics by learning optimal impedance. *Nature*, *414*(6862), 446–449.

Burssens, A., Schelpe, N., Vanhaecke, J., Dezillie, M., & Stockmans, F. (2015). Influence of wrist position on maximum grip force in a post-operative orthosis. *Prosthetics and orthotics international*, 0309364615605395.

Bützer, T., Dittli, J., Lieber, J., van Hedel, H. J., Meyer-Heim, A., Lambercy, O., & Gassert, R. (2019). PEXO-A Pediatric Whole Hand Exoskeleton for Grasping Assistance in Task-Oriented Training. *2019 IEEE 16th International Conference on Rehabilitation Robotics (ICORR)*, 108–114.

Bützer, T., Lambercy, O., Arata, J., & Gassert, R. (2020). Fully wearable actuated soft exoskeleton for grasping assistance in everyday activities. *Soft Robotics*.

Cameirão, M. S., i Badia, S. B., Oller, E. D., & Verschure, P. F. (2010). Neurorehabilitation using the virtual reality based Rehabilitation Gaming System: methodology, design, psychometrics, usability and validation. *Journal of neuroengineering and rehabilitation*, *7*(1), 48.

Canning, C., & Scheutz, M. (2013). Functional near-infrared spectroscopy in human-robot interaction. *Journal of Human-Robot Interaction*, *2*(3), 62–84.

Carey, L. M. (1995). Somatosensory loss after stroke. *Critical Reviews™ in Physical and Rehabilitation Medicine*, *7*(1).

Carey, L. M., Oke, L. E., & Matyas, T. A. (1996). Impaired limb position sense after stroke: a quantitative test for clinical use. *Archives of physical medicine and rehabilitation*, *77*(12), 1271–1278.

Bibliography

Castellini, C., Arquer, A., & Artigas, J. (2014). sEMG-based estimation of human stiffness: Towards impedance-controlled rehabilitation. *5th IEEE RAS/EMBS International Conference on Biomedical Robotics and Biomechatronics*, 604–609.

Chae, J., & Hart, R. (2003). Intramuscular hand neuroprosthesis for chronic stroke survivors. *Neurorehabilitation and neural repair, 17*(2), 109–117.

Chae, J., Yang, G., Park, B. K., & Labatia, I. (2002). Muscle weakness and cocontraction in upper limb hemiparesis: relationship to motor impairment and physical disability. *Neurorehabilitation and neural repair, 16*(3), 241–248.

Charters, E. (2003). The use of think-aloud methods in qualitative research an introduction to think-aloud methods. *Brock Education Journal, 12*(2).

Chen, J., Nichols, D., Brokaw, E. B., & Lum, P. S. (2017). Home-based Therapy after Stroke Using the Hand Spring Operated Movement Enhancer (HandSOME). *IEEE Transactions on Neural Systems and Rehabilitation Engineering*.

Choi, H., Kang, B. B., Jung, B.-K., & Cho, K.-J. (2019). Exo Wrist: A Soft Tendon Driven Wrist Wearable Robot with Active Anchor for Dart Throwing Motion in Hemiplegic Patients. *IEEE Robotics and Automation Letters*.

Choi, Y., Gordon, J., Park, H., & Schweighofer, N. (2011). Feasibility of the adaptive and automatic presentation of tasks (ADAPT) system for rehabilitation of upper extremity function post-stroke. *Journal of neuroengineering and rehabilitation, 8*(1), 42.

Cirstea, M., & Levin, M. F. (2000). Compensatory strategies for reaching in stroke. *Brain, 123*(5), 940–953.

Clancy, E. A., & Hogan, N. (1997). Relating agonist-antagonist electromyograms to joint torque during isometric, quasi-isotonic, nonfatiguing contractions. *IEEE Transactions on Biomedical Engineering, 44*(10), 1024–1028.

Colombo, R., Pisano, F., Mazzone, A., Delconte, C., Micera, S., Carrozza, M. C., Dario, P., & Minuco, G. (2007). Design strategies to improve patient motivation during robot-aided rehabilitation. *Journal of neuroengineering and rehabilitation, 4*(1), 3.

Corbett, E. A., Perreault, E. J., & Kuiken, T. A. (2011). Comparison of electromyography and force as interfaces for prosthetic control. *Journal of rehabilitation research and development, 48*(6), 629.

Cramer, S. C., & Bastings, E. P. (2000). Mapping clinically relevant plasticity after stroke. *Neuropharmacology, 39*(5), 842–851.

da Silva Cameirão, M., Bermudez i Badia, S., Duarte, E., & Verschure, P. F. (2011). Virtual reality based rehabilitation speeds up functional recovery of the upper extremities after stroke: a randomized controlled pilot study in the acute phase of stroke using the rehabilitation gaming system. *Restorative neurology and neuroscience, 29*(5), 287–298.

De Luca, C. J. (1997). The use of surface electromyography in biomechanics. *Journal of applied biomechanics, 13*(2), 135–163.

De Santis, A., Siciliano, B., De Luca, A., & Bicchi, A. (2008). An atlas of physical human–robot interaction. *Mechanism and Machine Theory, 43*(3), 253–270.

Dimeas, F., & Aspragathos, N. (2016). Online stability in human-robot cooperation with admittance control. *IEEE transactions on haptics, 9*(2), 267–278.

Ding, M., Ueda, J., & Ogasawara, T. (2008). Pinpointed muscle force control using a power-assisting device: System configuration and experiment. *Biomedical Robotics and Biomechatronics, 2008. BioRob 2008. 2nd IEEE RAS & EMBS International Conference on*, 181–186.

Dipietro, L., Krebs, H. I., Fasoli, S. E., Volpe, B. T., Stein, J., Bever, C., & Hogan, N. (2007). Changing motor synergies in chronic stroke. *Journal of neurophysiology*, *98*(2), 757–768.

Dombroski, C. E., Balsdon, M. E., & Froats, A. (2014). The use of a low cost 3D scanning and printing tool in the manufacture of custom-made foot orthoses: a preliminary study. *BMC research notes*, *7*(1), 1–4.

Dragusanu, M., Baldi, T. L., Iqbal, Z., Prattichizzo, D., & Malvezzi, M. (2020). Design, Development, and Control of a Tendon-actuated Exoskeleton for Wrist Rehabilitation and Training. *2020 IEEE International Conference on Robotics and Automation (ICRA)*, 1749–1754.

Enable. (2019). *Enabling The Future - A Global Network Of Passionate Volunteers Using 3D Printing To Give The World A "Helping Hand"*. Retrieved August 8, 2019, from https://enablingthefuture.org/

Eppinger, S., & Seering, W. (1986). On dynamic models of robot force control. *Proceedings. 1986 IEEE International Conference on Robotics and Automation, 3*, 29–34.

Faeh, D., Bopp, M., Group, S. N. C. S., et al. (2010). Educational inequalities in mortality and associated risk factors: German-versus French-speaking Switzerland. *BMC public health*, *10*(1), 567.

Fang, Y., Chen, X., Li, H., Lin, J., Huang, R., & Zeng, i. (2003). A study on additional early physiotherapy after stroke and factors affecting functional recovery. *Clinical rehabilitation*, *17*(6), 608–617.

Farina, D. (2006). Interpretation of the surface electromyogram in dynamic contractions. *Exercise and sport sciences reviews, 34*(3), 121–127.

Farina, D., Jiang, N., Rehbaum, H., Holobar, A., Graimann, B., Dietl, H., & Aszmann, O. C. (2014). The extraction of neural information from the surface EMG for the control of upper-limb prostheses: emerging avenues and challenges. *IEEE Transactions on Neural Systems and Rehabilitation Engineering, 22*(4), 797–809.

Farina, D., Merletti, R., Nazzaro, M., & Caruso, I. (2001). Effect of joint angle on EMG variables in leg and thigh muscles. *IEEE engineering in medicine and biology magazine, 20*(6), 62–71.

Farrell, T. R., & Weir, R. F. (2007). The optimal controller delay for myoelectric prostheses. *IEEE Transactions on neural systems and rehabilitation engineering, 15*(1), 111–118.

Feng, X., & Winters, J. M. (2005). UniTherapy: A computer-assisted motivating neurorehabilitation platform for teleassessment and remote therapy. *9th International Conference on Rehabilitation Robotics, 2005. ICORR 2005.*, 349–352.

Feys, H., De Weerdt, W., Nuyens, G., Van De Winckel, A., Selz, B., & Kiekens, C. (2000). Predicting motor recovery of the upper limb after stroke rehabilitation: value of a clinical examination. *Physiotherapy Research International, 5*(1), 1–18.

Bibliography

Fitts, S. S., Hammond, M. C., Kraft, G. H., & Nutter, P. B. (1989). Quantification of gaps in the EMG interference pattern in chronic hemiparesis. *Electroencephalography and clinical Neurophysiology, 73*(3), 225–232.

Fitzpatrick, A. P., Mohanned, M. I., Collins, P. K., & Gibson, I. (2017). Design of a patient specific, 3D printed arm cast. *KnE Engineering*, 135–142.

Fleischer, C., & Hommel, G. (2007). Calibration of an EMG-Based Body Model with six Muscles to control a Leg Exoskeleton. *Proceedings 2007 IEEE International Conference on Robotics and Automation*, 2514–2519.

Fong, J., Rouhani, H., & Tavakoli, M. (2019). A therapist-taught robotic system for assistance during gait therapy targeting foot drop. *IEEE Robotics and Automation Letters, 4*(2), 407–413.

Frost, G., Dowling, J., Dyson, K., & Bar-Or, O. (1997). Cocontraction in three age groups of children during treadmill locomotion. *Journal of Electromyography and Kinesiology, 7*(3), 179–186.

Gallagher, W., Gao, D., & Ueda, J. (2014). Improved stability of haptic human–robot interfaces using measurement of human arm stiffness. *Advanced Robotics, 28*(13), 869–882.

Gasser, B. W., Bennett, D. A., Durrough, C. M., & Goldfarb, M. (2017). Design and preliminary assessment of Vanderbilt hand exoskeleton. *2017 International Conference on Rehabilitation Robotics (ICORR)*, 1537–1542.

Gasser, B. W., & Goldfarb, M. (2015). Design and performance characterization of a hand orthosis prototype to aid activities of daily living in a post-stroke population. *2015 37th Annual International Conference of the IEEE Engineering in Medicine and Biology Society (EMBC)*, 3877–3880.

Gemperle, F., Kasabach, C., Stivoric, J., Bauer, M., & Martin, R. (1998). Design for wearability. *digest of papers. Second international symposium on wearable computers (cat. No. 98EX215)*, 116–122.

Georgi, M., Amma, C., & Schultz, T. (2015). Recognizing Hand and Finger Gestures with IMU based Motion and EMG based Muscle Activity Sensing. *BIOSIGNALS*, 99–108.

Ghez, C., Gordon, J., Ghilardi, M., Christakos, C., & Cooper, S. (1990). Roles of proprioceptive input in the programming of arm trajectories. *Cold spring harbor symposia on quantitative biology, 55*, 837–847.

Gopura, R., Bandara, D., Kiguchi, K., & Mann, G. K. (2016). Developments in hardware systems of active upper-limb exoskeleton robots: A review. *Robotics and Autonomous Systems, 75*, 203–220.

Gopura, R., & Kiguchi, K. (2008). A human forearm and wrist motion assist exoskeleton robot with EMG-based fuzzy-neuro control. *2008 2nd IEEE RAS & EMBS International Conference on Biomedical Robotics and Biomechatronics*, 550–555.

Grafakos, S., Dimeas, F., & Aspragathos, N. (2016). Variable admittance control in pHRI using EMG-based arm muscles co-activation. *2016 IEEE International Conference on Systems, Man, and Cybernetics (SMC)*, 001900–001905.

Graham, J., Wang, M., Frizzell, K., Watkins, C., Beredjiklian, P., & Rivlin, M. (2020). Conventional vs 3-dimensional printed cast wear comfort. *HAND, 15*(3), 388–392.

Grier, R. A. (2015). How high is high? A meta-analysis of NASA-TLX global workload scores. *Proceedings of the Human Factors and Ergonomics Society Annual Meeting, 59*(1), 1727–1731.

Gupta, A., & O'Malley, M. K. (2006). Design of a haptic arm exoskeleton for training and rehabilitation. *IEEE/ASME Transactions on mechatronics, 11*(3), 280–289.

Gupta, A., O'Malley, M. K., Patoglu, V., & Burgar, C. (2008). Design, control and performance of RiceWrist: a force feedback wrist exoskeleton for rehabilitation and training. *The International Journal of Robotics Research, 27*(2), 233–251.

Halaki, M., O'Dwyer, N., & Cathers, I. (2006). Systematic nonlinear relations between displacement amplitude and joint mechanics at the human wrist. *Journal of Biomechanics, 39*(12), 2171–2182.

Hall, M. J., Levant, S., & DeFrances, C. J. (2012). Hospitalization for stroke in US hospitals, 1989–2009. *Diabetes, 18*(23), 23.

Hargrove, L., Englehart, K., & Hudgins, B. (2008). A training strategy to reduce classification degradation due to electrode displacements in pattern recognition based myoelectric control. *Biomedical signal processing and control, 3*(2), 175–180.

Hart, S. G. (2006). NASA-task load index (NASA-TLX); 20 years later. *Proceedings of the human factors and ergonomics society annual meeting, 50*(9), 904–908.

Hasan, Z. (1992). Role of proprioceptors in neural control. *Current opinion in neurobiology, 2*(6), 824–829.

Hasegawa, Y., & Suzuki, T. (2015). Thin and active fixture to hold finger for easy attachment and comfort of grasping support exoskeleton. *2015 IEEE International Conference on Robotics and Automation (ICRA)*, 4973–4978.

Hashemi, J., Morin, E., Mousavi, P., & Hashtrudi-Zaad, K. (2014). Enhanced dynamic EMG-force estimation through calibration and PCI modeling. *IEEE Transactions on Neural Systems and Rehabilitation Engineering, 23*(1), 41–50.

Hayward, V., & Astley, O. R. (1996). Performance measures for haptic interfaces. *Robotics research* (pp. 195–206). Springer.

Hazelton, F. T., Smidt, G. L., Flatt, A. E., & Stephens, R. I. (1975). The influence of wrist position on the force produced by the finger flexors. *Journal of Biomechanics, 8*(5), 301–306.

Heo, P., Gu, G. M., Lee, S.-j., Rhee, K., & Kim, J. (2012). Current hand exoskeleton technologies for rehabilitation and assistive engineering. *International Journal of Precision Engineering and Manufacturing, 13*(5), 807–824.

Higuma, T., Kiguchi, K., & Arata, J. (2017). Low-Profile Two-Degree-of-Freedom Wrist Exoskeleton Device Using Multiple Spring Blades. *IEEE Robotics and Automation Letters, 3*(1), 305–311.

Ho, N., Tong, K., Hu, X., Fung, K., Wei, X., Rong, W., & Susanto, E. (2011). An EMG-driven exoskeleton hand robotic training device on chronic stroke subjects: task training system for stroke rehabilitation. *Rehabilitation Robotics (ICORR), 2011 IEEE International Conference on*, 1–5.

Bibliography

Hofmann, U. A., Bützer, T., Lambercy, O., & Gassert, R. (2018). Design and evaluation of a bowden-cable-based remote actuation system for wearable robotics. *IEEE Robotics and Automation Letters, 3*(3), 2101–2108.

Hogan, N., & Sternad, D. (2009). Sensitivity of smoothness measures to movement duration, amplitude, and arrests. *Journal of motor behavior, 41*(6), 529–534.

Houwink, A., Nijland, R. H., Geurts, A. C., & Kwakkel, G. (2013). Functional recovery of the paretic upper limb after stroke: who regains hand capacity? *Archives of physical medicine and rehabilitation, 94*(5), 839–844.

Hsieh, H.-C., Chien, L., & Lan, C.-C. (2015). Mechanical design of a gravity-balancing wearable exoskeleton for the motion enhancement of human upper limb. *2015 IEEE International Conference on Robotics and Automation (ICRA)*, 4992–4997.

Hsieh, Y.-W., Lin, K.-C., Wu, C.-Y., Shih, T.-Y., Li, M.-W., & Chen, C.-L. (2018). Comparison of proximal versus distal upper-limb robotic rehabilitation on motor performance after stroke: a cluster controlled trial. *Scientific reports, 8*(1), 1–11.

Hu, X., Tong, K.-Y., Song, R., Zheng, X. J., & Leung, W. W. (2009a). A comparison between electromyography-driven robot and passive motion device on wrist rehabilitation for chronic stroke. *Neurorehabilitation and neural repair, 23*(8), 837–846.

Hu, X., Tong, K., Song, R., Zheng, X., Lui, K., Leung, W., Ng, S., & Au-Yeung, S. (2009b). Quantitative evaluation of motor functional recovery process in chronic stroke patients during robot-assisted wrist training. *Journal of Electromyography and Kinesiology, 19*(4), 639–650.

Hu, X., Tong, R. K.-Y., Ho, N. S., Xue, J.-J., Rong, W., & Li, L. S. (2015). Wrist rehabilitation assisted by an electromyography-driven neuromuscular electrical stimulation robot after stroke. *Neurorehabilitation and neural repair, 29*(8), 767–776.

Huang, S., Cai, S., Li, G., Chen, Y., Ma, K., & Xie, L. (2019). SEMG-based detection of compensation caused by fatigue during rehabilitation therapy: A pilot study. *IEEE Access, 7*, 127055–127065.

Hwang, H.-J., Hahne, J. M., & Müller, K.-R. (2017). Real-time robustness evaluation of regression based myoelectric control against arm position change and donning/doffing. *PloS one, 12*(11).

iDryNeedle. (2021). *iDryNeedle the blog*. Retrieved March 5, 2021, from https://idryneedle. wordpress.com/2017/09/13/journal-club-dry-needling-on-contractile-properties-of-spastic-muscles-post-stroke

IDUN. (2020). *We enable the internet of Humans*. Retrieved November 20, 2020, from https://iduntechnologies.ch

IIT. (2021). *Start-it-up with WRISTBOT*. Retrieved March 5, 2021, from https://istituto-italiano-di-tecnologia.hivebrite.com/news/241798

Iqbal, J., Ahmad, O., & Malik, A. (2011). HEXOSYS II-towards realization of light mass robotics for the hand. *Multitopic Conference (INMIC), 2011 IEEE 14th International*, 115–119.

Ison, M., & Artemiadis, P. (2014). The role of muscle synergies in myoelectric control: trends and challenges for simultaneous multifunction control. *Journal of neural engineering, 11*(5), 051001.

Jiang, N., Englehart, K. B., & Parker, P. A. (2008). Extracting simultaneous and proportional neural control information for multiple-DOF prostheses from the surface electromyographic signal. *IEEE transactions on Biomedical Engineering, 56*(4), 1070–1080.

Johnson, M. J., Feng, X., Johnson, L. M., & Winters, J. M. (2007). Potential of a suite of robot/computer-assisted motivating systems for personalized, home-based, stroke rehabilitation. *Journal of NeuroEngineering and Rehabilitation, 4*(1), 6.

Joshi, A., Kale, S., Chandel, S., & Pal, D. K. (2015). Likert scale: Explored and explained. *Current Journal of Applied Science and Technology*, 396–403.

Jung, H.-Y. (2017). Rehabilitation in subacute and chronic stage after stroke. *Stroke revisited: diagnosis and treatment of ischemic stroke* (pp. 351–360). Springer.

Juszczak, M., Gallo, E., & Bushnik, T. (2018). Examining the effects of a powered exoskeleton on quality of life and secondary impairments in people living with spinal cord injury. *Topics in spinal cord injury rehabilitation, 24*(4), 336–342.

Kamper, D. G., Fischer, H. C., Cruz, E. G., & Rymer, W. Z. (2006). Weakness is the primary contributor to finger impairment in chronic stroke. *Archives of physical medicine and rehabilitation, 87*(9), 1262–1269.

Kessner, S. S., Bingel, U., & Thomalla, G. (2016). Somatosensory deficits after stroke: a scoping review. *Topics in Stroke Rehabilitation, 23*(2), 136–146.

Khokhar, Z. O., Xiao, Z. G., & Menon, C. (2010). Surface EMG pattern recognition for real-time control of a wrist exoskeleton. *Biomedical engineering online, 9*(1), 41.

Kilic, E. (2017). EMG based neural network and admittance control of an active wrist orthosis. *Journal of Mechanical Science and Technology, 31*(12), 6093–6106.

Kim, J., Kim, M., & Kim, K. (2016). Development of a wearable HCI controller through sEMG & IMU sensor fusion. *2016 13th International Conference on Ubiquitous Robots and Ambient Intelligence (URAI)*, 83–87.

Kim, M., Kim, K., & Chung, W. K. (2018a). Simple and fast compensation of sEMG interface rotation for robust hand motion recognition. *IEEE Transactions on Neural Systems and Rehabilitation Engineering, 26*(12), 2397–2406.

Kim, S., Nussbaum, M. A., Esfahani, M. I. M., Alemi, M. M., Jia, B., & Rashedi, E. (2018b). Assessing the influence of a passive, upper extremity exoskeletal vest for tasks requiring arm elevation: Part II–"Unexpected" effects on shoulder motion, balance, and spine loading. *Applied ergonomics, 70*, 323–330.

Kim, T. S., Park, D. D. H., Lee, Y. B., Han, D. G., su Shim, J., Lee, Y. J., Kim, P. C. W., et al. (2014). A study on the measurement of wrist motion range using the iPhone 4 gyroscope application. *Annals of plastic surgery, 73*(2), 215–218.

Kitago, T., & Krakauer, J. W. (2013). Motor learning principles for neurorehabilitation. *Handbook of clinical neurology* (pp. 93–103). Elsevier.

Kleim, J. A., & Jones, T. A. (2008). Principles of experience-dependent neural plasticity: implications for rehabilitation after brain damage. *Journal of speech, language, and hearing research*.

Bibliography

Klein, J., Spencer, S. J., & Reinkensmeyer, D. J. (2012). Breaking it down is better: haptic decomposition of complex movements aids in robot-assisted motor learning. *IEEE Transactions on Neural Systems and Rehabilitation Engineering, 20*(3), 268–275.

Kline, T., Kamper, D., & Schmit, B. (2005). Control system for pneumatically controlled glove to assist in grasp activities. *Rehabilitation Robotics, 2005. ICORR 2005. 9th International Conference on*, 78–81.

Koeneman, E., Schultz, R., Wolf, S., Herring, D., & Koeneman, J. (2004). A pneumatic muscle hand therapy device. *Engineering in Medicine and Biology Society, 2004. IEMBS'04. 26th Annual International Conference of the IEEE, 1*, 2711–2713.

Kozlowski, A., Bryce, T., & Dijkers, M. (2015). Time and effort required by persons with spinal cord injury to learn to use a powered exoskeleton for assisted walking. *Topics in spinal cord injury rehabilitation, 21*(2), 110–121.

Kuchenbecker, K. J., Park, J. G., & Niemeyer, G. n. (2003). Characterizing the human wrist for improved haptic interaction. *ASME International Mechanical Engineering Congress and Exposition, 37130*, 591–598.

Kwakkel, G. (2009). Intensity of practice after stroke: More is better. *Schweizer Archiv fur Neurologie und Psychiatrie, 160*(7), 295–298. https://doi.org/10.1080/09638280500534861

Kwakkel, G., Kollen, B., & Twisk, J. (2006). Impact of time on improvement of outcome after stroke. *Stroke, 37*(9), 2348–2353.

Kwakkel, G., Kollen, B. J., & Krebs, H. I. (2007). Effects of robot-assisted therapy on upper limb recovery after stroke: a systematic review. *Neurorehabilitation and neural repair*.

Kwakkel, G., Kollen, B. J., & Krebs, H. I. (2008). Effects of robot-assisted therapy on upper limb recovery after stroke: a systematic review. *Neurorehabilitation and neural repair, 22*(2), 111–121.

Kwakkel, G., Kollen, B. J., van der Grond, J., & Prevo, A. J. (2003). Probability of regaining dexterity in the flaccid upper limb: impact of severity of paresis and time since onset in acute stroke. *Stroke, 34*(9), 2181–2186.

Kwakkel, G., & Meskers, C. (2013). Effects of robotic therapy of the arm after stroke. *The Lancet. Neurology, 13*(2), 132–133.

Lai, J. C., Woo, J., Hui, E., & Chan, W. (2004). Telerehabilitation—a new model for community-based stroke rehabilitation. *Journal of telemedicine and telecare, 10*(4), 199–205.

Lambelet, C., Lyu, M., Woolley, D., Gassert, R., & Wenderoth, N. (2017). The eWrist—A wearable wrist exoskeleton with sEMG-based force control for stroke rehabilitation. *2017 International Conference on Rehabilitation Robotics (ICORR)*, 726–733.

Lambelet, C., Temiraliuly, D., Siegenthaler, M., Wirth, M., Woolley, D. G., Lambercy, O., Gassert, R., & Wenderoth, N. (2020). Characterization and wearability evaluation of a fully portable wrist exoskeleton for unsupervised training after stroke. *Journal of NeuroEngineering and Rehabilitation, 17*(1), 1–16.

Lambercy, O., Dovat, L., Yun, H., Wee, S. K., Kuah, C. W., Chua, K. S., Gassert, R., Milner, T. E., Teo, C. L., & Burdet, E. (2011). Effects of a robot-assisted training of grasp and pronation/supination in chronic stroke: a pilot study. *Journal of neuroengineering and rehabilitation, 8*(1), 63.

Lambercy, O., Ranzani, R., & Gassert, R. (2018). Robot-assisted rehabilitation of hand function. *Rehabilitation Robotics* (pp. 205–225). Elsevier.

Lance, J. W. (1980). The control of muscle tone, reflexes, and movement: Robert Wartenbeg Lecture. *Neurology*, *30*(12), 1303–1303.

Landi, C. T., Ferraguti, F., Sabattini, L., Secchi, C., & Fantuzzi, C. (2017). Admittance control parameter adaptation for physical human-robot interaction. *2017 IEEE International Conference on Robotics and Automation (ICRA)*, 2911–2916.

Lang, C. E., MacDonald, J. R., Reisman, D. S., Boyd, L., Kimberley, T. J., Schindler-Ivens, S. M., Hornby, T. G., Ross, S. A., & Scheets, P. L. (2009). Observation of amounts of movement practice provided during stroke rehabilitation. *Archives of physical medicine and rehabilitation*, *90*(10), 1692–1698.

Langhorne, P., Bernhardt, J., & Kwakkel, G. (2011). Stroke rehabilitation. *The Lancet, 377*(9778), 1693–1702.

Langhorne, P., Coupar, F., & Pollock, A. (2009). Motor recovery after stroke: a systematic review. *The Lancet Neurology*, *8*(8), 741–754.

Langhorne, P., Wagenaar, R., & Partridge, C. (1996). Physiotherapy after stroke: more is better? *Physiotherapy Research International*, *1*(2), 75–88.

Lapchak, P. A., & Zhang, J. H. (2017). The high cost of stroke and stroke cytoprotection research. *Translational stroke research*, *8*(4), 307–317.

Laredo, C., Zhao, Y., Rudilosso, S., Renú, A., Pariente, J. C., Chamorro, Á., & Urra, X. (2018). Prognostic significance of infarct size and location: the case of insular stroke. *Scientific reports*, *8*(1), 1–10.

LaStayo, P., & Hartzel, J. (1999). Dynamic versus static grip strength: how grip strength changes when the wrist is moved, and why dynamic grip strength may be a more functional measurement. *Journal of Hand Therapy*, *12*(3), 212–218.

Laver, K. E., Adey-Wakeling, Z., Crotty, M., Lannin, N. A., George, S., & Sherrington, C. (2020). Telerehabilitation services for stroke. *Cochrane Database of Systematic Reviews*, (1).

Lecours, A., Mayer-St-Onge, B., & Gosselin, C. (2012). Variable admittance control of a four-degree-of-freedom intelligent assist device. *2012 IEEE International Conference on Robotics and Automation*, 3903–3908.

Lee, G., Ding, Y., Bujanda, I. G., Karavas, N., Zhou, Y. M., & Walsh, C. J. (2017). Improved assistive profile tracking of soft exosuits for walking and jogging with off-board actuation. *2017 IEEE/RSJ International Conference on Intelligent Robots and Systems (IROS)*, 1699–1706.

Lee, S. I., Adans-Dester, C. P., Grimaldi, M., Dowling, A. V., Horak, P. C., Black-Schaffer, R. M., Bonato, P., & Gwin, J. T. (2018). Enabling stroke rehabilitation in home and community settings: a wearable sensor-based approach for upper-limb motor training. *IEEE journal of translational engineering in health and medicine, 6*, 1–11.

Lee, S. I., Adans-Dester, C., O'Brien, A., Diaz, G. V., Black-Schaffer, R., Patel, S., Zafonte, R., & Bonato, P. (2016). Using wearable motion sensors to estimate longitudinal changes in movement quality in stroke and traumatic brain injury survivors undergoing rehabilitation. *Archives of Physical Medicine and Rehabilitation, 97*(10), e117.

Bibliography

Leger, A. B., & Milner, T. E. (2000). Passive and active wrist joint stiffness following eccentric exercise. *European journal of applied physiology, 82*(5-6), 472–479.

Lenzi, T., De Rossi, S. M. M., Vitiello, N., & Carrozza, M. C. (2012). Intention-based EMG control for powered exoskeletons. *IEEE transactions on biomedical engineering, 59*(8), 2180–2190.

Leuenberger, K., Gonzenbach, R., Wachter, S., Luft, A., & Gassert, R. (2017). A method to qualitatively assess arm use in stroke survivors in the home environment. *Medical & biological engineering & computing, 55*(1), 141–150.

Lewis, J. R., & Sauro, J. (2009). The factor structure of the system usability scale. *International conference on human centered design*, 94–103.

Liarokapis, M. V., Zisimatos, A. G., Mavrogiannis, C. I., & Kyriakopoulos, K. J. (2014). Open-bionics: An open-source initiative for the creation of affordable, modular, light-weight, underactuated robot hands and prosthetic devices. *2nd ASU Rehabilitation Robotics Workshop.*

Liebesman, J., & Cafarelli, E. (1994). Physiology of range of motion in human joints: a critical review. *Critical reviews in physical and rehabilitation medicine, 6*, 131–131.

Liepert, J., Miltner, W., Bauder, H., Sommer, M., Dettmers, C., Taub, E., & Weiller, C. (1998). Motor cortex plasticity during constraint-induced movement therapy in stroke patients. *Neuroscience letters, 250*(1), 5–8.

Liepert, J., Tegenthoff, M., & Malin, J.-P. (1995). Changes of cortical motor area size during immobilization. *Electroencephalography and clinical neurophysiology/electromyography and motor control, 97*(6), 382–386.

Liepert, J., Bauder, H., Miltner, W. H., Taub, E., & Weiller, C. (2000). Treatment-induced cortical reorganization after stroke in humans. *Stroke, 31*(6), 1210–1216.

Liljegren, E. (2006). Usability in a medical technology context assessment of methods for usability evaluation of medical equipment. *International Journal of Industrial Ergonomics, 36*(4), 345–352.

Lipovskā, R., & Ferreira, H. A. (2015). Hand Therapist: a rehabilitation approach based on wearable technology and video gaming. *2015 IEEE 4th Portuguese Meeting on Bioengineering (ENBENG)*, 1–2.

Lloyd-Jones. (2009). Heart Disease and Stroke Statistics-2009 Update: A Report From the American Heart Association Statistics Committee and Stroke Statistics Subcommittee (vol 119, pg e21, 2009). *Circulation, 119*(3), E182–E182.

Lo, K., Stephenson, M., & Lockwood, C. (2019). The economic cost of robotic rehabilitation for adult stroke patients: a systematic review. *JBI Evidence Synthesis, 17*(4), 520–547.

Lobo-Prat, J., Keemink, A. Q., Stienen, A. H., Schouten, A. C., Veltink, P. H., & Koopman, B. F. (2014). Evaluation of EMG, force and joystick as control interfaces for active arm supports. *Journal of neuroengineering and rehabilitation, 11*(1), 68.

Lotze, M., Braun, C., Birbaumer, N., Anders, S., & Cohen, L. G. (2003). Motor learning elicited by voluntary drive. *Brain, 126*(4), 866–872.

Loureiro, R. C., Belda-Lois, J. M., Lima, E. R., Pons, J. L., Sanchez-Lacuesta, J. J., & Harwin, W. S. (2005). Upper limb tremor suppression in ADL via an orthosis incorporating a

controllable double viscous beam actuator. *Rehabilitation Robotics, 2005. ICORR 2005. 9th International Conference on*, 119–122.

Lum, P. S., Burgar, C. G., Shor, P. C., Majmundar, M., & Van der Loos, M. (2002). Robot-assisted movement training compared with conventional therapy techniques for the rehabilitation of upper-limb motor function after stroke. *Archives of physical medicine and rehabilitation, 83*(7), 952–959.

Lyu, M., Chen, W., Ding, X., Wang, J., Pei, Z., & Zhang, B. (2019). Development of an EMG-Controlled Knee Exoskeleton to Assist Home Rehabilitation in a Game Context. *Frontiers in Neurorobotics, 13*, 67.

Lyu, M., Lambelet, C., Woolley, D., Zhang, X., Chen, W., Ding, X., Gassert, R., & Wenderoth, N. (2017). Training wrist extensor function and detecting unwanted movement strategies in an EMG-controlled visuomotor task. *2017 International Conference on Rehabilitation Robotics (ICORR)*, 1549–1555.

Lyu, M., Lambelet, C., Woolley, D., Zhang, X., Chen, W., Ding, X., Gassert, R., & Wenderoth, N. (2020). Comparison of Particle Filter to Established Filtering Methods in Electromyography Biofeedback. *Biomedical Signal Processing and Control, 60*, 101949.

Maciejasz, P., Eschweiler, J., Gerlach-Hahn, K., Jansen-Troy, A., & Leonhardt, S. (2014). A survey on robotic devices for upper limb rehabilitation. *Journal of neuroengineering and rehabilitation, 11*(1), 3.

Mackay, J., & Mensah, G. A. (2004). *The atlas of heart disease and stroke.* World Health Organization.

Maclean, N., Pound, P., Wolfe, C., & Rudd, A. (2000). Qualitative analysis of stroke patients' motivation for rehabilitation. *Bmj, 321*(7268), 1051–1054.

Maclean, N., Pound, P., Wolfe, C., & Rudd, A. (2002). The concept of patient motivation: a qualitative analysis of stroke professionals' attitudes. *Stroke, 33*(2), 444–448.

Marini, F., Hughes, C. M., Squeri, V., Doglio, L., Moretti, P., Morasso, P., & Masia, L. (2017). Robotic wrist training after stroke: Adaptive modulation of assistance in pediatric rehabilitation. *Robotics and Autonomous Systems, 91*, 169–178.

Marras, W. S., & Schoenmarxlin, R. W. (1993). Wrist motions in industry. *Ergonomics, 36*(4), 341–351.

Martinez, J. A., Ng, P., Lu, S., Campagna, M. S., & Celik, O. (2013). Design of Wrist Gimbal: A forearm and wrist exoskeleton for stroke rehabilitation. *Rehabilitation Robotics (ICORR), 2013 IEEE International Conference on*, 1–6.

Marumoto, K., Hosomi, M., Koyama, T., Furukawa, K., Kodama, N., & Domen, K. (2011). The neural basis of constraint-induced movement therapy: A diffusion tensor imaging (DTI) study. *Neuroscience Research*, (71), e251.

Masiero, S., Armani, M., Ferlini, G., Rosati, G., & Rossi, A. (2014). Randomized trial of a robotic assistive device for the upper extremity during early inpatient stroke rehabilitation. *Neurorehabilitation and neural repair, 28*(4), 377–386.

Masson, S., Fortuna, F., Moura, F., Soriano, D., & do ABC, S. B. d. C. (2016). Integrating Myo armband for the control of myoelectric upper limb prosthesis. *Proceedings of the XXV Congresso Brasileiro de Engenharia Biomédica.*

Bibliography

Mateo, S., Revol, P., Fourtassi, M., Rossetti, Y., Collet, C., & Rode, G. (2013). Kinematic characteristics of tenodesis grasp in C6 quadriplegia. *Spinal cord*, *51*(2), 144–149.

Mauricio Ochoa, J., & Kamper, D. (2009). Development of an actuated cable orthotic glove to provide assistance of finger extension to stroke survivors. *Revista Ingenieríea Biomédica*, *3*(5), 75–82.

McKenna, C., Chen, P., & Barrett, A. (2017). Stroke: Impact on life and daily function. *Changes in the Brain* (pp. 87–115). Springer.

Menegaldo, L. L. (2017). Real-time muscle state estimation from EMG signals during isometric contractions using Kalman filters. *Biological Cybernetics*, *111*(5-6), 335–346.

Merritt, H. E. (1935). Worm gear performance. *Proceedings of the Institution of Mechanical Engineers*, *129*(1), 127–194.

Metzger, J.-C., Lambercy, O., & Gassert, R. (2015). Performance comparison of interaction control strategies on a hand rehabilitation robot. *2015 IEEE International Conference on Rehabilitation Robotics (ICORR)*, 846–851.

Meuleman, J., van Asseldonk, E., van Oort, G., Rietman, H., & van der Kooij, H. (2015). LOPES II—design and evaluation of an admittance controlled gait training robot with shadow-leg approach. *IEEE transactions on neural systems and rehabilitation engineering*, *24*(3), 352–363.

Meyer, J. T., Dittli, J., Stutz, A., Lambercy, O., & Gassert, R. (2020). A Method to Evaluate and Improve the Usability of a Robotic Hand Orthosis from the Caregiver Perspective. *2020 8th IEEE RAS/EMBS International Conference for Biomedical Robotics and Biomechatronics (BioRob)*, 605–610.

Miall, R. C., Kitchen, N. M., Nam, S.-H., Lefumat, H., Renault, A. G., Ørstavik, K., Cole, J. D., & Sarlegna, F. R. (2018). Proprioceptive loss and the perception, control and learning of arm movements in humans: evidence from sensory neuronopathy. *Experimental brain research*, *236*(8), 2137–2155.

Micera, S., Carrozza, M. C., Guglielmelli, E., Cappiello, G., Zaccone, F., Freschi, C., Colombo, R., Mazzone, A., Delconte, C., Pisano, F., et al. (2005). A simple robotic system for neurorehabilitation. *Autonomous Robots*, *19*(3), 271.

Miranda, A., Coelho, T., Forner-Cordero, A., & Siqueira, A. (2015). Directional stiffness attachment design for an upper limb exoskeleton. *2015 IEEE International Conference on Rehabilitation Robotics (ICORR)*, 446–450.

Montagnani, F., Controzzi, M., & Cipriani, C. (2015). Is it finger or wrist dexterity that is missing in current hand prostheses? *IEEE Transactions on Neural Systems and Rehabilitation Engineering*, *23*(4), 600–609.

Morales, R., Badesa, F. J., Garcíea-Aracil, N., Sabater, J. M., & Pérez-Vidal, C. (2011). Pneumatic robotic systems for upper limb rehabilitation. *Medical & biological engineering & computing*, *49*(10), 1145.

Moroney, W. F., Biers, D. W., & Eggemeier, F. T. (1995). Some measurement and methodological considerations in the application of subjective workload measurement techniques. *The international journal of aviation psychology*, *5*(1), 87–106.

Moubarak, S., Pham, M. T., Moreau, R., & Redarce, T. (2010). Gravity compensation of an upper extremity exoskeleton. *2010 Annual International Conference of the IEEE Engineering in Medicine and Biology*, 4489–4493.

Mulas, M., Folgheraiter, M., & Gini, G. (2005). An EMG-controlled exoskeleton for hand rehabilitation. *Rehabilitation Robotics, 2005. ICORR 2005. 9th International Conference on*, 371–374.

Murphy, T. H., & Corbett, D. (2009). Plasticity during stroke recovery: from synapse to behaviour. *Nature reviews neuroscience*, *10*(12), 861–872.

Nef, T., Mihelj, M., Colombo, G., & Riener, R. (2006). ARMin-robot for rehabilitation of the upper extremities. *Robotics and Automation, 2006. ICRA 2006. Proceedings 2006 IEEE International Conference on*, 3152–3157.

Neofect. (2020). *NeoMano: A Grasp Assist Device Gets Ready to Make a Debut!* Retrieved November 11, 2020, from https://www.neofect.com/us/blog/neomano-a-grasp-assist-device-gets-ready-to-make-a-debut

NeuroRehab. (2021). *NeuroRehab Directory*. Retrieved March 5, 2021, from https://www.neurorehabdirectory.com/rehab-products/inmotion-wrist

Nielsen, J., Clemmensen, T., & Yssing, C. (2002). Getting access to what goes on in people's heads?: reflections on the think-aloud technique. *Proceedings of the second Nordic conference on Human-computer interaction*, 101–110.

Nilsson, M., Ingvast, J., Wikander, J., & von Holst, H. (2012). The Soft Extra Muscle system for improving the grasping capability in neurological rehabilitation. *2012 IEEE-EMBS Conference on Biomedical Engineering and Sciences*, 412–417.

Norman, R. W., & Komi, P. V. (1979). Electromechanical delay in skeletal muscle under normal movement conditions. *Acta Physiologica Scandinavica*, *106*(3), 241–248.

Norouzi-Gheidari, N., Archambault, P. S., & Fung, J. (2012). Effects of robot-assisted therapy on stroke rehabilitation in upper limbs: systematic review and meta-analysis of the literature. *Journal of Rehabilitation Research & Development*, *49*(4).

Nycz, C. J., Bützer, T., Lambercy, O., Arata, J., Fischer, G. S., & Gassert, R. (2016). Design and characterization of a lightweight and fully portable remote actuation system for use with a hand exoskeleton. *IEEE Robotics and Automation Letters*, *1*(2), 976–983.

Nygren, T. E. (1991). Psychometric properties of subjective workload measurement techniques: Implications for their use in the assessment of perceived mental workload. *Human factors*, *33*(1), 17–33.

O Driscoll, S. W., & Giori, N. J. (2000). Continuous passive motion (CPM): theory and principles of clinical application. *Journal of rehabilitation research and development*, *37*(2), 179–188.

O'Driscoll, S. W., Horii, E., Ness, R., Cahalan, T. D., Richards, R. R., & An, K.-N. (1992). The relationship between wrist position, grasp size, and grip strength. *The Journal of hand surgery*, *17*(1), 169–177.

Ojaghihaghighi, S., Vahdati, S. S., Mikaeilpour, A., & Ramouz, A. (2017). Comparison of neurological clinical manifestation in patients with hemorrhagic and ischemic stroke. *World journal of emergency medicine*, *8*(1), 34.

Bibliography

Oldfield, R. C. (1971). The assessment and analysis of handedness: the Edinburgh inventory. *Neuropsychologia, 9*(1), 97–113.

OpenBCI. (2020). *Open Source Brain-Computer Interfaces.* Retrieved November 20, 2020, from https://openbci.com

Ostwald, S. K., Davis, S., Hersch, G., Kelley, C., & Godwin, K. M. (2008). Evidence-based educational guidelines for stroke survivors after discharge home. *The Journal of neuroscience nursing: journal of the American Association of Neuroscience Nurses, 40*(3), 173.

Ottenbacher, K. J., & Jannell, S. (1993). The results of clinical trials in stroke rehabilitation research. *Archives of neurology, 50*(1), 37–44.

Palmer, A. K., Werner, F. W., Murphy, D., & Glisson, R. (1985). Functional wrist motion: a biomechanical study. *The Journal of hand surgery, 10*(1), 39–46.

Patel, A. T., Duncan, P. W., Lai, S.-M., & Studenski, S. (2000). The relation between impairments and functional outcomes poststroke. *Archives of physical medicine and rehabilitation, 81*(10), 1357–1363.

Patel, S., Hughes, R., Hester, T., Stein, J., Akay, M., Dy, J. G., & Bonato, P. (2010). A novel approach to monitor rehabilitation outcomes in stroke survivors using wearable technology. *Proceedings of the IEEE, 98*(3), 450–461.

Pehlivan, A. U., Sergi, F., Erwin, A., Yozbatiran, N., Francisco, G. E., & O'Malley, M. K. (2014). Design and validation of the RiceWrist-S exoskeleton for robotic rehabilitation after incomplete spinal cord injury. *Robotica, 32*(8), 1415.

Penalver-Andres, J., Duarte, J., Vallery, H., Klamroth-Marganska, V., Riener, R., Marchal-Crespo, L., & Rauter, G. (2019). Do we need complex rehabilitation robots for training complex tasks? *2019 IEEE 16th International Conference on Rehabilitation Robotics (ICORR),* 1085–1090.

Perez, M. A., Lungholt, B. K., Nyborg, K., & Nielsen, J. B. (2004). Motor skill training induces changes in the excitability of the leg cortical area in healthy humans. *Experimental brain research, 159*(2), 197–205.

Perry, J. C., Trimble, S., Machado, L. G. C., Schroeder, J. S., Belloso, A., Rodriguez-de-Pablo, C., & Keller, T. (2016). Design of a spring-assisted exoskeleton module for wrist and hand rehabilitation. *Engineering in Medicine and Biology Society (EMBC), 2016 IEEE 38th Annual International Conference of the,* 594–597.

Pezent, E., Rose, C. G., Deshpande, A. D., & O'Malley, M. K. (2017). Design and characterization of the openwrist: A robotic wrist exoskeleton for coordinated hand-wrist rehabilitation. *2017 International Conference on Rehabilitation Robotics (ICORR),* 720–725.

Pham, M., Mengistu, Y., Do, H., & Sheng, W. (2018). Delivering home healthcare through a cloud-based smart home environment (CoSHE). *Future Generation Computer Systems, 81,* 129–140.

Pignolo, L. (2009). Robotics in neuro-rehabilitation. *Journal of Rehabilitation Medicine, 41*(12), 955–960.

Pila, O., Duret, C., Laborne, F.-X., Gracies, J.-M., Bayle, N., & Hutin, E. (2017). Pattern of improvement in upper limb pointing task kinematics after a 3-month training program

with robotic assistance in stroke. *Journal of neuroengineering and rehabilitation, 14*(1), 105.

Polygerinos, P., Wang, Z., Galloway, K. C., Wood, R. J., & Walsh, C. J. (2015). Soft robotic glove for combined assistance and at-home rehabilitation. *Robotics and Autonomous Systems, 73*, 135–143.

Power, V., O'Sullivan, L., de Eyto, A., Schülein, S., Nikamp, C., Bauer, C., Mueller, J., & Ortiz, J. (2016). Exploring user requirements for a lower body soft exoskeleton to assist mobility. *Proceedings of the 9th ACM International Conference on PErvasive Technologies Related to Assistive Environments*, 1–6.

Prange, G. B., Jannink, M. J., Groothuis-Oudshoorn, C. G., Hermens, H. J., & IJzerman, M. J. (2006). Systematic review of the effect of robot-aided therapy on recovery of the hemiparetic arm after stroke. *Journal of rehabilitation research and development, 43*(2), 171.

Proietti, T., Crocher, V., Roby-Brami, A., & Jarrasse, N. (2016). Upper-limb robotic exoskeletons for neurorehabilitation: a review on control strategies. *IEEE reviews in biomedical engineering, 9*, 4–14.

Proske, U., & Gandevia, S. C. (2012). The proprioceptive senses: their roles in signaling body shape, body position and movement, and muscle force. *Physiological reviews, 92*(4), 1651–1697.

Pryce, J. C. (1980). The wrist position between neutral and ulnar deviation that facilitates the maximum power grip strength. *Journal of biomechanics, 13*(6), 505509–507511.

Qiuyang, Q., Nam, C., Guo, Z., Huang, Y., Hu, X., Ng, S. C., Zheng, Y., & Poon, W. (2019). Distal versus proximal-an investigation on different supportive strategies by robots for upper limb rehabilitation after stroke: a randomized controlled trial. *Journal of neuroengineering and rehabilitation, 16*(1), 64.

Qlone. (2020). *3D SCAN ANY OBJECT*. Retrieved November 18, 2020, from https://www.qlone.pro

Radder, B., Prange-Lasonder, G. B., Kottink, A. I., Holmberg, J., Sletta, K., van Dijk, M., Meyer, T., Melendez-Calderon, A., Buurke, J. H., & Rietman, J. S. (2019). Home rehabilitation supported by a wearable soft-robotic device for improving hand function in older adults: A pilot randomized controlled trial. *PloS one, 14*(8), e0220544.

Raghavan, P. (2007). The nature of hand motor impairment after stroke and its treatment. *Current treatment options in cardiovascular medicine, 9*(3), 221–228.

Ramirez, L., Kim-Tenser, M. A., Sanossian, N., Cen, S., Wen, G., He, S., Mack, W. J., & Towfighi, A. (2016). Trends in acute ischemic stroke hospitalizations in the United States. *Journal of the American Heart Association, 5*(5), e003233.

Randazzo, L., Iturrate, I., Perdikis, S., & Millán, J. d. R. (2017). mano: A wearable hand exoskeleton for activities of daily living and neurorehabilitation. *IEEE Robotics and Automation Letters, 3*(1), 500–507.

Rathore, S. S., Hinn, A. R., Cooper, L. S., Tyroler, H. A., & Rosamond, W. D. (2002). Characterization of incident stroke signs and symptoms: findings from the atherosclerosis risk in communities study. *Stroke, 33*(11), 2718–2721.

Bibliography

Reding, M. J., & Potes, E. (1988). Rehabilitation outcome following initial unilateral hemispheric stroke. Life table analysis approach. *Stroke, 19*(11), 1354–1358.

Reimer, S. M., Lueth, T. C., & D'Angelo, L. T. (2014). Individualized arm shells towards an ergonomic design of exoskeleton robots. *2014 IEEE International Conference on Systems, Man, and Cybernetics (SMC)*, 3958–3965.

Resnik, L. (2011). Development and testing of new upper-limb prosthetic devices: Research designs for usability testing. *Journal of Rehabilitation Research & Development, 48*(6), 697.

Rose, C. G., Pezent, E., Kann, C. K., Deshpande, A. D., & O'Malley, M. K. (2018). Assessing Wrist Movement With Robotic Devices. *IEEE Transactions on Neural Systems and Rehabilitation Engineering, 26*(8), 1585–1595.

Rose, C. G., Sergi, F., Yun, Y., Madden, K., Deshpande, A. D., & O'Malley, M. K. (2015). Characterization of a hand-wrist exoskeleton, READAPT, via kinematic analysis of redundant pointing tasks. *2015 IEEE International Conference on Rehabilitation Robotics (ICORR)*, 205–210.

Rosenthal, R. (2005). Expectancy Effect by Experimenters. *Encyclopedia of Statistics in Behavioral Science.*

Rubio, S., Diéaz, E., Martién, J., & Puente, J. M. (2004). Evaluation of subjective mental workload: A comparison of SWAT, NASA-TLX, and workload profile methods. *Applied Psychology, 53*(1), 61–86.

Ryu, D., Song, J.-B., Kang, S., & Kim, M. (2008). Frequency domain stability observer and active damping control for stable haptic interaction. *IET Control Theory & Applications, 2*(4), 261–268.

Sangha, S., Elnady, A. M., & Menon, C. (2016). A compact robotic orthosis for wrist assistance. *2016 6th IEEE International Conference on Biomedical Robotics and Biomechatronics (BioRob)*, 1080–1085.

Sarlegna, F. R., & Sainburg, R. L. (2009). The roles of vision and proprioception in the planning of reaching movements. *Progress in motor control* (pp. 317–335). Springer.

Sasaki, D., Noritsugu, T., & Takaiwa, M. (2005). Development of active support splint driven by pneumatic soft actuator (ASSIST). *Robotics and Automation, 2005. ICRA 2005. Proceedings of the 2005 IEEE International Conference on*, 520–525.

Sawicki, G. S., & Ferris, D. P. (2009). A pneumatically powered knee-ankle-foot orthosis (KAFO) with myoelectric activation and inhibition. *Journal of neuroengineering and rehabilitation, 6*(1), 23.

Schabowsky, C. N., Godfrey, S. B., Holley, R. J., & Lum, P. S. (2010). Development and pilot testing of HEXORR: hand EXOskeleton rehabilitation robot. *Journal of neuroengineering and rehabilitation, 7*(1), 36.

Schaechter, J. D., Kraft, E., Hilliard, T. S., Dijkhuizen, R. M., Benner, T., Finklestein, S. P., Rosen, B. R., & Cramer, S. C. (2002). Motor recovery and cortical reorganization after constraint-induced movement therapy in stroke patients: a preliminary study. *Neurorehabilitation and neural repair, 16*(4), 326–338.

Schiele, A. (2009). Ergonomics of exoskeletons: Objective performance metrics. *World Haptics 2009-Third Joint EuroHaptics conference and Symposium on Haptic Interfaces for Virtual Environment and Teleoperator Systems*, 103–108.

Shadmehr, R., Smith, M. A., & Krakauer, J. W. (2010). Error correction, sensory prediction, and adaptation in motor control. *Annual review of neuroscience*, *33*, 89–108.

Shahmoradi, M. H., Akhaee, M. A., & Mirian, M. S. (2015). Combined classification and regression for simultaneous and proportional EMG control of wrist forces. *2015 23rd European Signal Processing Conference (EUSIPCO)*, 2426–2430.

Sherwood, L. (2015). *Human physiology: from cells to systems*. Cengage learning.

Singh, N., Saini, M., Anand, S., Kumar, N., Srivastava, M. P., & Mehndiratta, A. (2019). Robotic exoskeleton for wrist and fingers joint in post-stroke neuro-rehabilitation for low-resource settings. *IEEE Transactions on Neural Systems and Rehabilitation Engineering*, *27*(12), 2369–2377.

Sivan, M., Gallagher, J., Makower, S., Keeling, D., Bhakta, B., O'Connor, R. J., & Levesley, M. (2014). Home-based Computer Assisted Arm Rehabilitation (hCAAR) robotic device for upper limb exercise after stroke: results of a feasibility study in home setting. *Journal of neuroengineering and rehabilitation*, *11*(1), 163.

Smania, N., Montagnana, B., Faccioli, S., Fiaschi, A., & Aglioti, S. M. (2003). Rehabilitation of somatic sensation and related deficit of motor control in patients with pure sensory stroke. *Archives of physical medicine and rehabilitation*, *84*(11), 1692–1702.

Sober, S. J., & Sabes, P. N. (2003). Multisensory integration during motor planning. *Journal of Neuroscience*, *23*(18), 6982–6992.

Solomonow, M., Baratta, R. V., & D'Ambrosia, R. (1991). EMG-force relations of a single skeletal muscle acting across a joint: Dependence on joint angle. *Journal of Electromyography and Kinesiology*, *1*(1), 58–67.

Sommerfeld, D. K., Eek, E. U.-B., Svensson, A.-K., Holmqvist, L. W., & Von Arbin, M. H. (2004). Spasticity after stroke: its occurrence and association with motor impairments and activity limitations. *Stroke*, *35*(1), 134–139.

Song, R., Tong, K.-Y., Hu, X., & Zhou, W. (2013). Myoelectrically controlled wrist robot for stroke rehabilitation. *Journal of neuroengineering and rehabilitation*, *10*(1), 52.

Spagnuolo, G., Malosio, M., Scano, A., Caimmi, M., Legnani, G., & Tosatti, L. M. (2015). Passive and active gravity-compensation of LIGHTarm, an exoskeleton for the upper-limb rehabilitation. *2015 IEEE International Conference on Rehabilitation Robotics (ICORR)*, 440–445.

Squeri, V., Masia, L., Giannoni, P., Sandini, G., & Morasso, P. (2013). Wrist rehabilitation in chronic stroke patients by means of adaptive, progressive robot-aided therapy. *IEEE transactions on neural systems and rehabilitation engineering*, *22*(2), 312–325.

Stauffer, F., Thielen, M., Sauter, C., Chardonnens, S., Bachmann, S., Tybrandt, K., Peters, C., Hierold, C., & Vörös, J. (2018). Skin conformal polymer electrodes for clinical ECG and EEG recordings. *Advanced healthcare materials*, *7*(7), 1700994.

Stewart, A. M., Pretty, C. G., Adams, M., & Chen, X. (2017). Review of upper limb hybrid exoskeletons. *IFAC-PapersOnLine*, *50*(1), 15169–15178.

Bibliography

Su, F.-C., Chou, Y.-L., Yang, C.-S., Lin, G.-T., & An, K.-N. (2005). Movement of finger joints induced by synergistic wrist motion. *Clinical Biomechanics, 20*(5), 491–497.

Su, Y.-Y., Yu, Y.-L., Lin, C.-H., & Lan, C.-C. (2019). A compact wrist rehabilitation robot with accurate force/stiffness control and misalignment adaptation. *International Journal of Intelligent Robotics and Applications, 3*(1), 45–58.

Tagliamonte, N. L., Scorcia, M., Formica, D., Campolo, D., & Guglielmelli, E. (2011). Effects of impedance reduction of a robot for wrist rehabilitation on human motor strategies in healthy subjects during pointing tasks. *Advanced Robotics, 25*(5), 537–562.

Taub, E., Uswatte, G., Mark, V., & Morris, D. (2006). The learned nonuse phenomenon: implications for rehabilitation. *Eura Medicophys, 42*, 241–255.

Tefertiller, C., Hays, K., Jones, J., Jayaraman, A., Hartigan, C., Bushnik, T., & Forrest, G. F. (2017). Initial outcomes from a multicenter study utilizing the indego powered exoskeleton in spinal cord injury. *Topics in spinal cord injury rehabilitation, 24*(1), 78–85.

Teulings, H.-L., Contreras-Vidal, J. L., Stelmach, G. E., & Adler, C. H. (1997). Parkinsonism reduces coordination of fingers, wrist, and arm in fine motor control. *Experimental neurology, 146*(1), 159–170.

Thrift, A. G., Thayabaranathan, T., Howard, G., Howard, V. J., Rothwell, P. M., Feigin, V. L., Norrving, B., Donnan, G. A., & Cadilhac, D. A. (2017). Global stroke statistics. *International Journal of Stroke, 12*(1), 13–32.

Tyson, S. F., Hanley, M., Chillala, J., Selley, A. B., & Tallis, R. C. (2008). Sensory loss in hospital-admitted people with stroke: characteristics, associated factors, and relationship with function. *Neurorehabilitation and Neural Repair, 22*(2), 166–172.

Ueki, S., Kawasaki, H., Ito, S., Nishimoto, Y., Abe, M., Aoki, T., Ishigure, Y., Ojika, T., & Mouri, T. (2010). Development of a hand-assist robot with multi-degrees-of-freedom for rehabilitation therapy. *IEEE/ASME Transactions on mechatronics, 17*(1), 136–146.

Unity. (2020). *Unity for all.* Retrieved November 25, 2020, from https://unity.com/

Vahdat, S., Darainy, M., Thiel, A., & Ostry, D. J. (2019). A single session of robot-controlled proprioceptive training modulates functional connectivity of sensory motor networks and improves reaching accuracy in chronic stroke. *Neurorehabilitation and neural repair, 33*(1), 70–81.

Vallery, H., Duschau-Wicke, A., & Riener, R. (2009). Generalized elasticities improve patient-cooperative control of rehabilitation robots. *2009 IEEE International Conference on Rehabilitation Robotics*, 535–541.

Van Meulen, F. B., Klaassen, B., Held, J., Reenalda, J., Buurke, J. H., Van Beijnum, B.-J. F., Luft, A., & Veltink, P. H. (2016). Objective evaluation of the quality of movement in daily life after stroke. *Frontiers in bioengineering and biotechnology, 3*, 210.

van Andel, C. J., Wolterbeek, N., Doorenbosch, C. A., Veeger, D. H., & Harlaar, J. (2008). Complete 3D kinematics of upper extremity functional tasks. *Gait & posture, 27*(1), 120–127.

Veerbeek, J. M., Langbroek-Amersfoort, A. C., Van Wegen, E. E., Meskers, C. G., & Kwakkel, G. (2017). Effects of robot-assisted therapy for the upper limb after stroke: a systematic review and meta-analysis. *Neurorehabilitation and neural repair, 31*(2), 107–121.

Vidoni, E. D., & Boyd, L. A. (2009). Preserved motor learning after stroke is related to the degree of proprioceptive deficit. *Behavioral and Brain Functions*, *5*(1), 36.

Vinagre, B. M., Chen, Y. Q., & Petráš, I. (2003). Two direct Tustin discretization methods for fractional-order differentiator/integrator. *Journal of the franklin institute*, *340*(5), 349–362.

Virzi, R. A. (1992). Refining the test phase of usability evaluation: How many subjects is enough? *Human factors*, *34*(4), 457–468.

Volpe, B. T., Ferraro, M., Lynch, D., Christos, P., Krol, J., Trudell, C., Krebs, H. I., & Hogan, N. (2005). Robotics and other devices in the treatment of patients recovering from stroke. *Current neurology and neuroscience reports*, *5*(6), 465–470.

Volpe, B. T., Lynch, D., Rykman-Berland, A., Ferraro, M., Galgano, M., Hogan, N., & Krebs, H. I. (2008). Intensive sensorimotor arm training mediated by therapist or robot improves hemiparesis in patients with chronic stroke. *Neurorehabilitation and Neural Repair*, *22*(3), 305–310.

Wade, D., Langton-Hewer, R., Wood, V. A., Skilbeck, C., & Ismail, H. (1983). The hemiplegic arm after stroke: measurement and recovery. *Journal of Neurology, Neurosurgery & Psychiatry*, *46*(6), 521–524.

Wang, H., Patota, F., Buondonno, G., Haendl, M., De Luca, A., & Kosuge, K. (2015). Stability and variable admittance control in the physical interaction with a mobile robot. *International Journal of Advanced Robotic Systems*, *12*(12), 173.

Wang, H., Li, Y., Long, J., Yu, T., & Gu, Z. (2014). An asynchronous wheelchair control by hybrid EEG–EOG brain–computer interface. *Cognitive neurodynamics*, *8*(5), 399–409.

Ward, N. S., Brander, F., & Kelly, K. (2019). Intensive upper limb neurorehabilitation in chronic stroke: outcomes from the Queen Square programme. *J Neurol Neurosurg Psychiatry*, *90*(5), 498–506.

Webb, J., Xiao, Z. G., Aschenbrenner, K. P., Herrnstadt, G., & Menon, C. (2012). Towards a portable assistive arm exoskeleton for stroke patient rehabilitation controlled through a brain computer interface. *2012 4th IEEE RAS & EMBS International Conference on Biomedical Robotics and Biomechatronics (BioRob)*, 1299–1304.

Wege, A., & Zimmermann, A. (2007). Electromyography sensor based control for a hand exoskeleton. *Robotics and Biomimetics, 2007. ROBIO 2007. IEEE International Conference on*, 1470–1475.

Winward, C. E., Halligan, P. W., & Wade, D. T. (2007). Somatosensory recovery: a longitudinal study of the first 6 months after unilateral stroke. *Disability and rehabilitation*, *29*(4), 293–299.

Woldag, H., & Hummelsheim, H. (2002). Evidence-based physiotherapeutic concepts for improving arm and hand function in stroke patients. *Journal of neurology*, *249*(5), 518–528.

Wong, J. D., Kistemaker, D. A., Chin, A., & Gribble, P. L. (2012). Can proprioceptive training improve motor learning? *Journal of neurophysiology*, *108*(12), 3313–3321.

Bibliography

Wu, C.-L., Huang, M.-H., Lee, C.-L., Liu, C.-W., Lin, L.-J., & Chen, C.-H. (2006). Effect on spasticity after performance of dynamic-repeated-passive ankle joint motion exercise in chronic stroke patients. *The Kaohsiung journal of medical sciences, 22*(12), 610–617.

Wu, Q., Wang, X., & Du, F. (2016). Development and analysis of a gravity-balanced exoskeleton for active rehabilitation training of upper limb. *Proceedings of the Institution of Mechanical Engineers, Part C: Journal of Mechanical Engineering Science, 230*(20), 3777–3790.

Xiloyannis, M., Cappello, L., Khanh, D. B., Yen, S.-C., & Masia, L. (2016). Modelling and design of a synergy-based actuator for a tendon-driven soft robotic glove. *2016 6th IEEE International Conference on Biomedical Robotics and Biomechatronics (BioRob)*, 1213–1219.

Yekutiel, M. (2000). *Sensory re-education of the hand after stroke*. Wiley.

Yoshii, Y., Yuine, H., Kazuki, O., Tung, W.-l., & Ishii, T. (2015). Measurement of wrist flexion and extension torques in different forearm positions. *Biomedical engineering online, 14*(1), 115.

Zeng, G., & Hemami, A. (1997). An overview of robot force control. *Robotica, 15*(5), 473–482.

Zollo, L., Rossini, L., Bravi, M., Magrone, G., Sterzi, S., & Guglielmelli, E. (2011). Quantitative evaluation of upper-limb motor control in robot-aided rehabilitation. *Medical & biological engineering & computing, 49*(10), 1131.